Quantifying the impact of radiation therapy dose uncertainties on radiobiological treatment plan evaluation

by

Gavin Cranmer-Sargison

B.Sc., University of Victoria, 2003.

A Thesis Submitted in Partial Fulfillment of the
Requirements for the Degree of

MASTERS OF SCIENCE

in the Department of Physics and Astronomy.

Co - Supervisor: Dr. S. Zavgorodni

Co - Supervisor: Dr. M. J. Roney

Abstract

The goal of this study was to quantify the impact of dose uncertainty on radiobiological treatment plan evaluation. A formalism was developed for assessing the impact of dose uncertainty on survival fraction (SF). To distinguish between spatial and probabilistic dose variations, we define *equivalent stochastic dose* (ESD) as the voxel dose that gives an expected survival fraction for the randomly deposited dose. In the case where the probabilistic voxel dose follows a Gaussian distribution, we derive an analytic expression for SF(ESD). We show the analytic expression can account for multi-voxel dose distributions that incorporate both probabilistic and spatial dose heterogeneities. In addition, we incorporate dose uncertainty in the calculation of tumour control probability (TCP) using the ESD formalism. We verify the derivation and implementation of the derived expression using the Monte Carlo method for cases of 60 Gy and 70 Gy at 2 Gy per fraction. The results show that the derived formalism is an effective method for evaluating the radiobiological impact of dose uncertainties on treatment plan evaluation.

Contents

List of Tables

List of Figures

Acknowledgments

I would like to thank my family for their unconditional support and encouragement during the course of this project. I share the joy of completion with them, knowing this would not have been possible if not for their love. In addition, I thank Tammy Lavigne for her loving words of encouragement and strong character - this work would not have been possible without it. I thank my supervisors, Sergei Zavgorodni and Mike Roney for offering their expertise and guidance. I acknowledge Wayne Beckham as a true leader and thank him for his contribution to this work and much more. I appreciate everything Vitali Moiseenko has contributed to this work, to my own development and for the many great discussions over coffee. I am grateful to Andrew Jirasek for his thoughtful insights into graduate studies and for many great discussions. I thank Karl Bush, Gab Rosenbaum, Ian Nugent, Warren Shaw, Eric Harvey and Erin Barnett for being great friends and wish them all the best.

Dedication

I dedicate this thesis to my daughter, who I love more than life itself. She inspires me to strive to become more than I was yesterday, satisfied with the love of others, humbly pursuing my passion amongst the wonders of God's creation. I cherish each moment we're together, she brings a smile to my face, a tear to my eye, and will always be "my little beautiful".

Chapter 1

Introduction

1.1 Background

Today there is great optimism among patients diagnosed with one of the many forms of cancer. Though traumatic, the once ominous detection of a cancerous tumour is now met with a realization that the prognosis is good. In fact, now more than ever, patients diagnosed with cancer can anticipate a five year cure rate as a realistic therapeutic objective.

The historical understanding of cancer as a disease of overly rapid cellular proliferation made it logical to treat cancer patients with x-rays [1]. Within a few months of Roentgen's 1895 discovery of x-rays the biological effects of ionizing radiation were recognized. In fact, Grubbe [3] states that in 1896 the first patient was treated with x-rays for a far advance carcinoma of the breast with the resultant objective of tumour size reduction and subjective improvement in pain and discomfort being achieved. By the early 1930's Coutard [2] had developed a fractionated treatment scheme that remains the basis for current radiation therapy.

By the 1950's, technological advances had made the treatment of malignant disease possible at far higher x-ray energies than the early kV treatments. By the end of the decade, the "super-voltage roentgenotherapy" Van de Graaff generators, operat-

ing at 800-kV, were soon being replaced by linear accelerators and ^{60}Co teletherapy units [4] and so the beginning of the modern radiation oncology era had started.

In the past thirty years computer based treatment planning and the associated developments in medical imaging have each contributed to more sophisticated radiotherapeutic strategies. Yet, however impressive the current treatment techniques are, the goal of treatment has not changed. Quite simply, the goal of radiotherapy, as declared by The National Cancer Institute, is the complete destruction of an entire tumor or the shrinking of a tumor as a means of symptom relief.

In predicting and optimizing the effects of a radiotherapy treatment two processes must be well understood: the physics of ionizing radiation and the cellular response to the interactions of ionizing radiation. Since the aim of radiotherapy is to kill cancer cells while minimizing the damage to normal tissue, the expected effects of ionizing radiation to tumour, tissue and other irradiated organs must be well known [5].

Along with the many advances made in clinical radiotherapy, the study of cell response to ionizing radiation has too evolved. In fact, since the time when Gray and Read produced their pioneering results in a wooden hut behind the Mount Vernon Hospital, the field of radiobiology has developed to become a multidisciplinary field of research. Both experimental and theoretical research in radiobiology has contributed to clinical radiation therapy in a number of distinct ways.

The conceptual basis for the many forms of radiotherapy treatment has come from identifying the mechanisms and processes associated with the response of tissue and tumours to irradiation. Tumour control strategies based on these findings have influenced the clinical implementation of schedule choice, changes in fractionation and/or dose rate and the possible inclusion of chemotherapy into treatment regimes.

Carlos Perez, in his ASTRO[1] gold medal address defined the pillars of radiation oncology as: biology, physics and treatment planning, clinical knowledge, professional competence, socioeconomics, and politics. On these pillars rest rational therapy, clinical trials, and ongoing quality improvement [6]. These pillars are essential to quality patient care and emphasize the vast interdisciplinary nature of radiation oncology. As a requisite component of the radiotherapy team, medical physicists not only contribute to clinical operations but to the global understanding of the complex physical processes involved in cancer treatment. This involvement facilitates many cross-disciplinary studies such as radiobiological treatment plan evaluation.

Both radiobiologist and physicists have worked to develop quantitative evaluative methods used in scoring radiotherapy treatment plans. The majority of this work has formed around the understanding of the cellular response to ionizing radiation. In fact, understanding the characteristic curve associated with the cellular dose[2] response became an early area of research between these two scientific disciplines. The characteristic cellular dose response is often quantified using the concept of survival fraction; defined as the fractional number of cells surviving a fixed radiation dose. Derived from the survival fraction concept are a number of evaluative indices used to rank competing radiotherapy treatment plans. However, inherent in every radiotherapy treatment is an associated dose uncertainty which must be accounted for in the evaluative process.

---

[1] American Society for Therapeutic Radiology and Oncology

[2] Dose is defined as the energy E imparted to a finite volume V at a point P such that $D = \frac{dE}{dm}$.

1.2 Thesis outline

In this study, we employ the radiobiologically derived concept of survival fraction to quantify the potential affects of dose uncertainty on radiation therapy treatment plan evaluation. We develop a formalism for assessing the impact of both statistical and physical dose uncertainties (see below) on the radiobiologically based predictive indices of equivalent uniform dose (EUD) and tumour control probability (TCP)[3]. Dose uncertainties are divided into two categories: physical and statistical. Physical dose uncertainty is defined to be any physically discernible uncertainty resulting from systematic and/or random errors in treatment planning and/or delivery. Statistical dose uncertainty is associated exclusively with dose distributions calculated using Monte Carlo electron-photon transport algorithms. We will refer to all dose uncertainties that arise from either calculation or delivery as stochastic. In addition to the designation between physical and statistical dose uncertainty, we make a distinction between spatial and probabilistic dose heterogeneity; the later being an artificial dose heterogeneity resulting from physical or statistical dose uncertainties. We develop the concept of an *equivalent stochastic dose* (ESD) and derive an analytic expression for SF(ESD) as a means of assessing the impact of radiotherapy dose uncertainty.

Our discussion starts, in Chapter 2, with a review of the ICRU[4] volume definitions used in conformal radiation therapy. We continue with an overview of three dimensional conformal radiotherapy and explore a number of general techniques associated with intensity modulated radiation therapy (IMRT). We then describe the use of Monte Carlo methods in radiotherapy treatment planning, the Electron-Gamma-Shower (EGS) based BEAMnrc-DOSXYZnrc user code and how statistical dose un-

[3]See Chapter 3 for a full description of EUD and TCP

[4]International Commission on Radiation Units and Measurements

certainty is calculated in DOSXYZnrc. Chapter 2 concludes with a survey of physical radiotherapy dose uncertainties with a detailed exploration of both organ motion and patient position uncertainties.

Chapter 3 is devoted to developing the radiobiological background required to interpret the evaluative indices of equivalent uniform dose and tumour control probability. To appreciate these indices from a theoretical foundation, we first develop an understanding of cell kill and associate this with the concept of survival fraction. From the concept of survival fraction, we briefly examine treatment fractionation in radiotherapy, the concept of a biological effective dose, and quantify the characteristics of early and late responding tissue and tumour on survival fraction. We then examine the radiobiological treatment plan evaluative indices of EUD and TCP. To conclude the chapter, we explore how other researchers have worked to incorporate dose uncertainties into radiobiological treatment plan evaluation.

In Chapter 4, we start by defining statistical and physical dose uncertainties as used in this work. From the calculation of the expected survival fraction we develop our concept of *equivalent stochastic dose* (ESD). We then derive an analytic expression for SF(ESD) with the one assumption that the probabilistic dose to a voxel is distributed as a Gaussian probability density function. Using this analytic expression we then incorporate dose uncertainty into the calculation of TCP by calculating TCP as a function of ESD.

Chapter 5 is dedicated to quantifying the impact of dose uncertainties using our ESD concept. We explore how the expected survival fraction responds to increased dose uncertainty and compare this with the well documented response of survival fraction to spatial dose heterogeneity. Two common treatment prescriptions of 60 and 70 Gy at 2 Gy per fraction are modelled for increasing levels of dose uncertainty and the radiobiological response quantified using the ESD concept. This analysis is

extended to include TCP for the same two cases and the results contrasted to other studies. The chapter concludes with interpretation of ESD as the result of statistical or physical dose uncertainties and possible implications of ESD in treatment plan evaluation.

We end with a chapter devoted to concluding remarks and incorporate an appendix that includes published papers derived from this work.

Chapter 2

Conformal radiation therapy

The goal of radiation therapy is to eliminate cancerous cells within a patient tumour volume while minimizing damage to normal tissue and critical organs. To achieve an effective radiotherapy treatment, correct tumour localization is essential and therefore, tumour volumes, treatment volumes and other irradiated volumes must be clearly defined using a standard convention.

Delineating tumour volumes involves the use of accurate three dimensional (3D) patient image sets, clinical observation, palpation and surgical findings [7]. X-ray computed tomography (CT) is one of a number of 3D imaging techniques available to radiation therapy departments. In fact, CT imaging has become the standard modality used in tumour localization and clinical treatment planning [8]. High quality CT image sets can be used to ensure reliable clinical tumour volume delineation. In turn, this provides for higher treatment dose to smaller target volumes - which should result in less normal tissue damage. Tailoring treatment dose to a target while sparing normal tissue is referred to as conformal radiation therapy. Clearly, a convention for defining tumour volumes, accurate CT image sets, advanced beam collimation techniques and accurate dose calculation algorithms are essential in meeting the goal of conformal radiotherapy.

2.1 Volume definitions in radiotherapy

The International Commission on Radiation Units (ICRU) has in Report 50 and 62 recommended specifications for prescribing, recording and reporting standard volume(s) and dose(s) for most clinical radiotherapy treatment situations [9, 10]. In Report 50 the primary aim of radiotherapy is defined to be the radical treatment of malignant disease, where treatment outcome can only be interpreted if irradiation parameters such as the dose distribution in space and time are accurately correlated with the clinical and pathological extent of the disease.

Report 50 specifies a number of physical volumes that are to be defined prior to, and referenced during, treatment planning (See Figure 2.1). The Gross Tumour Volume (GTV) is the first required volume in the treatment planning process. GTV is defined as the gross palpable or visible/demonstrable extent and location of malignant growth. Generally, the region surrounding the GTV will also have high tumor cell density. Therefore, an additional volume is defined as the Clinical Target Volume (CTV). CTV consists of a tissue volume that contains a demonstrable GTV and/or subclinical microscopic malignant disease. Both GTV and CTV must be treated adequately in order to achieve the aim of therapy.

Throughout the treatment process the position and shape of the CTV should ideally be constant with respect to a common fixed coordinate system. Unfortunately, this is not the case as tumor size may change during the course of treatment and the tumour volume subject to internal movement. In addition, patient position variations may occur during treatment set-up and delivery. To address the geometric uncertainty due to tumour movement and patient set-up, Report 50 defines the Planning Target Volume (PTV) as a geometric concept used to select appropriate beam size and orientation; taking into consideration the net effect of all possible geometric

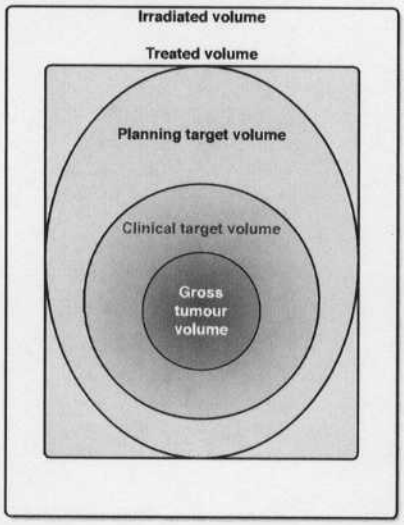

Figure 2.1: Schematic diagram showing the various volumes as defined in ICRU Report 50. The inner most region is defined as the Gross Tumor Volume (GTV) followed by the Clinical Target Volume (CTV), Planning Target Volume (PTV), Treated Volume and finally the Irradiated Volume.

variations. Accounting for all geometric variations ensures the prescribed dose is actually distributed throughout the CTV. PTV can therefore be envisioned as a static, geometric volume used only for treatment planning.

Other volumes specified in Report 50 are the Treated and Irradiated volumes: the former defined as the volume enclosed by an isodose surface selected by the radiation oncologist, and the later defined as the volume irradiated to a dose considered significant in relation to normal tissue tolerance. As projections onto a 2D plain, Fig. 2.1 illustrates the spatial relationship between the different Report 50 volumes.

As a supplement to Report 50, ICRU published Report 62 to formulate more accurate definitions related to volumes, margins, organs at risk, dose variations, and uncertainties that result from the technological advances in clinical imaging and treatment precision. Report 62 clearly specifies two coordinate systems and two reference points that are to be used in combination. The coordinates relate the positions of

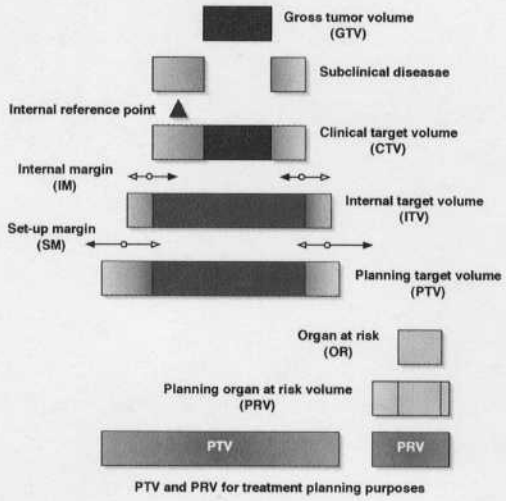

Figure 2.2: Schematic diagram showing the various volumes and margins as defined in ICRU Report 62. Included are the Gross Tumor Volume (GTV), Clinical Target Volume (CTV), Internal Margin (IM), Set-up Margin (SM), Planning Target Volume (PTV), Organ at Risk (OR), Planning Organ at Risk Volume(PRV).

tissues, organs and volumes in the patient with the position and orientations of the beams used for imaging and therapy. Graphically, the relationship between the defined volumes and margins can be seen in Fig. 2.2.

In conjunction with accurate patient set-up during imaging and therapy, ICRU Report 62 defines the Internal Reference Point as the point used for localization of GTV or CTV with respect to anatomical landmarks. The External Reference Point is defined as palpable or visible points located on or near the surface of the body or on the surface of an immobilization device. In addition, Report 62 specifies two independent coordinate systems that are associated with the patient position (internal) and the imaging system and treatment unit (external).

As an addition to the various volumes defined in Report 50, Report 62 incorporates margins to account for geometric variations and uncertainties (Fig 2.2). A planned treatment is a static composition of therapy beam orientations resulting in a

dose distribution that, in reality, does not inherently reflect the dynamic uncertainties in CTV size/location or patient position. Margins are included to incorporate changes in the position, size, and shape of both tissue and patient with respect to each of the coordinate systems.

An Internal Margin (IM) is added to the CTV to compensate for expected physiological movements and variations in tumour size, shape, and position during treatment. To distinguish the volume enclosed by the CTV surface plus an IM, from that of the PTV, an intermediate volume is defined as the Internal Target Volume (ITV) [11]. A Set-up Margin (SM) is incorporated to account for patient position, mechanical, and dosimetric uncertainties with respect to the external set of coordinates. The SM is added to the ITV to give the PTV previously defined in Report 50.

Figure 2.2 also includes an Organ at Risk (OAR) volume and the resulting Planning Organ at Risk Volume (PRV). An organ at risk is any normal tissue whose radiation sensitivity may significantly influence planning or the prescribed dose where the PRV is included to account for any movements of the OAR during treatment.

2.2 Techniques in conformal radiotherapy

CT image data can provide high quality anatomic information that, in turn, can be used to reveal the accurate location of tumours and critical structures [12]. With accurate three-dimensional tumour location, clinicians can define relevant ICRU volumes with increased confidence. Careful tumour volume localization combined with precise beam collimation techniques foreshadow the success of any radiation therapy treatment. To achieve the desired outcome of therapy, treatment fields should be made to conform to the tumour volume while sparing the critical structures [13].

As each treatment field is made to conform to the PTV, delivered dose may be escalated to produce a greater biological effect. In general, using a large number of beams set in various orientations can be planned to cover the required target while blocking out normal tissue and/or critical structures. Allowing multiple beams with varied orientations may provide sharp margins around the target, but as Langer [14] notes, should be created with the penumbra of one beam placed in the interior of another. Khan [15] adds that in the design of conformal fields, sufficient margins must be given between the PTV and any field boundary to ensure adequate coverage. With sufficient margins, PTV dose can be made to incorporate cross-beam profile penumbra and lateral radiation transport as a function of depth, radial distance and tissue density.

Webb [16] broadly divides conformal therapy techniques into two categories: those which employ geometric field shaping alone and those which also modulate the fluence[1] intensity across the geometrically-shaped field. Throughout this work, geometric field shaping techniques will be referred to as 3D conformal radiation therapy (CRT), whereas techniques that incorporate modulated fluence intensities will be referred to as intensity modulated radiation therapy (IMRT). The complexities associated with treating patients using conformal and modulated techniques are numerous and the scope of the subject vast. In the following sections we will explore essential aspects of both three dimensional conformal therapy and intensity modulated radiation therapy.

[1]Fluence is defined, for a mono-energetic photon beam, as the ratio of the number of photons dN passing through a cross sectional area dA perpendicular to the beam direction, such that $\Phi = \frac{dN}{dA}$.

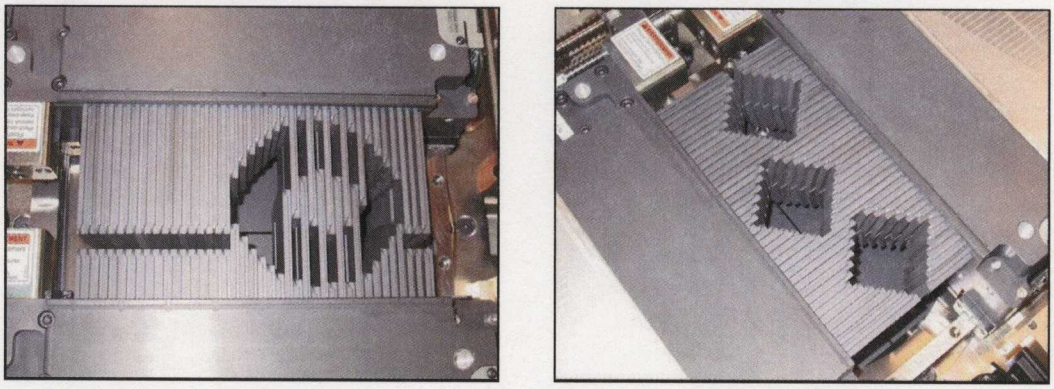

Figure 2.3: Two images of the Varian Millennium multi-leaf collimator taken during an electronics quality assurance test. Note the rounded leaf ends and the intricate tongue-and-groove configuration used for inter-leaf positioning.

2.2.1 Three-dimensional conformal radiation therapy

For most deep seated tumours a realistic tumour dose can only be achieved by using a combination of several beams. In fact, acceptable isodose distributions are generally only achieved using a combination of therapy beams with appropriate energy, size, weighting and gantry angle. Combined in the appropriate manner, a treatment plan can be made to give a therapeutic dose over the target volume while minimizing acute and/or late side affects. Beam shaping has traditionally been achieved through the use of alloy blocks individually made to collimate each field to a specific shape. The blocks are placed in a tray attached to the machine head and must be changed for each field. A typical conformal treatment uses 3 to 5 fields, therefore, the time require to prepare and set-up the collimating blocks can become considerable.

An alternate approach to collimating conformal therapy beams was developed by Takahashi [17]. This method uses a large number of rectangular wedged fields, each at different gantry angles, made to approximately conform to the target volume. The total dose distribution that results from the this method can be made to pro-

duce a high tumour dose. However, this method is limited by the rectangular beam collimation and therefore is not truly conformal. By using beam shaping blocks this approach can be made to produce highly conformal dose distributions but again the time allocated for block preparation and set-up becomes problematic.

Today, three-dimensional conformal radiotherapy generally refers to multi-field treatments, where each field is shaped with a multi-leaf collimator (MLC). Boyer [18] sets out beam shaping in the following manner:

- Accelerated electrons strike a tungsten target producing a shower of high energy photons.
- A fixed primary collimator first attenuates all but the forward-directed bremsstrahlung cone.
- The cone of radiation passes through a sealed, parallel-plate ionization chamber. The resulting ionization current is used to monitor and control the machine output.
- The beam next passes through a set of motorized tungsten blocks that reduce the circular cross section of the cone to a rectangular field circumscribing the desired field shape.
- Finally, the individual leaves of the MLC are set to the boundaries of the desired field shape.

Multi-leaf collimators are clinically the most sophisticated method for generating arbitrary shaped radiotherapy fields, yet the utility of MLC collimation is not restricted to just conformal treatments.

2.2.2 Intensity modulated radiation therapy

In the previous section, conformal therapy techniques were explored and the benefit of using a multi-leaf collimator outlined. However, the application of the MLC does not stop with conforming two-dimensional treatment fields to a PTV. As Brahme [19] states, the ultimate step in therapy development was to allow full freedom in the shape of the delivered beams both with regard to beam energy, beam direction and beam profile. Freedom in beam profile implies modulation of the beam intensity across each field. Traditional conformal therapy techniques use field intensities that are either uniform or change uniformly with the addition of a wedge filter. The intensity profile of a modulated field need not observe such a restriction and can be made to produce non-traditional fluence maps. This freedom suggests that features of conventional dose distributions expected from conformal therapy need no longer be preserved, and new features created so that treatment plans can be made to enhance the sparing of normal tissue and critical structures.

Bortfeld *et al* [21] frames the problem of optimizing the dose distribution for conformation radiotherapy with intensity modulated external beams as a problem similar to the reconstructing a 3D image from its 2D projections, as demonstrated in Figure 2.4.

There are two general methods used to produce IMRT beams shaped with a multi-leaf collimator. The first is to use a series of discrete conformal fields each located at the same gantry angle. The treatment machine is turned on to give a conformal dose for the first field. Each pair of multi-leaves are then moved to a set of different positions. This produces a new conformal field and the machine is once again turned on. This results in a series of fractional conformal doses given at that same gantry angle. The total dose is therefore the sum of the fractional doses

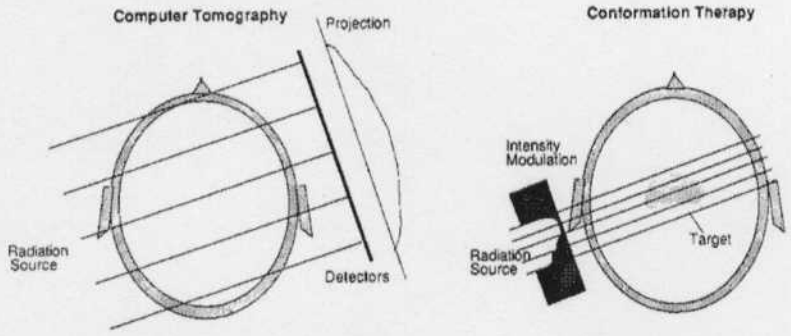

Figure 2.4: Taken from Bortfeld *et al* [21], this image demonstrates how optimizing the dose distribution for conformation radiotherapy with intensity modulated external beams is similar to the problem of reconstructing a 3D image from its 2D projections.

delivered through each conformal field and results in a modulated dose distribution. This technique is referred to as step-and-shoot intensity modulation and finds many applications in radiotherapy. Figure 2.5 shows four different conformal fields used in an example step-and-shoot treatment.

A second IMRT technique used in radiotherapy is a dynamic method where the leaves are moved while the treatment machine is on; this is referred to as dynamic multi-leaf collimation (dMLC). Having the fluence intensity modulated as a dynamic process does pose a number of difficulties. One key requirement is to interpret the desired intensity modulation into a set of instructions used to drive the leaves across the treatment field. A simple solution for calculating the leaf positions as a function of time was presented by Boyer [22] and Boyer and Strait [23]. This method relates the desired beam intensity to the velocity of each leaf-pair. This is a very intuitive solution that assumes the leading leaf is moving at the maximum possible velocity and varies the velocity of the trailing leaf to produce the desired intensity modulation.

However, optimizing field intensities to maximize the tumour dose, while minimizing dose to normal tissue, is computationally not trivial. Optimization uses

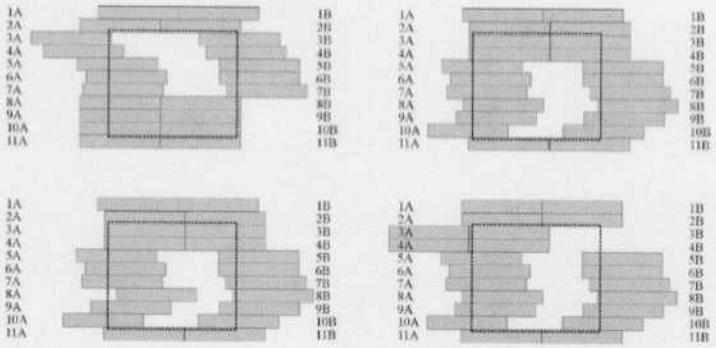

Figure 2.5: Shown are four multi-leaf collimated fields used in an example step-and-shoot IMRT treatment (Taken from [20]).

an objective function constrained by the prescribed dose to the target volume and OARs. As it is impossible to deliver negative dose, there are restrictions on the parameters used in optimizing beam weights that produce modulated field intensities. One method implemented by Webb [24] uses a model of simulated annealing to derive beam element weights for a known dose prescription. This technique starts with all the elemental beam weights set to zero and assigns discrete weights offered randomly to each of the beam elements. After each offering the dose distribution that results from the current ensemble is compared with the prescription distribution and the process iterated until there is a match.

One characteristic of modulating the beam intensity across the treatment field is the possibility of an inhomogeneous dose distribution within the tumour volume. At first this might be thought undesirable, but as De Meerleer [25] notes, the use of inhomogeneous dose distributions may provide a higher dose to the tumor without increasing normal tissue doses. This is the primary benefit in modulating the beam intensity across each field, yet, the overall goal of tumour control must not be compromised. Goitein and Niemierko [26] warn that optimization of field intensities should produce dose distributions that are homogeneous throughout the target

volume and strongly caution against the all too-ready acceptance of significant dose non-uniformity as being an unavoidable consequence of optimization.

2.3 The Monte Carlo method in radiotherapy treatment planning

The Monte Carlo method, used in the simulation of radiation transport, employs computer generated random numbers and the knowledge of the probability distributions governing the individual interactions of electrons and photons in materials to simulate the trajectories or histories of individual particles [27]. As a large number of histories are modelled the result approaches the average photon and electron distribution - calculated to within a statistical uncertainty. The ability to simulate radiotherapy treatments using this method clearly facilitates the calculation of accurate dose distributions. When compared to analytic techniques, Monte Carlo simulation is a superior method for modelling dose deposition in regions of varying material density. In fact, Cranmer-Sargison *et al* [28] showed that at an extreme water-lung interface the difference between dose deposition calculated using an analytic technique with that of Monte Carlo data (consistent with experimental measurement) can be as much as 14%.

There are several fundamental differences between Monte Carlo calculated dose distributions and those calculated using traditional analytic algorithms [29]. One important difference is the inherent statistical uncertainty associated with Monte Carlo calculated values. This uncertainty arises from the random sampling used in the Monte Carlo method and is therefore not present in dose distributions calculated using analytic techniques.

At the root of the Monte Carlo method is a simple computational structure where

a process is modelled by producing a large number of possible outcomes. For N events, the mean and variance of a simulation are calculated as

$$\mu = \frac{1}{N}\sum_{i=1}^{N} x_i \tag{2.1}$$

and

$$\sigma^2 = \frac{1}{N-1}\sum_{i=1}^{N} (x_i - \mu)^2 \tag{2.2}$$

where μ is the mean, σ^2 is the variance and x_i is considered an independent event[2]. The statistical uncertainty on the mean is calculated such that

$$\delta = \frac{\sigma}{\sqrt{N}} \tag{2.3}$$

where one can see that the accuracy of a Monte Carlo simulation is proportional to $1/\sqrt{N}$ [30].

With an ability to model various materials and geometric configurations, the Monte Carlo method can be used to simulate physical situations. One example would be modelling the head of a medical linear accelerator. Many individuals have contributed to produce the Electron-Gamma-Shower (EGS) code [31] for high energy electron and photon transport. To extend the original application of EGS to model photon-electron energies common in radiation therapy the OMEGA (Ottawa Madison Electron Gamma Algorithm) [32] project developed EGS4. The OMEGA project also produced a set of routines that enable a user to define geometries for both medical linear accelerators and phantom configurations.

2.3.1 BEAMnrc and DOSXYZnrc

The OMEGA project was a collaborative effort between the National Research Council of Canada and the University of Wisconsin-Madison. The goal was to develop a

[2]One event is considered independent of another if the occurrence of one gives no information about whether or not the other will occur.

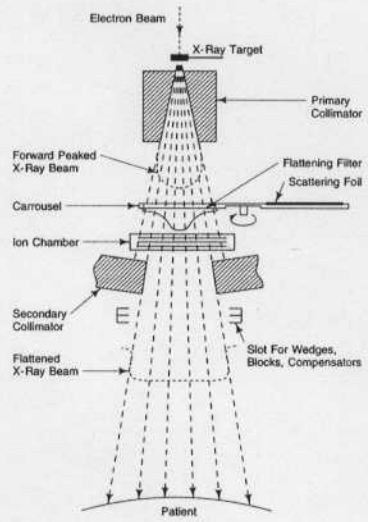

Figure 2.6: Diagram showing the components in a typical medical linear accelerator head (Taken from [33]). The important components used in a BEAM model are the bremsstrahlung target, primary collimator, flattening filter, monitor unit chamber (ion chamber) and secondary collimator jaws.

full 3D electron beam simulation based on Monte Carlo techniques that could be used to calculate the dose to a radiotherapy patient. Developed as part of the OMEGA project, BEAM and DOSXYZ are user code additions to the original EGS4 Monte Carlo system[3]. The following is a brief overview of the BEAM and DOSXYZ formalism for modelling a medical linear accelerator.

BEAM was designed to simulate the radiation beam produced by Co^{60} units and medical linear accelerators. The convention used in building a model of an accelerator is to define the z-axis of the simulation as the beam central axis; this axis is then used as the origin for all other spatial requirements. One builds a BEAM model of a linear accelerator head (Fig. 2.6) by configuring a series of component modules (CM) to dimensions provided by the manufacturer. Typical component modules used in

[3]With the addition of the EGSnrc code came what are now known as BEAMnrc and DOSXYZnrc.

accelerator modeling are: SLABS, CONS3R, FLATFILT, CHAMBER and JAWS.

The primary output of a BEAM simulation is a phase space file. This file contains information on all the particles crossing the xy-plane located at a fixed point along the z-axis. The xy-plane is referred to as a scoring plane; any number of scoring planes can be defined and located anywhere in the accelerator head. A phase space file contains information on each particle: the energy (E), the xy-position (X,Y), the direction cosines with respect to the x and y-axis (U,V), the direction cosine of the angle with respect to the z-axis (SIGN(W)), the particle weight (WT), the charge (IQ), the number of times the particle has crossed the scoring plane (NPASS) and other particle history information (LATCH) [34].

DOSXYZnrc is the most recent version of the original DOSXYZ user code developed as part of the OMEGA project. DOSXYZnrc, used in combination with the EGSnrc Monte Carlo simulation code, facilitates the calculation of dose distributions within a rectilinear phantom [35]. The code allows sources such as monoenergetic diverging or parallel beams, phase-space data generated by BEAMnrc simulations, or a model-based beam reconstruction produced by BEAMDP [36]. Photon-electron transport is simulated in a Cartesian volume and energy deposition scored in designated volume elements (voxels). Each voxel is assigned a physical density that represents the true material confined to that volume element. The dimensions are variable yet are typically smaller than 1.0 cm^{-3}. For any given simulation a phantom is configured as an array of voxels.

CT based phantoms can be modelled in DOSXYZnrc by processing the CT data using the program *ctcreate*. This allows the calculation of dose distributions in phantoms derived from patient CT data sets. The program reads in a CT data-set and converts it to a material density in the corresponding volume elements. Kawrakow *et al* [37] found a simple relationship between the mass density of a material and it's

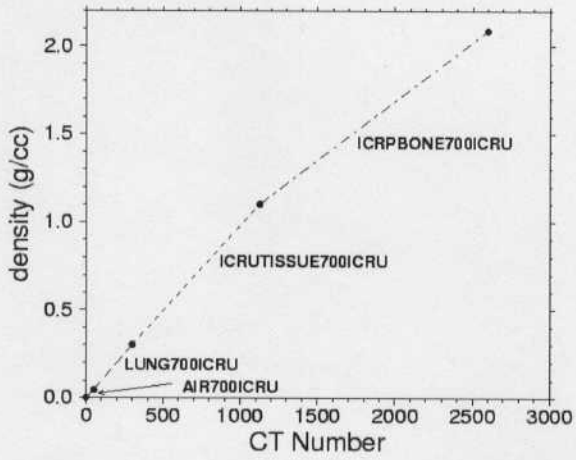

Figure 2.7: The DOSXYZnrc default ramp for converting CT-number to material density (Taken from [35]). Indicated in the figure are the ICRU standardized points for "Air", "Lung", "Tissue" and "Bone".

mass scattering and stopping powers. The authors then develop a conversion between Hounsfield number and mass density as a function of CT-scanner x-ray energy (E_x). From this work a conversion ramp (Fig. 2.7) relating CT-number and material density is included in DOSXYZnrc. The ICRU standardized materials used to characterize the default ramp are "Air", "Lung", "Tissue" and "Bone" where material densities between the fixed points are linearly interpolated.

In DOSXYZnrc statistics are handled by grouping scored quantities on a history-by-history basis. Uncertainties ($s_{\bar{X}}$) are determined for each scored quantity X_i (in our case dose to a voxel) as statistically independent events, such that

$$s_{\bar{X}} = \sqrt{\frac{1}{N-1}\left(\frac{\sum_{i=1}^{N} X_i^2}{N} - \left(\frac{\sum_{i=1}^{N} X_i}{N}\right)^2\right)} \tag{2.4}$$

where N is the total number of independent events and is always equal to the total number of primary histories [38]. Using this method, a statistical dose uncertainty for each voxel can be calculated as a function of initial history number. For phase

space sources generated using BEAMnrc there is potentially more than one particle in the file that may be traced back to the same initial primary history. Therefore, to account for a common initial history, the history-by-history technique groups all particles according to the primary history that generated each and calculates the uncertainty accordingly.

To increase the number of particles simulated in a DOSXYZnrc run the phase space file may be re-sampled. NRCYCL is an input parameter used to define the number of times each particle in a phase space file will be re-used. Along with particle recycling, ISMOOTH is used to redistribute the recycled particles about the central axis of the accelerator beam. As long as the simulated linear accelerator geometry and field size are each symmetric, and centered on the central beam axis, the ability to redistribute the phase space file allows for a reduction of systematic uncertainties in small data sets (particularly import for small field sizes). The ability to recycle phase space data becomes important as calculation time becomes clinically very important.

2.3.2 Developments in the application of the Monte Carlo method

Two important advances made recently in Monte Carlo simulations of radiotherapy treatment plans include: the ability to model the time varying multi-leaf positions inherent in dynamic IMRT plans, and establishing an absolute dosimetric frame of reference as a function of the number of initial electron histories. Combined, these two developments have made it possible to simulated a real radiotherapy treatment, calibrated to an actual treatment machine. This has made Monte Carlo simulation a clinically viable independent source of treatment planning and dose verification.

Incorporating dynamic intensity modulation into Monte Carlo simulations

The complexities associated with using the Monte Carlo method to model static and dynamic multi-leaf collimation is well documented [39–42]. The geometry of the multi-leaves present difficulties in modelling due to their intricate tongue-and-groove configuration and rounded leaf-edge. The difficulty in simulating a dynamic leaf sequence is the incorporation of time within an otherwise time independent model. Siebers *et al* [43] solved both these problems by making a number of elegant approximations to produce an accurate, fast, and efficient dMLC particle transport model that can be incorporated into Monte Carlo dose computations.

MLC geometry is modelled by separating each leaf into a set of layers corresponding to simplified geometric regions. When stacked, the layers form the inter-leaf tongue-and-groove configuration. With a set of simplified geometric regions defined for each leaf, radiation transport can be made in a region-by-region manner. To make the model efficient, the authors only model photon attenuation and Compton scatter interactions. The amount of attenuation material an individual particle traverses is determined by adding up all the individual geometric leaf regions in the particles path. Modelling the leaves using the layered leaf geometry and approximating the photon interactions was shown by the authors to produce a correct photon fluence. This was confirmed experimentally by performing static depth dose and profile measurements made with the field completely blocked by the MLC leaves.

To incorporate leaf motion into the model the authors use leaf positions read from the MLC leaf sequence file. This is the same file normally sent from the treatment planning system to the treatment machine and specifies the position of each leaf as a function of beam on time. Beam on time is calculated in monitor units which are machine specific and quantifies the output. The model developed by Siebers *et al*

uses the same method for calculating leaf positions as does the treatment planning system. Once all the physical leaf positions are determined as a function of monitor units, particles are read from a phase space file and transported through the MLC and scored in a another phase space located in the same position.

Absolute dosimetry in Monte Carlo simulations

To correctly model radiotherapy treatment plans using the Monte Carlo method an absolute dosimetric reference frame must be established. The reference frame is a requirement if Monte Carlo dose distributions are to be clinically useful. Therefore, the clinical interpretation of a Monte Carlo dose distribution that is dosimetrically correct must be related back to a standards laboratory calibration of the modelled treatment machine. To date, Popescu *et al* [44] have developed the most detailed method for determining an absolute dosimetric reference frame to be used in Monte Carlo simulations.

The authors explain the simulation set-up in the follow manner: a phase space is scored under the fixed component modules of the linac. Then, this phase space is used as a source for simulations through the variable components, such as the jaws and the multileaf collimator. The MC simulation of the fixed components of the linac are referred to as the BEAM_A simulation, resulting in a phase space A scored above the jaws and a dose $D_{ch}^{forward}$ accumulated in the monitor chamber due to the beam entering the chamber from above. This phase space is then used as a source for a BEAM_B simulation, resulting in a phase space B scored below the jaws and a dose D_{ch}^{back} accumulated in the monitor chamber due to the particles backscattered from the jaws. The inclusion of the mirror and monitor chamber in the BEAM_B simulation allows one to obtain the backscattered dose for every simulated field, separately from the forward dose, while increasing insignificantly the CPU time per history.

With the phase space designations and monitor unit chamber dose scored for both forward and backward scattered particles, the authors establish a convention for calculating the dose as a function of monitor units. The final form of the dose-MU equation implemented by Popescu *et al* is

$$D_{xyz,abs} = D_{xyz} \frac{\left(D_{ch}^{forward} + D_{ch}^{back}\left(10 \times 10\right)\right)}{\left(D_{ch}^{forward} + D_{ch}^{back}\right)} \left(\frac{D_{xyz,abs}^{cal}}{D_{xyz}^{cal}}\right) \cdot U \tag{2.5}$$

where $D_{xyz,abs}$ is the absolute dose, D_{xyz} the relative MC dose, $\left(\frac{D_{xyz,abs}^{cal}}{D_{xyz}^{cal}}\right)$ a constant relating the relative MC dose with an absolute dose determined under standard calibration conditions and U the specified monitor units. This is a very simple formula that relates relative MC dose to an absolute dosimetric reference frame associated with standard calibration conditions. The method is easily implemented and the potential benefits to clinical MC application of great importance.

2.4 Dose uncertainty in radiation therapy

Throughout this chapter we have seen that producing precise tumour dose requires the use of high quality 3D patient image sets, conformal treatment techniques and comprehensive dose calculation algorithms. In combination, accurate 3D image data, sophisticated dose calculations and treatment methods have evolved to where dose distributions can now be truly tailored for each patient. These refinements have also been incorporated in the current ICRU convention for reporting and recording patient dose. However, defining clinical volumes and assigning margins around a CTV does not negate the presence of dose uncertainties found in all delivered treatments. In fact, as methods of delivering and reporting dose distributions have become more sophisticated, the need for accurate dose uncertainty estimates has also increased.

A multi-institution analysis of dose uncertainties in treatment planning was con-

ducted by Urie *et al* [45] in the early part of the last decade. This study reports that uncertainties associated with patient anatomy include variations in the delineation of target volumes and normal tissues, and the effects of positional uncertainties due to physiological motion and set-up reproducibility. As many others have found, these uncertainties were deemed to have a potential impact on dose to the target and could result in significantly altered tumour control. In addition, the study accounted for treatment machine related uncertainties such as daily variations in output, compensator misregistration and mechanical misalignment of treatment fields. The magnitude of these uncertainties were considered small as clinical quality assurance protocols would highlight the problem and correct for them as they develop.

In this section we will explore the most prevalent dose uncertainty sources and investigate how they have been quantified. As the literature reveals, this topic has long been the source of both theoretical and clinical research. To thoroughly cover this topic would be beyond the scope of this thesis. For this project we will focus on organ motion and patient position uncertainties, how they impact patient CT data and explore the validity of calculated dose distributions as accurate representations of delivered treatments.

2.4.1 Organ position uncertainty

To address the management of organ motion, Langen and Jones [46] studied various sources of organ motion and separated them into three categories: organ motion due to patient position changes, motion that occurs in-between fractions (inter-fraction) and that which occurs during treatment (intra-fraction)[4].

Organ motion due to positional changes are generally the result of a change in

[4]Dose fractionation is used to deposit a total tumour dose in a number of smaller fractional doses. Typically, treatment occurs over a number of weeks with one fraction delivered each day.

patient position between imaging and treatment. The magnitude of the motion is usually dependent on anatomical site and will vary from one patient to another. Inter-fractional organ motion occurs when the CTV position changes on a day-to-day level and is typically associated with organs that are adjacent to the digestive system. Another source of inter-fractional organ motion, which may affect the relative CTV position, is patient weight gain or loss. Respiratory and cardiac motions are considered the main source of intra-fractional organ motion and are prevalent throughout the thorax and abdomen. The authors [46] reviewed the literature and summarized the impact of the different organ motions, yet comment that methods used to compensate for the internal motion are often resource intensive and that implementation must be weighed against the potential risk to clinical outcomes. However, if not addressed, it is obvious that all three types of organ motion will impact treatment and the corresponding outcome.

It is well documented that patient CT data can potentially be compromised during acquisition due to organ motion. This creates a problem with the anatomic accuracy which can propagate throughout the whole planning process. Gagné and Robinson [47] showed that the presence of internal motion of various volumes produce a wide range of image distortions which were found to depend on object size and the extent of motion. The authors investigated the variation in image integrity due to motion artifacts and explored the fluctuations in regional electron density. The work clearly demonstrates that internal organ motion does produce spatial electron density variations that do not accurately represent the true distribution. The authors voice their concern for the reliability of modern radiotherapy treatment planning which is reliant on CT number fidelity.

Booth and Zavgorodni [48] modelled the dosimetric consequences of organ motion at CT imaging on radiotherapy treatment planning and quantified the results for

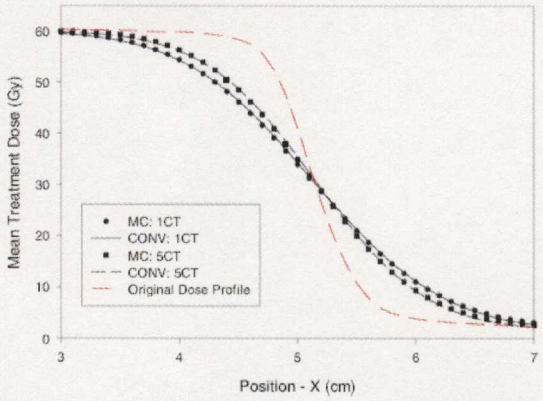

Figure 2.8: Dose profile data calculated for a single field on a static CT data set and convolved CT data sets (Taken from [48]). The data labeled original represents a dose profile associated with no organ motion. The other profiles represent the smeared profiles that result from organ motion during CT image acquisition calculated using Monte Carlo (MC) and convolution (CONV) techniques.

various simple geometric beam configurations. The authors explored how a single-field dose distribution, delivering a dose of 60 Gy in 30 fractions, was degraded by organ motion in CT imaging. It was found that incorporating CT uncertainty smeared the delivered dose. When compared to an ideal profile, the maximum discrepancy could be as much as 14 Gy. As seen in Fig. 2.8, the mean treatment dose was clearly less than the original in the upper penumbra and greater in the lower penumbra due to the simulated organ motion.

To account for internal organ motion during treatment Schaly *et al* [49] quantified dose uncertainties for a clinical prostate treatment. The authors found significant localized dose differences due to systematic voxel motion in a single fraction as well as in 15 cumulative fractions. The results of this study show that for one fraction the largest positive dose differences in the rectum, bladder and seminal vesicles were 29%, 2% and 24% respectively and for 15 cumulative fractions the dose uncertainty may be as high as 23%, 32% and 18% when compared to the planned dose. These

results show that internal motion may have a substantial impact on clinical dose distributions especially if internal volumes move during imaging and treatment.

Breath-hold techniques have been devised to minimize the affect of internal organ motion during imaging and treatment. Balter *et al* [50] explored the impact of patient breathing on CT data sets used in treatment planning and found a significant influence on organ position due to patient ventilation. In addition, the authors investigated differences in organ volume, radiation path length, and predicted treatment outcome for free-breathing and inhale/exhale breathing techniques. An important conclusion drawn from this work was that errors in physical organ volumes derived from free-breathing CT data sets can lead to significant differences in evaluation when compared to either inhale or exhale regimes. Chetty *et al* [51] found that changing from an asymmetric breathing function to one that is symmetric produced an increase in hot/cold spots of $\pm 15\%$ relative to the static plan. The authors state that this level of variation can have a substantial impact on the outcome of a planned treatment and again emphasizes the need for accurate assessment of organ motion during imaging and treatment.

2.4.2 Patient position uncertainty

A second geometric concern that leads to dose uncertainty is the reproducibility of intra and inter-fraction patient position. This has long been a source of concern for clinicians and as treatment techniques have evolved the requirements for correct patient position have increased. Goitein [52] states that it is potentially misleading to present a single dose distribution as the true dose distribution characterizing a patient's treatment. This early paper assumed that systematic rather than random positional errors were dominant and that the latter could be accounted for with increased margins. Unfortunately, accounting for random patient position, by adjusting

margin size, is in many cases unrealistic as tumours may be located near organs at risk and/or critical structures. From a therapeutic perspective, increasing normal tissue dose compromises treatment objectives and could pose substantial post treatment complications. Therefore, a generic increase in the size of the set-up margin cannot be assumed as the sole solution to patient positional uncertainty.

Recently, Craig *et al* [53] investigated the shift invariance of planned treatments and quantified the dose uncertainty in various anatomic regions. Shift invariance refers to the static nature of the CT image and planned treatment with respect to the actual patient position during treatment. Any inter-fraction patient movement essentially results in a physical shift of the planned dose distribution by the same magnitude in the opposite direction of the positioning off set. As a means of quantifying the impact of potential patient movement the authors simulated treatment by randomly sampling the patient position at each fraction. For each fraction the dose distribution was calculated with the treatment fields shifted with respect to the patient CT data. The total treatment dose distribution was calculated as the mean distribution over the total number of fractions. When compared to the initial static treatment plan the authors found dose uncertainties of 3% for a prostate plan, 17% for a lung plan and 13% for a sinus plan. In each case, the greatest dose uncertainty was located near the beam penumbra. This is consistent with other findings and generally accepted as the most problematic. One can see that making an assumption as to the static nature of a planned treatment could become problematic if the inter-fraction patient position uncertainty is not correctly taken into account.

Chapter 3

Radiobiological models

In the previous chapter we stated that the goal of radiotherapy was to completely eliminate cancerous cells within a patient tumour volume while minimizing the damage to normal tissue and critical organs. However, predicting the probability of controlling the tumour cannot be made by evaluating dose distributions alone and must incorporate the evaluation of radiobiologically derived predictive indices.

In this chapter we will survey a kinetic reaction-rate based model of cell kill and the linear quadratic formalism. Time-dose relationships and cell radiosensitivity will be explored and implications drawn from the discussion. To quantify the radiobiological effect of treatment, we will set out in detail the survival fraction based evaluative indices of equivalent uniform dose (EUD) and tumour control probability (TCP).

3.1 Introduction to radiobiological models

It is widely accepted that radiotherapy based cell kill results from DNA[1] double-strand breaks (DSB). Cell kill is generally defined as the inability to replicate in a colony forming fashion and given the complexity of biological systems has not been a simple process to decipher. A number of different models have emerged - each

[1]Deoxyribonucleic acid (DNA) is a large molecule that has a characteristic double-helix structure consisting of two strands, each made up of a sequence of nucleotides.

reproducing the characteristic shape of experimental cell survival curves with varying degrees of accuracy.

Radiotherapy DNA damage is the result of either direct radiation damage or that caused by free radicals produced in water by ionizing radiation. After ionization a water molecule is left with a net positive charge and quickly forms into a hydrogen ion H^+ and an uncharged OH radical. The OH radical is highly reactive and within a biological system interacts with essential macromolecules responsible for the survival and proper function of cells. The most important reactions are those that damage the cell DNA. The result of DNA damage is a cell's inability to replicate. This is defined as cell kill and constitutes the primary goal of radiation therapy treatment.

3.1.1 Cell kill and survival fraction

As an early model of cell kill, target theory assumed that a cell was inactivated after the DNA region responsible for maintaining reproductive abilities is damaged [54–56]. A target was defined as the DNA region with reproductive ability, and damage to this region defined as a hit. The first version of target theory assumed that only one hit was needed to inactivate the cell and is referred to as single-target, single-hit inactivation. However, this model did not produce survival curves consistent with experiment. To account for the shoulder associated with experimental survival curves, the single-target, single-hit model was generalized to a multi-target, single-hit model. Unfortunately, this extension of target theory did not predict the correct cellular response at low dose; where there is strong experimental evidence for significant cell kill [57] .

A more elegant derivation of cell survival was proposed by Chadwick and Leenhouts in their 1973 paper entitled "A Molecular Theory of Cell Survival" [58]. In this work the authors assume that cell kill is the result of double-strand breaks in the

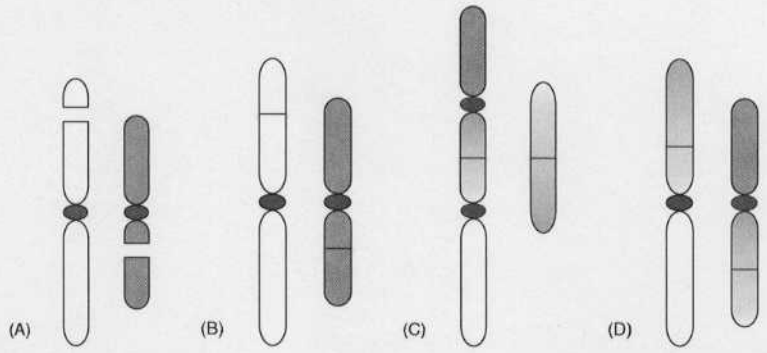

Figure 3.1: Shown above are: (A) two chromosomes each with a DSB, (B) viable restitution of each chromosome, (C) lethal binary misrepair (dicentric and acentric formation), and (D) viable binary misrepair (translocation).

DNA helix. Unlike target theory, Chadwick and Leenhouts gave a clear derivation of cell survival that includes both cell repair and an ionization dependent variable[2] [59]. However, this model has now been superseded by kinetic models of cell survival. One example is the repair-misrepair (RMR) model [60] which incorporates DNA double-strand break damage, repair and misrepair.

Reaction rate equations: repair-misrepair model

Reaction rate models [61] link dose response to the underlying production of DSB damage. Through the equations of ordinary chemical kinetics, production, repair and misrepair rates are used to characterize the average per cell DSB number produced by low LET radiation. It has been shown that the number of DSB per cell per Gy is approximately 40 [62,63]. However, only a fraction of the DSB participate in reactions which can be lethal. Figure 3.1 (A) shows two chromosomes each with one DSB. The subsequent diagrams (B), (C) and (D) show the possible ways in which the DSB can be "repaired" or "misrepaired".

[2]The dependence is characterized through the ionizing particles linear energy transfer (LET).

After production, most DSB undergo restitution (Figure 3.1 (B)), where the two free ends are rejoined to restore the overall continuity of the chromosome. However, a small portion are found to be clonogenically lethal and instead undergo illegitimate restitution. An illegitimate restitution is therefore considered a lethal lesion, rendering the cell inactive.

Two chromosomes each having one DSB may however form a lethal lesion referred to as a dicentric chromosome aberration (Figure 3.1 (C)). The formation of a dicentric leaves behind an acentric fragment and in combination destroys the clonogenic viability of the cell. In the RMR kinetic theory the formation of a dicentric is considered a lethal binary misrepair. The two DSB shown in Figure 3.1 (A) can also lead to translocation shown in Figure 3.1 (D). Translocation does involve large scale cellular rearrangements, yet does not generally alter cell survival and is therefore considered viable binary misrepair. Figure 3.2 shows the damage producing pathways where one and two-track action clearly leads to different dose response.

As outlined by Sachs *et al* [64], the RMR kinetic reaction-rate model is based on the assumption that a uniform population of many non-cycling cells are irradiated to a total dose D. The model can be applied for a dose delivered acutely or in a protracted regime and uses per-cell average rates for DSB production (δ), restitution (λ) , and a binary removal rate constant (κ) to estimate the average number of DSB as a function of time ($U(t)$). The time rate of change of the average number of DSB is given as follows [60]:

$$\frac{dU}{dt} = \delta \dot{D} - \lambda U - \kappa U^2. \tag{3.1}$$

Equation (3.1) therefore specifies the rate at which DSB are produced and removed and can be solved to give the average number of DSB as a function of time. The formation of DSB does however produce lethal lesions through illegitimate restitution

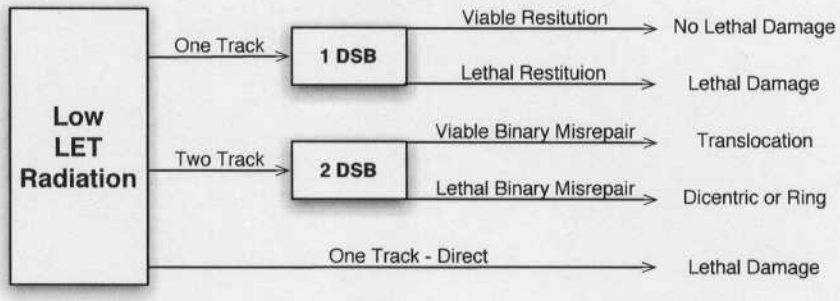

Figure 3.2: The possible pathways lethal DNA damage may occur in the RMR kinetic theory. Each track is considered an independent event that results from either primary high energy particles or all resulting secondary particles.

and lethal binary misrepair. The per-cell average rate of forming lethal lesions is taken as the sum of two terms, lethal restitution and lethal binary misrepair, such that

$$\frac{dL}{dt} = (1-\phi)\,\lambda U + \frac{\kappa}{4}U^2. \tag{3.2}$$

The constant ϕ represents the proportion of all restitutions that are viable and the $1/4$ characterizes the fraction of all binary repairs that form lethal dicentrics. The fraction of clonogenic cells that survive is then

$$\frac{dS}{dt} = -\left(\frac{dL}{dt}\right) S. \tag{3.3}$$

Since $S=1$ before radiation starts, the solution to Eq. (3.3) is

$$S\,(t) = exp\,\{-L\,(t)\}\,. \tag{3.4}$$

The Linear-quadratic (LQ) formalism relates the fraction of surviving clonogens with one and two-track action in terms of the damage coefficients α and β respectively. For a total dose D the survival fraction is given as,

$$lnS = -\alpha D - \beta G D^2, \tag{3.5}$$

where G is the generalized Lea-Catcheside dose protraction factor, and specifies how repair during any regime of irradiation decreases the effects of lethal misrepair. Therefore, the factor systematically accounts for the effects of any protracted dose delivery and is calculated as follows:

$$G = \frac{2}{D^2} \int_{-\infty}^{\infty} \dot{D}(t) \int_{-\infty}^{t} e^{-\lambda(t-t')} \dot{D}(t)\, dt'. \tag{3.6}$$

Under certain conditions the LQ formalism is found to be a solution to the RMR kinetic reaction-rate model. The two restrictions that must hold are: (1) the predominant removal of DSB must occur through restitution and (2) survival can only be determined after misrepair has run its full course. The LQ parameters α and β can then be defined from the representative model such that

$$\alpha = \delta(1 - \phi) \tag{3.7}$$

and

$$\beta = (\phi - 3/4)\frac{\kappa\delta^2}{2\lambda}. \tag{3.8}$$

Given these restrictions the dose and dose rate must be sufficiently small, that is

$$D \ll \frac{\alpha(\phi - 3/4)}{2\beta(1 - \phi)} \approx 17\,\mathrm{Gy} \tag{3.9}$$

and

$$\dot{D} \ll \lambda \frac{\alpha(\phi - 3/4)}{2\beta(1 - \phi)} \approx 8\,\mathrm{Gy} \cdot \mathrm{h}^{-1}. \tag{3.10}$$

3.1.2 Radiotherapy treatment fractionation

In the previous section we developed an equation that gives the fractional number of cells within a volume that survive a total dose D. However, most clinical radiotherapy treatments are not given at one time. In fact, dose fractionation is used to deposit a total tumour dose in a number of small fractional doses. This is done to reduce

late effects to normal tissues yet gain efficient tumour cell kill. Having the dose rate protracted in a fractionated regime corresponds to a Lea-Catcheside factor of $G=\frac{1}{n}$; where n is the number of treatment fractions.

The basis for fractionation in radiotherapy can be conceptually substantiated through the four R's of radiobiology: repair, reassortment, repopulation and reoxygenation [65]. Repair is simply the restoration of the integrity of damaged macromolecules. Reassortment is the return of cells towards a natural distribution within the cell cycle following the selective killing within certain phases of the cycle. Repopulation is the proliferation of clonogens[3], and reoxygenation the process by which surviving hypoxic clonogenic cells become better oxygenated during the period after irradiation. Fractionation helps spare normal tissues through repair and repopulation and increases tumour cell kill due to reassortment and reoxygenation [66]. Therefore, optimizing the dose fractionation schedule to accommodate the various effects becomes an important clinical concern.

The idea behind dose fractionation is to divide the total dose into a number of smaller dose fractions. Experimental data suggests that there is a consistent difference in dose response between early and late responding tissue/tumour [4]. Generally, tumours are considered "early responding" and most other tissues considered "late responding". Fowler [67] states that overall time has little effect on the total isoeffect[5] dose for late responding tissues because by definition they proliferate very little in the six weeks or so of radiotherapy, but for early reacting tissues there can be a

[3]A clonogenic cell is simply defined as a cell that proliferates at a high rate and is capable of colony formation.

[4]Response is defined here to be the end result of cell irradiation. We note the end result can be measured as cell kill, local control or early/late complications.

[5]Isoeffect is used to describe different treatment schedules that produce essentially the same biological effect.

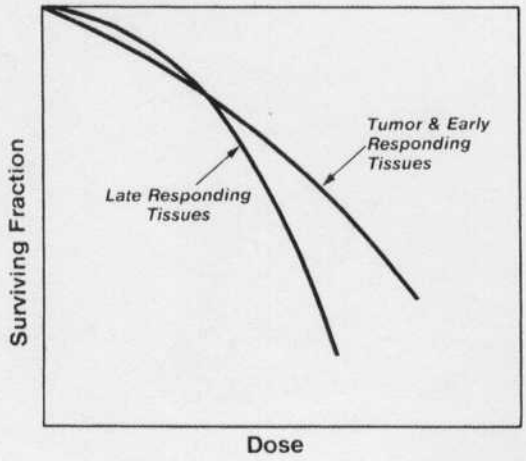

Figure 3.3: Dose response relationship for early and late responding tumour and tissue. One can see that changing the fractionation schedule will change the biological response of late responding tissue more that early responding tumours.

large effect of overall time. The author continues to explain that tumours proliferate fast even if their overall tumour volume is being reduced, and that prolonging the time between fractional dose may result in reduced cell kill but will not reduce late reactions. However, if the time between fractions is reduced such that the treatment is made continuous the original acute effects will again become problematic.

To account for treatment fractionation, Eq. (3.5) can be re-written such that

$$SF\left(d,n\right)=\exp\left\{-n\left(\alpha d+\beta d^{2}\right)\right\} \tag{3.11}$$

where the total dose delivered in n fractions is $D=nd$. The biological effective dose (BED) is used as a comparitive index between competing fractionation schemes. Defined by Fowler [68], the biological effective dose is

$$BED=nd\left(1+\frac{d}{\alpha/\beta}\right). \tag{3.12}$$

The ratio α/β represents the dose at which the cell kill contributions from the linear and quadratic components are equal: high ratios ($\backsim$ 10 Gy) indicating early respond-

Tissue/organ		α/β **ratio (Gy)**
	Early reactions	
Skin	Erythema	8.8
	Erythema	12.3
	Desquamation	11.2
Oral mucosa	Mucositis	9.3
	Mucositis	15.0
	Late reactions	
Nerve	Brachial plexopathy	2.0
	Optic neuropathy	1.6
Lung	Pneumonitis	4.0
	Lung fibrosis	3.1
	Tumours	
Head and neck		
- Larynx		14.5
- Vocal cord		13.0
- Buccal mucosa		7.2
- Tonsil		6.6
- Various		10.5

Table 3.1: Typical α/β ratios for human normal tissues and tumours.

ing tissues and/or tumours and low ratios ($\backsim$ 1.5 to 3.0 Gy) indicating late responding tissues. The α/β ratio also indicates the degree of curvature associated with a dose response curve: large values (early responding) correspond to low curvature and small values (late responding) correspond to high curvature.

Figure 3.3 shows two qualitative examples of dose response curves where the relative curvature is associated with late responding tissue and early responding tumours. Table 3.1 is a list of typical α/β ratios for human normal tissues and tumours.

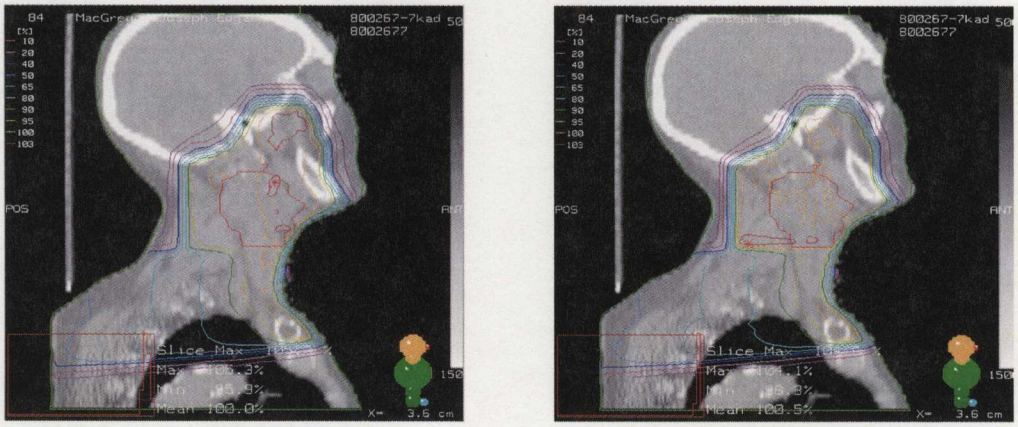

Figure 3.4: Isodose distributions generated by a commercial treatment planning system for both a CRT (left) and an IMRT (right) head-and-neck treatment plan.

3.2 Radiobiological treatment plan evaluation

The process of planning a course of radiotherapy treatment involves the choosing and arranging of radiation beams around a patient in order to provide a high dose at the site of the tumour and as low a dose as possible everywhere else [69]. This would at first seem to be a relatively simple operation given the highly refined techniques now available to clinicians. This however has not always been the case and for many years computer analysis of planned treatments was not available. After the clinical implementation of CT imaging, early computer based treatment planning systems were outfitted with evaluative tools such as the 2 and 3-dimensional isodose display as well as dose volume histogram (DVH) functionality.

A 2-dimensional isodose display (Figure 3.4) consists of an isodose distribution overlaid on a patient CT data set. This type of display shows the regional dose to the target and other structures of interest. To generate a 3-dimensional isodose distribution a set of 2D image sections are stacked side-by-side.

Dose volume histograms (Figure 3.5) are used to simplify the process of ana-

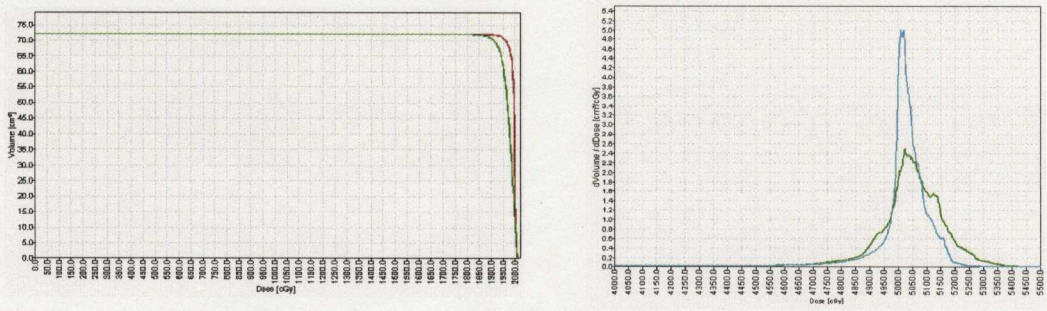

Figure 3.5: Dose volume histogram (left) and differential dose volume histogram (right) generated by a commercial treatment planning system for both a CRT and an IMRT head-and-neck dose distribution.

lyzing 3D dose distributions. A DVH represents the volume (or percentage of the total volume) that receives a dose in a given range. However, even though the DVH eliminates the subjectivity of isodose analysis it does not necessarily put forth a definitive score or ranking of planned treatments. At best, DVHs can indicate potential problems by highlighting hot and cold spots within a structure, but does obscure information about the precise geometric position of these regions [70]. In addition, the non-linear response of tissue/tumour to dose further complicates the evaluation of planned treatments.

However, if treatment plan evaluation can be made with an index that incorporates tissue/tumour dose response a more robust indicator could potentially be developed to rank planned treatments. Incorporating the cellular response to dose fluctuations, Niemierko [71] developed the concept of equivalent uniform dose (EUD)as a means of quantitatively comparing inhomogeneous dose distributions. Tumour control probability (TCP) is another evaluative index that uses survival fraction as the basis for comparison, but extends the application of Poisson statistics to incorporate the concept of "tumour control". These two evaluative indices both have radiobiological roots and will be developed in the following sections.

3.2.1 Equivalent uniform dose (EUD)

The first assumption made in the development of EUD is that an irradiated tumour is composed of a large number of independent clonogens, and that random cell kill is correctly described using the concept of survival fraction. One can consider any two *different* dose distributions as equivalent if the corresponding survival fractions are equal. Using this statement, Niemierko defined EUD in the following manner: For any dose distribution, the corresponding Equivalent Uniform Dose is the dose (in Gy), which, when distributed uniformly across the target volume, causes the survival of the same number of clonogens.

We have seen that the fraction of surviving clonogens in any arbitrary volume V, irradiated with a homogeneously distributed dose D, is calculated using Eq. (3.5). If the total volume is divided into a set of sub-volumes, each with a uniform cell distribution, the effective survival fraction for the whole volume can be calculated as a weighted average. The mean survival fraction, taken over all N irradiated sub-volumes, is calculated such that

$$\overline{SF}\left(\{D_k\}\right) = \sum_{k=1}^{M} v_k \cdot SF\left(D_k\right) \tag{3.13}$$

where v_k is the partial volume corresponding to the dose D_k. $\overline{SF}\left(\{D_k\}\right)$ can be calculated, when all partial volume elements are identical, such that

$$\overline{SF}\left(\{D_k\}\right) = \frac{1}{M} \sum_{k=1}^{M} SF\left(D_k\right). \tag{3.14}$$

Given a spatially non-uniform dose distribution, one can equate the same number of surviving clonogens with a uniform target dose, defined as EUD, such that

$$SF\left(EUD\right) = \overline{SF}\left(\{D_k\}\right). \tag{3.15}$$

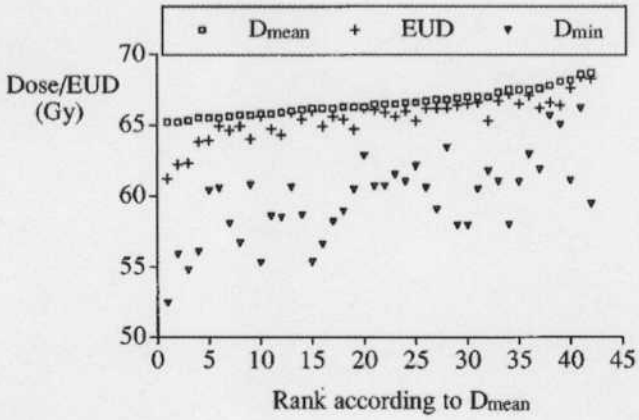

Figure 3.6: Taken from the original EUD paper by Niemierko [71], this graph shows a number of example plans evaluated using the EUD formalism. Compared to a mean and/or minimum dose evaluation only, EUD evaluation incorporates the entire spatial dose distribution in a manner more suitable for evaluation of competing treatment plans.

Using Eqs. (3.5), (3.11) and (3.15) we find that

$$EUD^2 + \frac{n\alpha}{\beta} EUD + \frac{n}{\beta} ln\left\{\overline{SF}\left(\{D_i\}\right)\right\} = 0 \tag{3.16}$$

which is a quadratic function of EUD. Therefore, an expression for EUD is obtained such that,

$$EUD = \frac{1}{2}\sqrt{\frac{\alpha^2 n^2}{\beta^2} - \frac{4n}{\beta} ln\left\{\overline{SF}\left(\{D_k\}\right)\right\}} - \frac{n\alpha}{2\beta}, \tag{3.17}$$

where the mean survival fraction is calculated over all N dose points within the volume.

Given the simplicity of EUD it has become a common evaluative index used to determine the quality of clinical treatment plans. However, there are a number of characteristics associated with EUD that must be understood before correct interpretation of a treatment plan can be made. The first characteristic associated with EUD is that for any given target volume, EUD is always greater than or equal to the minimum dose and less than or equal to the mean dose. The only case where

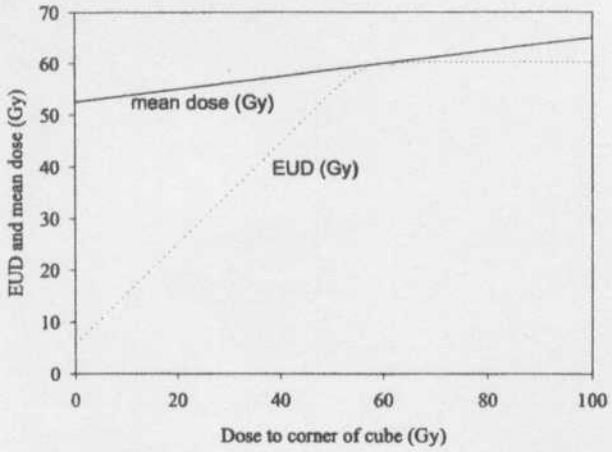

Figure 3.7: EUD and the mean dose calculated when one volume element receives a low dose [72]. One can see that EUD responds to the low dose in a more dramatic fashion when compared to the mean.

EUD is equal to the mean and minimum dose is when the volume is uniformly irradiated. Niemierko reports that for a set of clinical treatment plans, the range of minimum doses is much larger than the range of mean doses or EUDs, and that for each planned treatment the minimum dose may correspond to just one or two volume elements within the target.

Figure 3.6 is taken from the original EUD paper by Niemierko. For many of the planned treatments the difference between the mean dose and minimum dose is relatively large, yet for the same plan EUD is usually very close to the mean. Therefore, when evaluating competing dose distributions EUD may provide a better quantitative estimate of dose uniformity when compared to evaluation based on the mean and minimum dose.

In comparison to the change in mean dose, Halloway *et al* [72] explored the effect that small, low dose, volumes have on EUD. Given the non-linear response of survival fraction to dose, it is expected that EUD will demonstrate a dramatic change

in comparison to the mean dose given an extreme low dose volume element. As an example of this, the authors simulated a cubic tumour with on corner receiving a varying dose where the remaining volume received a constant dose of 60 Gy. Figure 3.7 shows that in comparison to the mean dose, EUD reveals that cold spots can have a large impact on overall cell kill but hot spots in this case greater than 60 Gy do not.

3.2.2 Tumor control probability (TCP)

In deriving the LQ formalism cellular radiation damage was considered a random event where after a given time a cell either survives with complete functionality (restitution or translocation) or is damaged leaving it unable to proliferate (lethal damage or dicentric formation). The concept of tumour control probability evolves from the assumption that control is only achieved if no clonogens survive. Let N be the average number of cells that survive treatment and n be the actual number of cells that survive. Using Poisson statistics to quantify the probabilistic effect of an event that can produce only two possible outcomes, the probability that n cells survive treatment is given as

$$P(n) = \frac{N^n}{n!} e^{-N}. \tag{3.18}$$

If all clonogenic cells are damaged leaving them unable to proliferate, that is $n = 0$, Eq.(3.18) gives

$$P(0) = e^{-N} \tag{3.19}$$

and is defined as the tumour control probability. Again, N is the expected number of cells that survive treatment and, therefore, can be calculated using the survival fraction equation. In general, TCP is given as

$$TCP(D) = exp\{-N_0 \cdot SF(D)\} \tag{3.20}$$

where D is the total treatment dose and N_0 is the initial number of clonogenic cells. From Eq. (3.20) one can see that TCP values range between 0 and 1; where complete tumour control results in a score of TCP = 1.

Webb and Nahum [73] extended this model to include inhomogeneous distributions of dose and clonogenic cell density. Let us divide the total volume into sufficiently small volume elements v_k such that the dose D_k and cell density ρ_k for each volume element are considered uniform. The product $\rho_k v_k$ gives the number of clonogens in each volume element. Tumour control for the total volume is calculated such that,

$$TCP = \prod_{k=1}^{K} exp\left\{-\rho_k v_k \left(\alpha_k D_k + \frac{\beta_k}{n} D_k^2\right)\right\}, \tag{3.21}$$

where the radiosensitivity has also been specified for each volume element .

From Eq. (3.21) one can see that complete tumour control is only achieved if each $TCP_k = 1$. The volume element dose dependence of TCP leads naturally to the uniform-dose theorem presented by Webb *et al* [74]. The authors prove that the physical dose distribution that maximizes TCP for a fixed total dose is a uniform dose distribution, but state, that the proof in no way implies that either such a distribution can be realized in practice or that it is necessarily the best planning outcome given other treatment planning constraints.

Niemierko and Goitein [75] extend the TCP concept to incorporate a tumour that is not uniformly irradiated. As with Webb and Nahum the authors state the goal of the model is not to provide an accurate assessment of the absolute TCP, but, to estimate the relative difference in TCP which might reasonably be predicted between two not too dissimilar planned treatments. The convention proposed by Niemierko and Goitein is to calculate TCP for an individual patient (indicated by

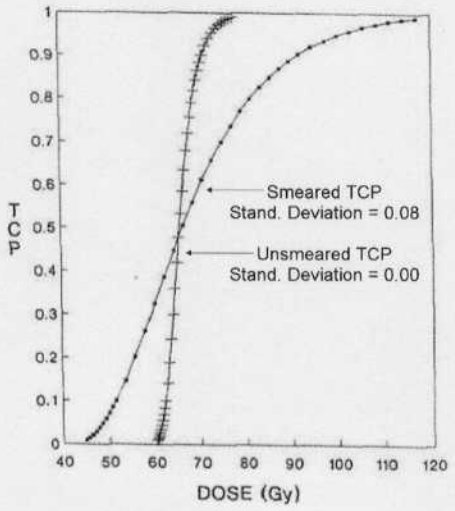

Figure 3.8: Taken from Webb and Nahum [73], this plot shows TCP as a function of dose for an unsmeared constant α and α smeared over a population average: $\alpha = 0.35$ Gy^{-1} with a standard deviation of 0.0 and 0.08 Gy^{-1} for the unsmeared and smeared cases respectively.

the *ind* subscript), as a function of the mean inter-voxel survival fraction, is

$$TCP_{ind} = exp\left\{-\rho V \cdot \sum_{i=1}^{N} v_i \cdot \overline{SF}_i\right\}. \tag{3.22}$$

$\overline{SF}_i$ is an average survival fraction that incorporates an intra-tumour cell radiosensitivity variation. However, if we neglect the variation in the intra-voxel radiosensitivity and focus on the averaging of SF over the tumour volume, Eq. (3.22) can be written as,

$$TCP = exp\left\{-N_0 \cdot \sum_{i=1}^{N} v_i \cdot SF_i\right\}, \tag{3.23}$$

where we have removed the *ind* subscript for simplicity. Using Eqs. (3.13) and (3.15), we find that TCP calculated using Eq. (3.23) is simply TCP as a function of EUD and can be written as

$$TCP = exp\left\{-\rho V \cdot SF\left(EUD\right)\right\}. \tag{3.24}$$

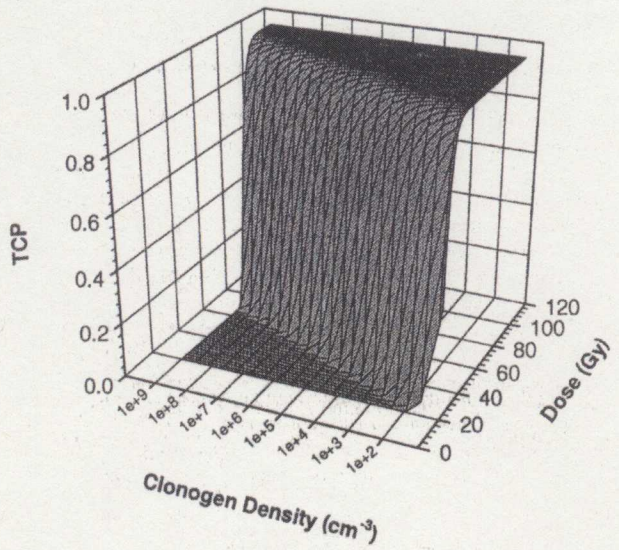

Figure 3.9: Taken from Ebert and Hoban [78], this graph shows the distribution of TCP as a function of dose and cell density for a constant volume of 100 cm^3. One can see from that for a constant integral dose, TCP changes significantly for varying cell densities.

In general, theoretical and actual experimental TCP curves are different. One explanation for this is that curves derived from actual experimental treatment outcomes are indicative of the population as a whole and do not reflect any one particular tumour. To account for this population heterogeneity the radiosensitivity can be specified as a distribution and from that TCP curves calculated as shown in Fig. 3.8. Webb and Nahum showed that good clinical TCP curves could be matched to experimental data compiled by Brenner [76] by specifying α as a Gaussian distribution with a mean of 0.35 Gy^{-1} and a standard deviation of 0.08 Gy^{-1}. However, variations in patient specific cell sensitivity is hypothesized to be small and therefore will produce TCP curves closer to the steeper theoretical case [77].

Incorporated in the exponential expression for TCP is the clonogenic cell density. Ebert and Hoban [78] investigated TCP characteristics for tumours with a heteroge-

neous distribution of cell density. Figure 3.9 represents the distribution of TCP as a function of dose and cell density for a constant volume of 100 cm^3. One can see that for a constant total dose, TCP changes significantly for varying cell densities. The authors state that in order to prescribe a dose distribution throughout a tumour which maximizes the tumour control probability, knowledge of the cell density and radiosensitivity within the tumour is required. This however should not be used as a treatment objective but is simply the optimal condition for a fixed tumour dose.

3.3 Incorporating dose uncertainty into radiobiological plan evaluation

A number of investigators [79, 80] have explored the global effects of Monte Carlo uncertainty on calculated dose distributions and dose volume histograms, whereas others have specifically investigated the effects of Monte Carlo uncertainty on radiobiological predictive indices [81]. It has been shown that an increase in Monte Carlo dose uncertainty broadens the dose volume histogram which results in an underestimate of the tumour control probability. It is generally agreed that an average dose uncertainty of 2% will not noticeably change TCP and if the uncertainty in the radiosensitivity parameters increases, the relative impact of Monte Carlo uncertainty will be reduced. However, each of these investigations used radiobiological evaluative methods without explicitly incorporating the voxel dose uncertainty. The studies only looked at how the dose uncertainty impacted the evaluation of the whole dose distribution. In none of the studies was there an explicit incorporation of the voxel dose uncertainty into the evaluation. Developing an evaluative index that incorporates the voxel dose uncertainty explicitly would present a more useful evaluative tool that could potentially be used to correct for the statistical degradation.

As one approach to incorporating voxel dose uncertainty into radiobiological treatment plan evaluation, Zavgorodni [82] investigated how inter-fraction dose variations could potentially impact the biological equivalent dose. An analytic expression was derived for BED that incorporated the effects of inter-fraction dose fluctuations given that the total delivered dose was fixed. Zavgorodni showed that as the inter-fraction dose variance increases the biological effect increases linearly. It was also shown that the effect was more prevalent for normal tissue than tumours which is a result of the lower α/β ratio for normal tissue.

Although useful, BED is not used directly in routine clinical treatment plan evaluation and will therefore find limited application. Although there has been some work done to include dose uncertainties into the evaluation of TCP there has however been little work done to explicitly incorporate dose uncertainty into EUD treatment plan evaluation and therefore will form the focus of this investigation.

Chapter 4

Equivalent stochastic dose

4.1 Introduction

As discussed previously, there are a number of inherent uncertainties associated with simulated and delivered radiotherapy dose distributions. Two broad categorizations can be made to separate dose uncertainties that result from the planning process with those associated with treatment delivery. Treatment planning dose uncertainties can result from the well documented limitations in patient CT data sets, the assumed static nature of clinical treatment plans, and the statistical uncertainty inherent in Monte Carlo dose calculations. Uncertainties associated with treatment delivery are essentially geometric and mainly due to patient set-up errors as well as internal organ motion and tumour size variations. Quantifying the impact of dose uncertainties is fundamental to quality patient care and has become an important issue in current radiotherapy research.

Many have investigated the application and potential limitations associated with using convolution techniques to model the impact of patient position and organ motion uncertainties on planned dose distributions. To account for inter-fraction patient set-up fluctuations, Leong [83] applied the convolution technique to beam profile data and produced modified dose profiles. The modified profiles were then used to calculate

clinical isodose distributions. Lujan *et al* [84] quantified patient set-up uncertainties by calculating the standard deviation between convolved and static dose distributions. The average dose was calculated by convolving the planned dose distribution with a 3D Gaussian probability density function. This method assumed rigid body motion, no change in external patient contour, no organ deformation and an infinite number of small fractions.

Clinically, the most problematic assumption made by Lujan *et al* was the infinite number of fractions. To access the validity of using a finite number of treatment fractions in convolution techniques, McCarter and Beckham [86] quantified the difference between convolved and simulated dose distributions that modelled patient set-up uncertainties over a discrete number of treatment fractions. It was found that for as few as 15 fractions, convolving the static plan with a Gaussian impulse response function more accurately described the delivered dose distribution. The authors state that if the number of fractions is greater than 15 the convolution method may be a reliable technique for describing the dose actually delivered to a patient.

Both Rudat *et al* [87] and Song *et al* [88] model the influence of patient positioning errors as a convolution between the 3D dose distribution and an error function describing random geometric set-up uncertainties. To account for rotational and translation set-up uncertainties Bel *et al* [89] derived approximate margin sizes for prostate treatments by convolving the static dose distribution with Gaussian distributed probability density functions.

To extend the convolution technique to Monte Carlo calculated dose distributions, Beckham *et al* [90] investigated the difference between fluence convolution and dose matrix convolution. The fluence convolution method consists of convolving a Monte Carlo generated incident photon fluence with a 2-dimensional Gaussian probability density function. The authors state that fluence-convolution effectively decouples the

treatment beam from the patient, and more closely resembles the reality of particle fluence distributions for many individual beam-patient configurations. As an extension of this work, Stapleton *et al* [91] implemented the fluence convolution method to include Monte Carlo calculated dynamic IMRT treatment plans.

Researchers have also explored the effects a Monte Carlo uncertainty on calculated dose distributions and dose volume histograms (DVHs). In fact, there have been a number of specific investigations into the effects of Monte Carlo uncertainty on radiobiological predictive indices as outlined at the end of the previous chapter.

In this chapter, the impact of dose uncertainty on survival fraction will be investigated. We refer to all dose uncertainties that arise from either calculation or delivery as stochastic. To account for voxel dose uncertainty, we calculate the expected survival fraction for the random dose deposition and associate this with an *equivalent stochastic dose* (ESD). Mathematically, the expression for the expected survival fraction is identical to that used by Niemierko in defining EUD (Section 3.2.1). For a probability density function $f(D)$, that represents the probabilistic voxel dose, SF(ESD) can be calculated by convolving $SF(D)$ with $f(D)$. In the case where the probability density function follows a Gaussian distribution an analytic expression is derived for SF(ESD). To account for both physical and statistical dose uncertainties associated with clinical dose distributions the analytic expression is extended to subsume both intra-voxel dose uncertainty as well as inter-voxel mean dose fluctuations[1].

[1]Intra will be taken to mean "within one voxel" and inter to mean "between any two or more voxels".

4.2 Defining physical and statistical dose uncertainty

Throughout this work we assume that all dose uncertainties are the result of a random process depositing a mean dose D in a volume element V. Given the assumed random nature of the voxel dose each D has an associated uncertainty σD. In this work we make a distinction between physical and statistical dose uncertainties. Physical dose uncertainty is defined to be any physically discernible dose uncertainty that results from systematic and/or random errors in treatment planning and/or delivery. Statistical dose uncertainty is associated exclusively with dose distributions calculated using Monte Carlo electron-photon transport algorithms[2]. We emphasis that statistical dose uncertainty as defined here must be viewed as artificial with respect to the actual delivered dose.

In addition to discriminating between physical and statistical dose uncertainty a distinction is made between physical and probabilistic dose heterogeneity. Physical dose heterogeneity is defined to be the result of any systematic inter-voxel dose non-uniformity, whereas probabilistic dose heterogeneity is defined to be the result of both physical and statistical dose uncertainties. Figure 4.1 represents a subset of voxels located within a spatially uniform dose distribution. One can see that the voxel dose uncertainty creates a probabilistic dose heterogeneity characterized by the inter-voxel mean dose fluctuation.

[2]One example of a dose distribution calculated using the Monte Carlo method would be an EGSnrc based BEAMnrc-DOSXYZnrc simulation.

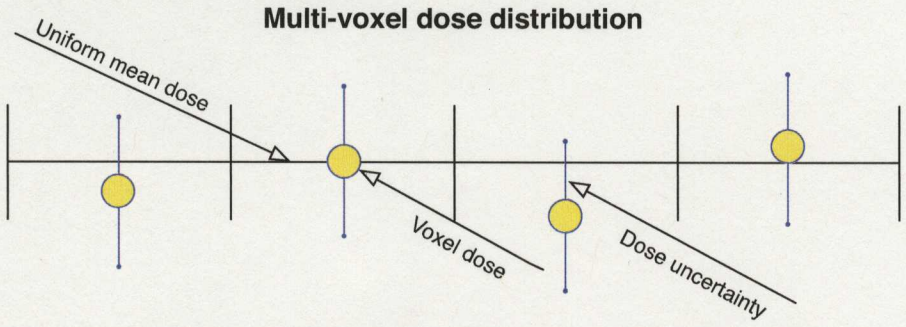

Figure 4.1: A subset of voxels in a spatially uniform multi-voxel dose distribution where each voxel dose has an associated uncertainty. As a result of the dose uncertainty there is a probabilistic inter-voxel dose heterogeneity generated within the distribution.

4.3 Calculating the expected survival fraction for a single voxel

A discrete random variable is defined as any variable that can only assume values from a discrete set $\{x_1, x_2, ..., x_N\}$. The expectation value of any discrete random variable is calculated such that

$$E(X) = \sum_{i=1}^{N} x_i p_i \tag{4.1}$$

where p_i represents the probability that x_i occurs, and must satisfy

$$p_i \geq 0 \tag{4.2}$$

and

$$\sum_{i=1}^{N} p_i = 1. \tag{4.3}$$

However, if the probability of each x_i is the same, we find that

$$p_i = \frac{1}{N}. \tag{4.4}$$

Therefore, the expected value for a discrete random variable, where each element of the set $\{x_1, x_2, ..., x_N\}$ has an equal probability of occurrence, is calculated such that

$$E(X) = \frac{1}{N}\sum_{i=1}^{N} x_i. \tag{4.5}$$

Now, let us use these very simple characteristics of a discrete random variable to calculate the expected survival fraction for a voxel dose that has an associated uncertainty. Consider a volume element V, where the total dose delivered is the result of some random process. We assume the dose in each voxel is deposited through a series of independent events and can only take discrete values characterized by the set $\{D_i\}$. Given the random nature of the dose deposited in V, we calculate the expected survival fraction as

$$\overline{SF}(\{D_i\}) = \frac{1}{N}\sum_{i=1}^{N} SF(D_i) \tag{4.6}$$

where N is the number of discrete D_i from the set $\{D_i\}$. For each D_i we calculate the survival fraction, in the simplest case, as

$$SF(D_i) = \exp\left\{-\alpha D_i - \frac{\beta}{n} D_i^2\right\} \tag{4.7}$$

where α and β are radiosensitivity parameters and n the number of fractions in the planned treatment[3].

We define the *equivalent stochastic dose* as the dose to a voxel that results in a survival fraction that is equivalent to the expected survival fraction calculated from the set $\{D_i\}$. SF(ESD) can therefore be equated with Eq. (4.6) such that,

$$SF(ESD) = \overline{SF}(\{D_i\}). \tag{4.8}$$

Analogous to the derivation of EUD (Eqs. (3.13) to (3.17)) an expression for ESD is

[3]Cell proliferation is not considered for the sake of simplicity.

obtained such that,

$$ESD = \frac{1}{2}\sqrt{\frac{\alpha^2 n^2}{\beta^2} - \frac{4n}{\beta} ln\left\{\overline{SF}\left(\{D_i\}\right)\right\}} - \frac{n\alpha}{2\beta}. \tag{4.9}$$

In defining *equivalent stochastic dose* the dose to a voxel was assumed to be a discrete random variable; where each D_i was assumed to have an equal probability of occurrence. It must be noted that this is not strictly the case. In general, the probabilistic dose to a voxel will be a continuous random variable distributed according to some function. Assuming the D_i's were discrete and equally probable helped demonstrate a mathematical equivalence between EUD and ESD. The connection was made so that we could use many of the known characteristics associated with EUD in our evaluation of ESD.

Let us now assume the probabilistic dose to a voxel is a continuous random variable distributed according to a probability density function. The expectation value of a continuous random variable is calculated such that

$$E\left(X\right) = \int_a^b xp\left(x\right)dx \tag{4.10}$$

where $p\left(x\right)$ represents the probability density of the random variable over the interval $a \leq X \leq b$. The distribution $p\left(x\right)$ must satisfy

$$p\left(x\right) \geq 0 \tag{4.11}$$

and

$$\int_a^b p\left(x\right)\, dx = 1. \tag{4.12}$$

Let us now choose any continuous function $h\left(x\right)$ and define a new continuous random variable such that $Y = h\left(X\right)$. The expectation value of the continuous random function is

$$E\left(h\left(X\right)\right) = \int_a^b h\left(x\right)p\left(x\right)dx \tag{4.13}$$

where in general $E(h(X)) \neq h(E(X))$ [92].

For the case where the probability density function is given as $p(x - x')$ the expectation value can be calculated as a convolution; where the convolution of any two functions g and h is defined as

$$(g * h)(x) = \int_{-\infty}^{\infty} g(x')\, h(x - x')\, dx'. \tag{4.14}$$

The convolution given above is often written as $g(x) \otimes h(x)$ [93] where the shift in $h(x)$ is assumed.

We now calculate the expected survival fraction as a convolution between SF(D) and a function that characterizes the probabilistic dose to the voxel. This approach is consistent with that of Leong, Lujan *et al*, Rudat *et al*, Song *et al* and Bel *et al*; where the influence of patient positioning errors were taken into account using convolution techniques. Our approach is also consistent with Roberts and Hendry's [94] calculation of an average TCP as a convolution. The authors show that a convolution can be used to account for inter-patient variations in clonogen number, cell radiosensitivity and repopulation rate in the evaluation of an average TCP.

Let us follow this convention and assume the mean voxel dose to be a continuos random variable distributed according to a probability density function $f_v(D)$. The expected survival fraction is calculated by convolving Eq. (4.7) with the probability density function $f_v(D)$. That is,

$$\overline{SF}(D, \sigma) = \int_{0}^{\infty} SF(D')\, f_v(D - D', \sigma)\, dD' \tag{4.15}$$

where the distribution $f_v(D)$ is now uniquely defined as a function of the mean voxel dose and the standard deviation. This results in a *smeared* survival fraction which can be equated with a survival fraction calculated as a function of ESD, that is,

$$SF(ESD) = \overline{SF}(D, \sigma). \tag{4.16}$$

For notational simplicity we write Eq. (4.16) as

$$SF\left(ESD\right) = SF\left(D\right) \otimes f_v\left(D\right) \tag{4.17}$$

and calculate ESD as before,

$$ESD = \frac{1}{2}\sqrt{\frac{\alpha^2 n^2}{\beta^2} - \frac{4n}{\beta} ln\left\{\overline{SF}\left(D,\sigma\right)\right\}} - \frac{n\alpha}{2\beta}. \tag{4.18}$$

4.4 Calculating the expected survival fraction for a multi-voxel dose distribution

So far we have only considered SF(ESD) for a single voxel and have shown this to be mathematically equivalent to convoluting $SF\left(D\right)$ with $f_v\left(D\right)$. Now, let us look at a multi-voxel dose distribution where the dose in each voxel has an associated uncertainty. Given the assumed random nature associated with the deposited dose, each voxel dose will converge to a different mean value D_k. Using Eq. (4.17) an ESD_k can be calculated for each voxel. This produces a distribution of ESD_k as seen in Fig. 4.2. The expected survival fraction for the multi-voxel domain can then be expressed as,

$$\overline{SF}\left(\{ESD_k\}\right) = \frac{1}{M}\sum_{k=1}^{M} SF\left(ESD_k\right), \tag{4.19}$$

where M is the number of voxels in the distribution. When the number of voxels is large, calculating the expected survival fraction again results in a convolution.

The definition of ESD, given in Eq. (4.17), is now amended to subsume both the voxel dose uncertainty as well as the inter-voxel ESD fluctuation by including the probability density function $f_m\left(D\right)$ which represents the distribution of ESD_k.

Equation (4.17) has to this point reflected the probabilistic nature of the intra-voxel dose. Now, survival fraction has to be further convolved with $f_m\left(D\right)$ to reflect the variability in the inter-voxel mean dose. As a result, the equivalent stochastic dose,

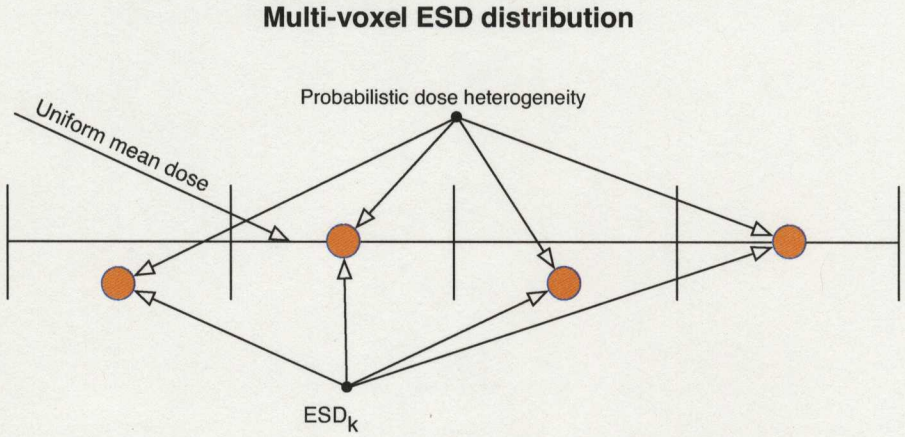

Figure 4.2: A subset of voxels in a spatially uniform multi-voxel dose distribution subject to mean voxel dose fluctuations. As a result the distribution of ESD_k will produce a probabilistic dose heterogeneity as defined in this work.

for a spatially uniform multi-voxel dose distribution, subject to voxel dose uncertainty becomes

$$SF\left(ESD\right) = SF\left(D\right) \otimes f_v\left(D\right) \otimes f_m\left(D\right). \tag{4.20}$$

This reveals that intra-voxel dose uncertainty does produce a probabilistic inter-voxel dose heterogeneity which can be accounted for in a similar fashion to a physical dose heterogeneity (Eq. (A.1)).

Given a dose distribution that is not spatially uniform, another distribution representing the spatial dose heterogeneity can be included in Eq. (4.20). We define an *equivalent uniform stochastic dose* (EUSD) that encompasses voxel dose uncertainty, inter-voxel noise as well as a spatial dose non-uniformity. The survival fraction associated with EUSD, for a known spatial dose distribution, is then

$$SF\left(EUSD\right) = SF\left(D\right) \otimes f_v\left(D\right) \otimes f_m\left(D\right) \otimes g\left(D\right), \tag{4.21}$$

where $g\left(D\right)$ represents the distribution of dose about a mean value. The distribution

is easily derived from the differential dose volume histogram (dDVH) generated by commercial treatment planning systems.

4.5 An analytic expression for calculating the expected survival fraction

Let us explicitly calculate a specific case of Eq. (4.17) where the probability density function is assumed Gaussian. Statistical dose uncertainty has been associated with Monte Carlo calculations only and therefore using a Gaussian distribution follows naturally assuming the sample size is large. Lujan *et al* verified using Gaussian distributions to model patient set-up uncertainties by fitting Gaussian distributions to clinical data along the anterior-posterior, left-right, and superior-inferior axes. Cho *et al* [95] also verified using Gaussian distributions to model preparation and execution errors, yet does note that non-normally distributed displacement errors, such as the periodic breathing motion where the time at exhalation is greater than at inhalation, have also been studied.

Let us write a Gaussian distribution with a mean dose D as,

$$f\left(D - D'; \sigma^2\right) = \frac{1}{\sqrt{2\pi}\sigma} \exp\left\{-\frac{(D - D')^2}{2\sigma^2}\right\}, \tag{4.22}$$

where D' extends over the range $0 \leq D' \leq \infty$ and σ is the standard deviation in the probabilistic voxel dose. If we now substitute Eqs. (4.7) and (4.22) into Eq. (4.17), the survival fraction associated with the *equivalent stochastic dose* becomes

$$SF(ESD) = \frac{1}{\sqrt{2\pi}\sigma} \int \exp\left\{-\alpha D' - \frac{\beta}{n} D'^2 - \frac{(D - D')^2}{2\sigma^2}\right\} dD'. \tag{4.23}$$

One can see that the exponential term is quadratic in D', therefore we can write the

integral as

$$SF(ESD) = \frac{1}{\sqrt{2\pi}\sigma} \int \exp\left\{ -\left[D'^2 \left(\frac{\beta}{n} + \frac{1}{2\sigma^2} \right) + D' \left(\alpha - \frac{D}{\sigma^2} \right) + \frac{D^2}{2\sigma^2} \right] \right\} dD'. \tag{4.24}$$

Upon integration over all positive dose values ($0 \leq D' \leq \infty$) an analytic solution is found, giving

$$SF(ESD) = \frac{1}{2^{3/2}\sigma} \left(\frac{\beta}{n} + \frac{1}{2\sigma^2} \right)^{-1/2} \left(1 - erf \left(\frac{\alpha - \frac{D}{\sigma^2}}{2\sqrt{\frac{\beta}{n} + \frac{1}{2\sigma^2}}} \right) \right)$$

$$\exp\left\{ \frac{\left(\left(\alpha - \frac{D}{\sigma^2} \right)^2 - 4\left(\frac{\beta}{n} + \frac{1}{2\sigma^2} \right) \frac{D^2}{2\sigma^2} \right)}{4\left(\frac{\beta}{n} + \frac{1}{2\sigma^2} \right)} \right\}, \tag{4.25}$$

where SF(ESD) can now be calculated knowing only the mean voxel dose and associated standard deviation. ESD can be calculated by substituting Eq. (4.25) into Eq. (4.18) as the expected survival fraction.

It is well known that the convolution of any number of independent Gaussian distributions is itself Gaussian. Therefore, Eq. (4.25) can be applied to encompass not only a random voxel dose but can be made to account for a multi-voxel dose distribution that is subject to inter-voxel noise as well as a spatial non-uniformity where each is assumed independent. A set of convolved independent Gaussian distributions, with one centered about a mean dose D and the others centered about zero, can be represented by modifying Eq. (4.22) such that

$$f\left(D - D'; \sum \sigma_k^2 \right) = \frac{1}{\sqrt{2\pi \sum \sigma_k^2}} \exp\left\{ -\frac{(D - D')^2}{2\sum \sigma_k^2} \right\}. \tag{4.26}$$

Equation (4.25) can be used to account for both intra and inter-voxel mean dose fluctuations as well as a specific dose non-uniformity. An example of this would be the case where $f_v(D)$, $f_m(D)$ and $g(D)$ of Eq. (4.21) are independent and each take the form of a Gaussian. However, if the distributions $f_v(D)$, $f_m(D)$ and $g(D)$ are

not Gaussian the convolution can be performed numerically using the appropriate probability density functions.

4.6 Incorporating ESD into the calculation of TCP

In the previous sections we made a clear distinction between the interpretation of ESD and EUD. It was shown that the ESD formalism may be used to quantify the radiobiological impact of dose uncertainty on treatment plan evaluations knowing only $D \pm \sigma D$ for each voxel. Incorporating voxel dose uncertainty into the calculation of TCP then becomes a natural extension of the initial ESD concept.

The tumour control probability for each voxel, calculated as a function of the expected survival fraction, can be written as

$$TCP\left(\overline{SF_k}\left(\{D_i\}\right)\right) = exp\left\{-N_0\left(\frac{1}{N}\sum_{i=1}^{N} SF\left(D_i\right)\right)\right\} \tag{4.27}$$

where k is the voxel index and N_0 is the initial number of clonogenic cells in each voxel. Using the definition of SF(ESD), given in Eq. (4.6), we can write Eq. (4.27) such that

$$TCP\left(SF_k\left(ESD\right)\right) = TCP\left(\overline{SF_k}\left(\{D_i\}\right)\right). \tag{4.28}$$

For notational simplicity we make the following definition

$$TCP_k\left(ESD\right) = TCP\left(SF_k\left(ESD\right)\right). \tag{4.29}$$

Let us investigate TCP_k(ESD) further by substituting Eq. (4.6) into the second half of Eq. (4.27). The inclusion of the dose uncertainty in the form of an average

survival fraction then gives

$$\begin{aligned} TCP_k\left(\overline{SF}\left(\{D_i\}\right)\right) &= exp\left\{-N_0\left(\frac{1}{N}\sum_{i=1}^{N} SF\left(D_i\right)\right)\right\} \\ &= \left(exp\left\{-N_0\sum_{i=1}^{N} SF\left(D_i\right)\right\}\right)^{1/N} \\ &= \left(\prod_{i=1}^{N} exp\left\{-N_0 \cdot SF\left(D_i\right)\right\}\right)^{1/N} \end{aligned} \tag{4.30}$$

which is the equation for the geometric mean of $\mathrm{TCP}_k\left(\{D_i\}\right)$.

Given the probabilistic dose distribution to the voxel, calculating TCP as a function of the mean expected survival fraction is analogous to the calculation of TCP_{ind} proposed by Niemierko and Goitein [75] to account for a non-uniform, multi-voxel dose distribution. The authors define TCP_{ind} as the tumour control probability of the *individual*, such that

$$TCP_{ind} = exp\left\{-\rho V \cdot \sum_{i=1}^{N}\left(v_i \cdot \overline{SF}_i\right)\right\} \tag{4.31}$$

where i is the voxel index and $\overline{SF_i}$ is an average survival fraction that takes into account cell radiosensitivity variations within each voxel. Calculating $\overline{SF}_i$ to account for the cell radiosensitivity variations adds a layer of detail not directly associated with our incorporation of dose uncertainty and therefore will be treated as a special case of SF_i. Upon inspection, one can see that the mean survival fraction calculated in Eq. (4.31) is just SF(EUD) as outlined in Section 3.2.2. Therefore, TCP_{ind} is simply TCP(EUD). This is analogous to our proposed TCP_k(ESD) given a probabilistic voxel dose distribution - as opposed to the spatial non-uniformity used in defining EUD. Again we see that accounting for spatial and probabilistic dose heterogeneity can be made using similar analytic techniques, yet note that an emphasis must be placed on correct interpretation.

For a multi-voxel dose distribution the convention for calculating TCP over the whole volume requires a decision as to which model will be used. We have seen that Niemierko and Goitein propose using the mean survival fraction as outlined in Eq. (4.31), yet the authors do caution that the purpose of the model is not to provide an accurate assessment of the absolute TCP, but to estimate the relative difference between two not too dissimilar situations.

In contrast to the method of calculating TCP from the mean expected survival fraction, Webb and Nahum propose calculating TCP on a voxel-by-voxel basis with the total tumour control calculated as the product of all TCP_k over the tumour volume (Eq. (3.21)). For the purpose of this work we will adopt the convention proposed by Niemierko and Goitein as a means of calculating TCP for a multi-voxel dose distribution. However, we do not advocate that the model used here is superior to that proposed by Webb and Nahum and note that incorporating $\mathrm{TCP}_k(\mathrm{ESD})$ into the calculation of TCP as a product over all TCP_k could still serve as an evaluative means of assessing dose uncertainty.

To extend our analysis of dose uncertainty to incorporate inter-voxel mean dose fluctuations, as well as spatial dose non-uniformities, we defined an equivalent uniform stochastic dose as the dose that results in the mean expected survival fraction for a multi-voxel dose distribution that incorporates an intra-voxel dose uncertainty, inter-voxel mean dose fluctuations and a spatial dose non-uniformity. The analytic expression derived in Eq. (4.25) in combination with Eq. (4.26) can be used to calculate SF(EUSD), if we assume $f_v(D)$, $f_m(D)$ and $g(D)$ of Eq. (4.21) each take the form of a Gaussian.

Using the derived expression to calculate ESD for each voxel, TCP can be assessed

for a multi-voxel dose distribution such that

$$TCP\left(\overline{SF}\left(\{ESD_k\}\right)\right) = exp\left\{-N_0\left(\frac{1}{M}\sum_{k=1}^{M} SF\left(ESD_k\right)\right)\right\}. \tag{4.32}$$

In-turn, this can be written as

$$TCP\left(SF\left(EUSD\right)\right) = TCP\left(\overline{SF}\left(\{ESD_k\}\right)\right). \tag{4.33}$$

Again, for notational simplicity we make the following definition

$$TCP\left(EUSD\right) = TCP\left(SF\left(EUSD\right)\right). \tag{4.34}$$

In the derivation of Eq. (4.31) Niemierko and Goitein account for non-uniform dose distributions by calculating SF(EUD). In the previous section we investigated the interpretation of ESD with respect to EUD and found the indices to be mathematically equivalent. Therefore, we can incorporate EUSD into the TCP calculation of a multi-voxel dose distribution by simply replacing the expected survival fraction in Eq. (4.31) with the analytic expression of Eq. (4.25), in combination with Eq. (4.26), to account for the inter-voxel mean dose fluctuations and spatial dose heterogeneity.

4.7 Verification of the equivalent stochastic dose formalism

The derivation and implementation of Eq. (4.25) was verified using Monte Carlo modelling. This verification was performed for three cases: a randomly delivered dose to a single voxel, a randomly delivered spatially uniform multi-voxel dose distribution and a randomly delivered spatially non-uniform multi-voxel dose distribution. To extend the verification we also incorporated ESD and EUSD into the calculation of tumour control probability for each of the cases. Finally we calculated three real clinical IMRT dose distributions using the Monte Carlo method and evaluated the results using the derived formalism for various levels of statistical dose uncertainty.

Verification of the derived expression was performed using the Matlab software environment. Monte Carlo code was written to simulate the probabilistic voxel dose as outlined in the following sections. The clinical IMRT dose distributions were calculated using a computer cluster running the BEAMnrc-DOSXYZnrc Monte Carlo code. A Varian 2100 series accelerator head was modelled using manufacture specifications. For a nominal 6 MV photon beam the incident electron energy and spatial distribution on the x-ray target was set (and previously tested) as outlined in Cranmer-Sargison [28]. Intensity modulation was modelled using the dMLC particle transport code developed by Siebers *et al* [43]. To establish an absolute dosimetric Monte Carlo output each simulation was run using the linac segmentation and phase space set-up developed by Popescu *et al* [44]. To give the desired level of statistical uncertainty each simulation was run with an appropriate history number.

Verification of ESD and EUSD using the Monte Carlo method

To model a voxel dose delivered through a stochastic process, values of D_v were randomly generated 1.0×10^5 times from a Gaussian probability density function $f_v(D)$. The simulation was run with a standard deviation that increased in 0.5% increments from 0.5% to 25%. The mean expected survival fraction was calculated at each level of uncertainty and compared to that predicted by Eq. (4.25). This range of standard deviations was chosen to cover potential physical and statistical dose uncertainties not only in the PTV, but also in any organs at risk (OARs), where both physical (due to beam penumbra) and statistical (due to lower number of particles transported through these regions) uncertainties are usually high.

As a further test, an inter-voxel ESD uncertainty was introduced into a multi-voxel phantom. Each mean voxel dose (D_m) was first sampled from a Gaussian distribution $f_m(D)$ centered about a uniform multi-voxel mean dose D. To represent

a volume of interest, the number of voxels was fixed at $j = 2.5 \times 10^3$. To model voxel dose uncertainty, values of D_v were randomly generated 1.0×10^5 times from a Gaussian probability density function $f_v(D)$ centered about $D_m = 0$. The standard deviation of $f_v(D)$ was assumed to be equal to that of $f_m(D)$. The mean expected survival fraction was calculated for each level of uncertainty and compared to that predicted using Eq. (4.25); where the total variance incorporated both the variance of $f_v(D)$ and $f_m(D)$.

In a similar manner to Ebert [96], a spatially non-uniform dose distribution was also modelled. The standard deviation of the physical dose distribution was taken to be the same as that of the statistical distributions $f_v(D)$ and $f_m(D)$. The mean values of this normally distributed multi-voxel dose (D_g) were sampled 2.5×10^3 times from a Gaussian distribution centered on the prescribed mean dose D. The inter-voxel ESD uncertainty and intra-voxel dose uncertainty were each modelled as above. The results where compared with those derived using Eq. (4.25) noting that the variance was now the sum of three variances.

TCP as a function of ESD and EUSD

In addition to verifying SF(ESD), TCP as a function of SF(ESD) was also modelled for the three cases of a randomly deposited voxel dose, a uniform dose delivered randomly to a multi-voxel phantom and a randomly delivered spatially non-uniform dose to a multi-voxel phantom. However, given that the analytic form of ESD and EUSD had already been verified, we used the analytic form of Eq. (4.25) to calculate the mean expected survival fraction as a function of increasing dose uncertainty (0.5% increments from 0.5% to 25%) for cases of 60 and 70 Gy at 2 Gy per fraction.

To incorporate fluctuations in the inter-voxel mean dose a multi-voxel phantom was modelled as above. Each mean voxel dose (D_m) was first sampled from a Gaussian

distribution $f_m(D)$ centered about a uniform multi-voxel mean dose D. A volume of interest was simulated with the number of voxels fixed at $j = 2.5 \times 10^3$. To model voxel dose uncertainty ESD was calculated for each D_m using Eq. (4.25). TCP_k was evaluated using Eq. (4.34) for each voxel as a function of the mean expected survival fraction for each level of dose uncertainty. TCP as a function of SF(EUSD) was calculated using Eqs. (4.25) and (4.26) and compared to TCP calculated using Eq. (4.33) where the average survival fraction of ESD was taken over the whole distribution.

A spatially non-uniform dose distribution was also modelled where the standard deviation of the physical dose distribution was taken to be the same as that of the statistical distributions $f_v(D)$ and $f_m(D)$. For each case a plot of TCP as a function of dose uncertainty were generated for various combinations of α, α/β and clonogen density.

Chapter 5

Quantifying the impact of dose uncertainties using the concept of equivalent stochastic dose

5.1 Introduction

In this chapter we explore the results obtained through the verification and application of equivalent stochastic dose. The impact of dose uncertainty is evaluated using the ESD concept for the case of a single voxel, a spatially uniform multi-voxel dose distribution as well as a spatially non-uniform multi-voxel dose distribution. Tumour control probability as a function of equivalent stochastic dose is investigated for various combinations of radiosensitivity and cell density at the intra and inter-voxel level.

5.2 Expected survival fraction calculated for various levels of dose uncertainty

As a function of mean voxel dose and uncertainty (Section 4.6) an analytic expression was derived for the expected survival fraction. The only assumption made in the derivation was that the probabilistic dose to a voxel follows a Gaussian probability density function. Using Eq. (4.25) the impact of dose uncertainty on survival fraction

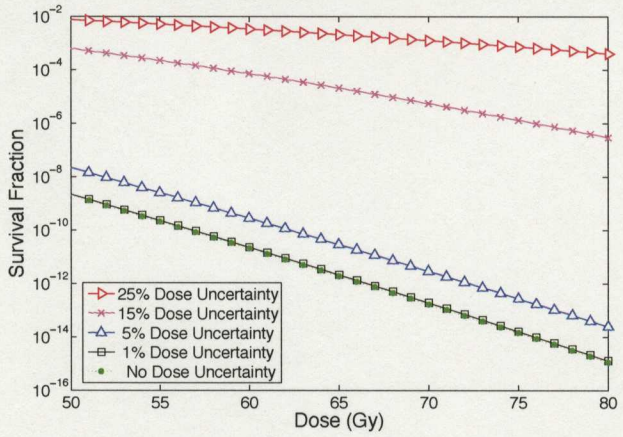

Figure 5.1: SF as a function of dose for various levels of dose uncertainty calculated using Eq. (4.25). The modelled treatment was fixed at 2 Gy per fraction, with $\alpha = 0.30$ Gy^{-1} and $\alpha/\beta = 10$ Gy. The SF with no dose uncertainty was calculated using the LQ equation (Eq. (4.7)).

was first evaluated as a function of mean voxel dose with increasing levels of dose uncertainty.

Figure 5.1 is a plot of survival fraction, for a clinically relevant dose range, calculated with an increasing level of dose uncertainty. At each level the calculated survival fraction responds in a manner that is consistent with the known response to increased spatial dose heterogeneity. The incorporation of a probabilistic dose heterogeneity reveals the well documented effect of dose non-uniformity on the calculation of survival fraction. However, in our case the dose non-uniformity is not spatial but probabilistic. The fact that a reduction in survival fraction is not restricted to spatial dose heterogeneity follows from the mathematical equivalence of ESD and EUD. In either case, the non-linear response of survival fraction to dose variations manifests itself in the same manner.

One can see that the difference between the case of no dose uncertainty and the case of 1.0% uncertainty is negligible, but as the dose uncertainty increases to 25% the

survival fraction increases by $\backsim 7$ orders of magnitude. In addition to the escalating number of surviving clonogens, the slope of the survival fraction curve is reduced by the increasing dose uncertainty. For each level of dose uncertainty this reduction represents a relative decrease in cell kill with respect to an equivalent increase in voxel dose. In fact, a mean voxel dose escalation, in combination with an amplification in dose uncertainty, results in a greater probability of low dose. This in-turn produces a reduced biological response and must be taken into consideration when developing dose escalation protocols.

The declining slope in survival fraction is, in our case, solely due to the increased uncertainty in the mean voxel dose. Unlike the results in other studies, where the reduction in biological response is due to spatial dose heterogeneity, our results show that random dose deposition can impact radiobiological plan evaluation. As seen in Fig. 5.1, the result of dose uncertainty on the evaluation of survival fraction can be large and therefore must be accounted for if correct treatment plan evaluation is to be made.

Tomé and Fowler [97] note that physical target sub-volumes as small as 1% receiving a cold dose lower than the prescribed dose by substantially more than 10% can be detrimental. The authors state that even when 80% of the target receives a 10% boost, particular attention has to be paid to small-volume cold regions in the target. Analogous to the effect of spatial cold dose sub-volumes, an increase in dose uncertainty gives rise to a greater probability in low dose. This in-turn produces what we refer to as "probabilistic cold spots". The declining survival fraction, as a function of increased dose uncertainty, highlights the fact that "probabilistic cold spots" have a large influence on overall cell kill while "probabilistic hot spots" have a minimal radiobiological impact. This is essentially what Tomé and Fowler are reporting, yet the "hot" and "cold" spots in their case are spatial sub-volumes and not probabilistic.

It should be noted that the decrease in survival fraction shown in Fig. 5.1 was modelled for a fixed fractional dose of 2 Gy, $\alpha = 0.30$ Gy^{-1} and $\alpha/\beta = 10$ Gy. As these parameters change so will the relative decrease in cell kill with respect to an equivalent increase in voxel dose.

5.3 Equivalent stochastic dose for various levels of dose uncertainty

In the previous section we explored how the radiobiological response of survival fraction was affected by increased dose uncertainty. It was found that the number of surviving clonogens increased as the dose uncertainty increased. To further explore this radiobiological reduction, an equivalent stochastic dose was calculated from the expected survival fraction using Eq. (4.18).

To quantify the impact of probabilistic dose deposition, ESD and EUSD will be evaluated for various radiobiological parameters attributed to tissue and tumour. Monte Carlo data is included in the results as an independent verification of the derivation and implementation of the formalism presented in this work.

Figures 5.2 and 5.3 represent ESD for a single voxel calculated using Eq. (4.25) and verified with Monte Carlo data. The derived expression correctly accounts for the modelled stochastic voxel dose for various combinations of α and α/β. At increased levels of dose uncertainty the impact of the stochastic process is evident in the reduced ESD. In fact, as the voxel dose uncertainty increases the difference between the two cases of 60 and 70 Gy decreases. The reduction in the relative difference between the two cases is again the result of the non-linear response of survival fraction to dose variations.

Table 5.1 gives the ratio of ESD with respect to the prescribed mean dose of

either 60 or 70 Gy modelled at 2 Gy per fraction. The table reveals that for a dose uncertainty up to 5% the ratio of mean prescribed dose to ESD is the same for both the 60 and 70 Gy cases. However, as the dose uncertainty increases beyond this level the relative impact on ESD for the 70 Gy case becomes greater than for the 60 Gy case. At increased levels of dose uncertainty the radiobiological degradation is more readily precipitated for greater prescribed voxel dose. For higher dose values the "probabilistic cold spots" span a greater range than for the lower prescribed voxel dose. The increased reduction is an indication that dose uncertainty will potentially have a greater relative radiobiological effect for treatments that incorporate dose escalation protocols and highlights the need for accurate voxel dose uncertainty estimation.

Shown in Figs. 5.4 and 5.5 are calculated (Eq. (4.25)) and Monte Carlo generated data for a spatially uniform multi-voxel dose distribution that incorporates a fluctuation on the inter-voxel mean dose as well as intra-voxel dose uncertainty. Equation (4.25) correctly models the random mean voxel dose and is clearly capable of simulating both voxel dose uncertainty and probabilistic inter-voxel dose heterogeneity for various combinations of α and α/β.

Comparing Figs. 5.4 and 5.5 with Figs. 5.2 and 5.3 respectively, one can see the radiobiological reduction, at each level of dose uncertainty, is less for a single voxel than for a spatially uniform multi-voxel dose distribution subject to inter-voxel mean dose fluctuations. When compared to the case for a single voxel the increased radiobiological degradation revealed in the multi-voxel dose distribution is solely due to the inherent fluctuation in the inter-voxel mean dose. Using the concept of EUSD the impact can be quantified and reported as a single value.

Table 5.2 represents the ratio of EUSD with respect to the prescribed uniform multi-voxel mean dose. Given that the multi-voxel mean dose is subject to stochastic

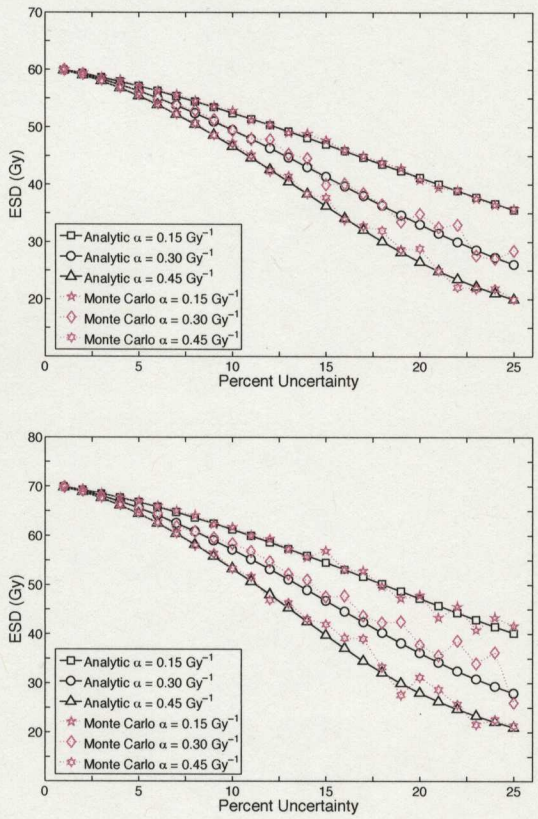

Figure 5.2: Single voxel dose modelled at 60 Gy (top) and 70 Gy (bottom) at 2 Gy per fraction. The radiosensitivity parameter $\alpha = 0.15$, 0.30, 0.45 Gy^{-1} and the ratio $\alpha/\beta = 10$ Gy.

fluctuations, the relative reduction at increasing levels of dose uncertainty is naturally greater than for the single voxel. The ratio of EUSD to prescribed mean dose again reveals that at a dose uncertainty up to 5% the relative impact for the cases of 60 and 70 Gy are equivalent and as the dose uncertainty increases beyond that level the reduction in EUSD is greater for the prescribed 70 Gy.

Figures 5.6 and 5.7 represent data calculated using Eq. (4.25) and Monte Carlo generated data for a spatial dose non-uniformity that incorporates inter-voxel mean dose fluctuations as well as an intra-voxel dose uncertainty. Equation (4.25) correctly

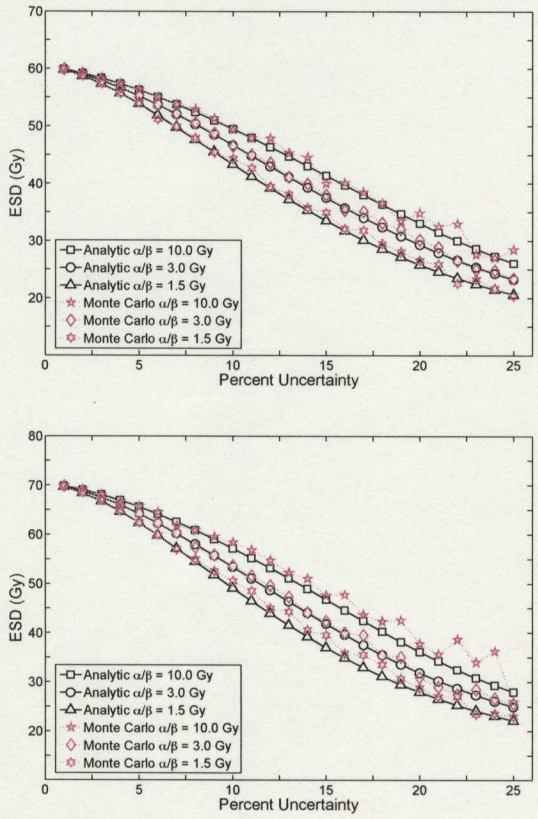

Figure 5.3: Single voxel dose modelled at 60 Gy (top) and 70 Gy (bottom) at 2 Gy per fraction. The radiosensitivity parameter $\alpha = 0.30$ Gy^{-1} and the ratio $\alpha/\beta = 1.5$, 3.0, 10.0 Gy.

models the spatial non-uniformity and is clearly capable of simulating both stochastic and spatial dose heterogeneity. Incorporating a spatial non-uniformity into the modelled multi-voxel dose distribution results in a further reduction in EUSD when compared to the spatially uniform case. Figures 5.6 and 5.7 again reveal the inherent reduction in the radiobiological response on tumour and tissues with different α and α/β values - due not only to the stochastic dose deposition but in this case a spatial dose heterogeneity.

Table 5.3 displays the ratio of EUSD to the planned mean doses of 60 and 70

	Relative ESD 60 Gy treatment plan			Relative ESD 70 Gy treatment plan		
Percent Dose Uncertainty	α (Gy^{-1}) 0.15	0.30	0.45	α (Gy^{-1}) 0.15	0.30	0.45
2%	0.989	0.987	0.984	0.990	0.987	0.984
5%	0.953	0.938	0.924	0.955	0.938	0.921
10%	0.875	0.825	0.778	0.876	0.871	0.762
15%	0.784	0.690	0.605	0.780	0.669	0.569
25%	0.593	0.435	0.334	0.574	0.400	0.300
	α/β (Gy) 1.5	3.0	10.0	α/β (Gy) 1.5	3.0	10.0
2%	0.979	0.984	0.987	0.978	0.983	0.987
5%	0.898	0.921	0.938	0.891	0.918	0.938
10%	0.723	0.778	0.825	0.702	0.763	0.817
15%	0.559	0.625	0.690	0.529	0.598	0.669
25%	0.344	0.388	0.435	0.316	0.357	0.400

Table 5.1: Relative ESD taken with respect to the mean dose of 60 Gy and 70 Gy at 2 Gy per fraction for various α values ($\alpha/\beta = 10.0$ Gy) for a single voxel and various α/β values ($\alpha = 0.30$ Gy^{-1}) for a single voxel.

Gy at 2 Gy per fraction. It is apparent that dose uncertainty has a greater effect on radiosensitive tumours ($\alpha = 0.45$ Gy^{-1}) and less affect on radioresistant ($\alpha = 0.15$ Gy^{-1}) ones. For a dose heterogeneity and uncertainty of 2% the relative difference between the mean dose and EUSD is on average 2%, however, the difference inflates to a point where a dose heterogeneity and uncertainty of 25% results in a reduction in EUSD by 75%. Once again, by comparing the cases of 60 and 70 Gy one can see that the relative reduction in EUSD is more significant for higher dose.

One feature that is apparent in Tables 5.1, 5.2 and 5.3 is that as the α/β ratio increases so does the equivalent stochastic dose. This indicates that the dose variations are affecting late responding tissues to a greater degree than early responding

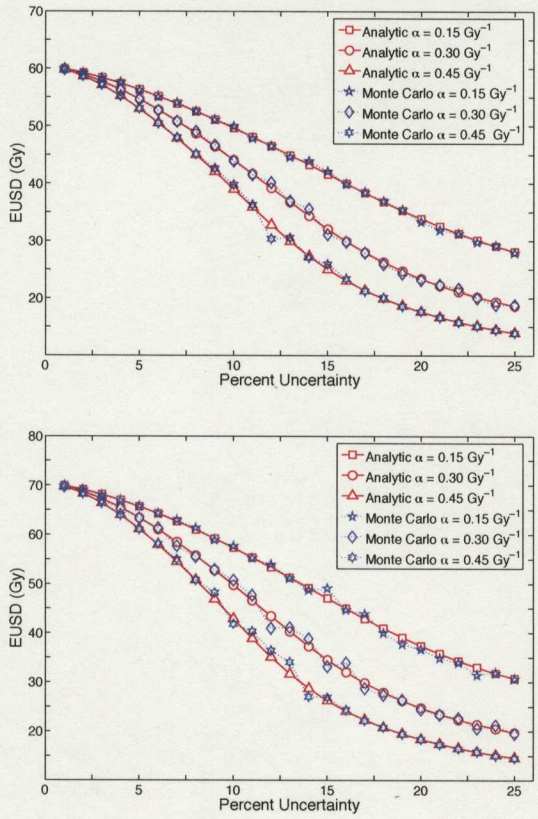

Figure 5.4: Spatially uniform multi-voxel ESD modelled at 60 Gy (top) and 70 Gy (bottom) at 2 Gy per fraction. The radiosensitivity parameter $\alpha = 0.15$, 0.30, 0.45 Gy^{-1} and the ratio $\alpha/\beta = 10$ Gy.

ones. At levels of dose non-uniformity and uncertainty above 5%, variations in the α/β ratio affect EUSD less than variations in α. This is due to the high number of fractions (30 and 35) used in each case and is consistent with the known relative importance between α and β values in fractionated treatments.

In each case, the ratio of EUSD to prescribed mean dose was less than 1 but greater than the probabilistic minimum dose ($D = 0$ Gy). This is consistent with one of the characteristics of EUD explored in Section 3.2.1 and follows naturally given the mathematical definitions of EUD and ESD. Niemierko stated that for clinical treat-

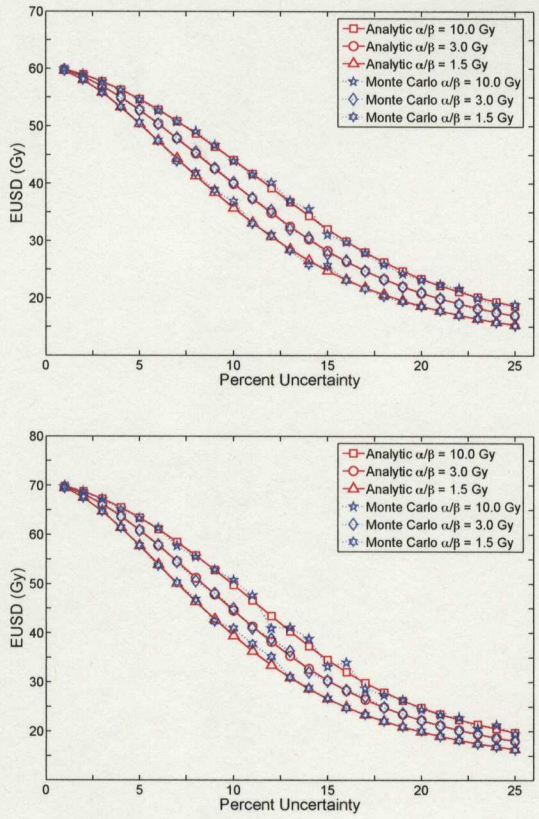

Figure 5.5: Spatially uniform multi-voxel ESD modelled at 60 Gy (top) and 70 Gy (bottom) at 2 Gy per fraction. The radiosensitivity parameter $\alpha = 0.30$ Gy^{-1} and the ratio $\alpha/\beta = 1.5$, 3.0, 10.0 Gy.

ment plans the range of minimum dose is much larger than the range of mean dose or EUD, and that the minimum dose might correspond to a very small number of physical volume elements. However, in the calculation of ESD, the range of probabilistic dose minima ($D = 0$ Gy) will be constant for all levels of dose uncertainty. What will change is the probability that any given low dose occurs. This is conceptually very different to EUD where it is the the number of volume elements within a target receiving the reduced dose that varies.

	Relative EUSD 60 Gy treatment plan			Relative EUSD 70 Gy treatment plan		
Percent Dose Uncertainty	α (Gy^{-1}) 0.15	0.30	0.45	α (Gy^{-1}) 0.15	0.30	0.45
2%	0.987	0.982	0.977	0.987	0.981	0.975
5%	0.939	0.910	0.883	0.938	0905	0.873
10%	0.827	0.734	0.649	0.818	0.710	0.612
15%	0.693	0.534	0.417	0.672	0.493	0.375
25%	0.468	0.310	0.232	0.439	0.281	0.208
	α/β (Gy) 1.5	3.0	10.0	α/β (Gy) 1.5	3.0	10.0
2%	0.967	0.976	0.982	0.964	0.974	0.981
5%	0.839	0.879	0.910	0.824	0.869	0.905
10%	0.595	0.665	0.734	0.563	0.636	0.710
15%	0.412	0.470	0.534	0.380	0.433	0.493
25%	0.255	0.282	0.310	0.233	0.257	0.281

Table 5.2: Relative EUSD taken with respect to the mean dose of 60 Gy and 70 Gy at 2 Gy per fraction for various α values ($\alpha/\beta = 10.0$ Gy) and various α/β values ($\alpha = 0.30$ Gy^{-1}) for a spatially uniform multi-voxel dose distribution.

5.4 Evaluation of TCP as a function of ESD for various levels of dose uncertainty

The concept of an equivalent uniform dose is not the only evaluative convention used in radiotherapy. Another common quantitative index derived from survival fraction is the probability of tumour control. Incorporating both physical and statistical dose uncertainties into the calculation of TCP is a natural extension to the analysis already shown and essential for comprehensive evaluation of radiotherapy treatment plans.

No evaluative index has emerged as being clearly superior and given there are number of unique characteristics to both EUD and TCP (and other evaluative indices), we now complement our initial analysis by assessing the impact of dose un-

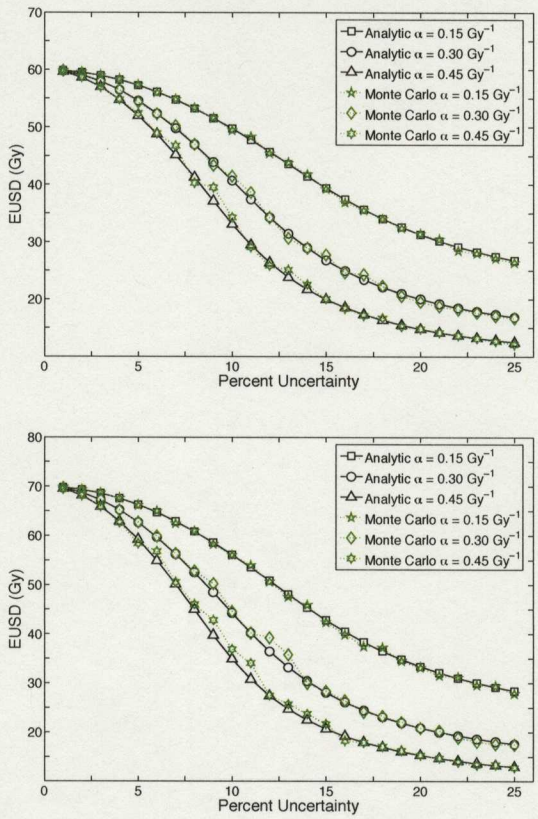

Figure 5.6: Spatially non-unifrom multi-voxel dose distribution modelled at 60 Gy (top) and 70 Gy (bottom) at 2 Gy per fraction. The radiosensitivity parameter $\alpha =$ 0.15, 0.30, 0.45 Gy^{-1} and the ratio $\alpha/\beta = 10$ Gy.

certainty on TCP. We calculate TCP using the convention proposed by Niemierko and Goitein; where TCP is evaluated as a function of the mean survival fraction. Given ESD is derived from the mean expected survival fraction, using this TCP convention follows naturally. We explore TCP(ESD) and TCP(EUSD) for the case of a single voxel, a spatially uniform multi-voxel dose distribution, as well as a spatially non-uniform multi-voxel dose distribution.

Shown in Fig. 5.8 are single voxel (1 cm^3) TCP values calculated as a function of ESD, which accounts for the increasing dose uncertainty, for the two cases of 60 and

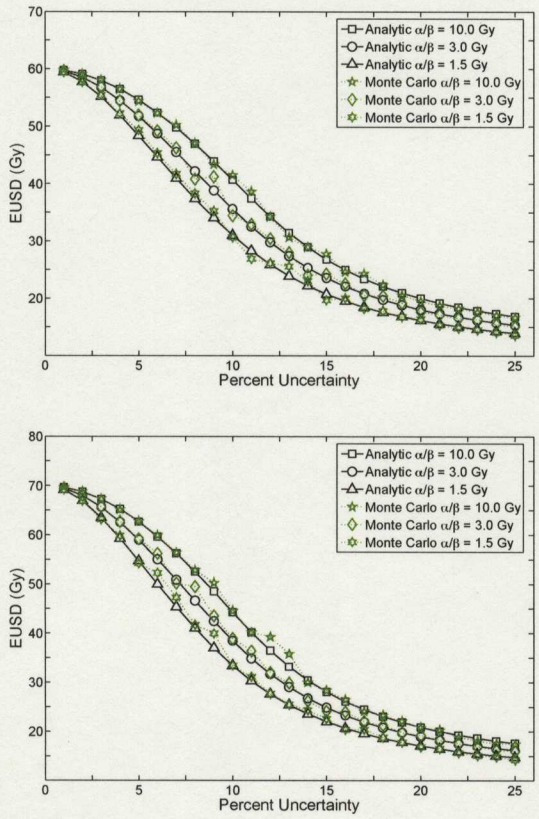

Figure 5.7: Spatially non-uniform multi-voxel dose distribution modelled at 60 Gy (top) and 70 Gy (bottom) at 2 Gy per fraction. The radiosensitivity parameter $\alpha = 0.30$ Gy^{-1} and the ratio $\alpha/\beta = 1.5$, 3.0, 10.0 Gy.

70 Gy at 2 Gy per fraction. Each case was calculated with various combinations of cell radiosensitivity, α/β ratio and cell density. A baseline combination of parameters ($\alpha = 0.30$ Gy^{-1}, $\alpha/\beta = 10.0$ Gy and $\rho = 10^8$ cm^{-3}) was used and is shown in each graph for comparative purposes. In general, one can see that as the dose uncertainty increases TCP decreases. As the dose uncertainty increases the equivalent stochastic dose decreases; this in turn produces a reduced TCP.

Shown in the top row of Fig. 5.8 are the reductions in TCP as a function of dose uncertainty for various α values. One can see that TCP transitions between control

	Relative EUSD 60 Gy treatment plan			Relative EUSD 70 Gy treatment plan		
Percent Dose Uncertainty	α (Gy^{-1}) 0.15	0.30	0.45	α (Gy^{-1}) 0.15	0.30	0.45
2%	0.992	0.985	0.977	0.991	0.983	0.974
5%	0.955	0.906	0.867	0.947	0.896	0.847
10%	0.829	0.692	0.552	0.803	0.633	0.499
15%	0.657	0.462	0.334	0.612	0.402	0.296
25%	0.447	0.280	0.208	0.406	0.252	0.185
	α/β (Gy) 1.5	3.0	10.0	α/β (Gy) 1.5	3.0	10.0
2%	0.963	0.976	0.985	0.965	0.972	0.983
5%	0.807	0.863	0.906	0.782	0.843	0.895
10%	0.517	0.594	0.692	0.477	0.550	0.633
15%	0.415	0.394	0.462	0.315	0.356	0.402
25%	0.233	0.257	0.280	0.211	0.231	0.252

Table 5.3: Relative EUSD taken with respect to the mean dose of 60 Gy and 70 Gy at 2 Gy per fraction for various α values (α/β = 10.0 Gy) and various α/β values ($\alpha = 0.30$ Gy^{-1}) for a spatially non-uniform multi-voxel dose distribution.

and no control at various levels of dose uncertainty. This variation is due only to the changing radiosensitivity (α=0.30 Gy^{-1} and 0.45 Gy^{-1}). In fact, when α=0.15 Gy^{-1} we find TCP=0 for all levels of dose uncertainty. This is an indicator that there will never be tumour control for this prescribed dose and radiosensitivity combination. Given there is never tumour control the dose uncertainty will not have any impact on the radiobiological outcome.

One characteristic revealed by increasing the radiosensitivity parameter α was that the TCP decrease occurred at increasing levels of dose uncertainty - the more radiosensitive the tumour - the less sensitive TCP evaluation was to dose uncertainty. However, for higher radiosensitivities the transition between control and no control

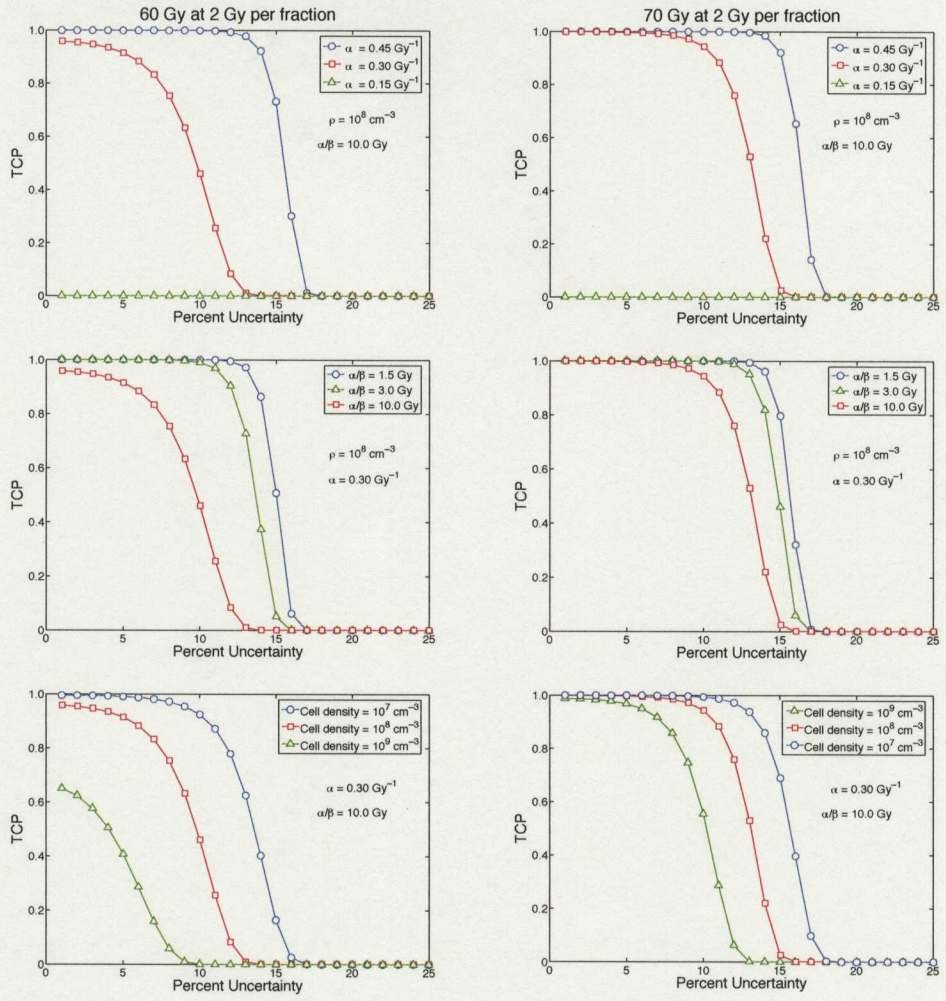

Figure 5.8: Tumour control probability versus dose uncertainty for a single voxel that incorporates an intra-voxel dose uncertainty modelled at 60 and 70 Gy at 2 Gy per fraction.

was found to occur over a very narrow dose uncertainty range. This is evident for both the 60 and 70 Gy cases yet is more pronounced for the latter.

The variation in TCP for different values of α/β, shown in the second row of Fig. 5.8, indicates that a decrease in the α/β ratio results in a greater overall biological response. The data reveals that TCP is reduced at lower dose uncertainty levels

when the α/β ratio is increased. That is, TCP calculated with a greater β, resulting from a lower α/β ratio, gives rise to a TCP fall-off that occurs at higher levels of dose uncertainty. However, when compared to the variation of α (for a fixed α/β ratio) the difference between TCP calculated with the various α/β ratios occurs over a smaller range of dose uncertainty.

Shown in the third row of Fig. 5.8 are TCP values calculated, for a fixed voxel size of 1 cm^3 with various cell densities, as a function of the mean expected survival fraction. One can see that TCP for the 60 Gy case is less than 1 for a cell density of 10^9 cm^{-3} (α=0.30 Gy^{-1} and α/β=10.0 Gy), however, when the prescribed mean voxel dose is 70 Gy, TCP = 1 for a dose uncertainty up to approximately 5%. For a cell density of 10^7 and 10^8 cm^{-3}, both the 60 and 70 Gy cases degrade from TCP = 1 to TCP = 0 as the dose uncertainty increases. This shows the sensitivity of TCP to clonogen number and emphasizes that TCP should be used as an absolute predictor with caution and that variations in TCP can be substantial when the dose uncertainties are high and the cell densities are not well known.

So far each TCP example has been evaluated for a single voxel. To extend the application of TCP as a function of ESD, or more correctly EUSD, we evaluated TCP(EUSD) for a spatially uniform multi-voxel dose distribution that incorporates a fluctuation in the inter-voxel mean dose as well as intra-voxel dose uncertainty.

However, as noted earlier, the calculation of TCP for a multi-voxel dose distribution can be made using two different conventions. In this work, we have chosen to evaluate TCP for the multi-voxel dose distribution using Eq. (4.31). This amounts to calculating TCP($\overline{SF}(\{D_k\})$)=TCP(EUD) for a multi-voxel dose distribution. As we are assessing the impact of dose uncertainty, each voxel dose element becomes ESD_k. Therefore, the evaluation over the whole multi-voxel dose distribution becomes TCP($\overline{SF}(\{ESD_k\})$)=TCP(EUSD), where the evaluation can be made

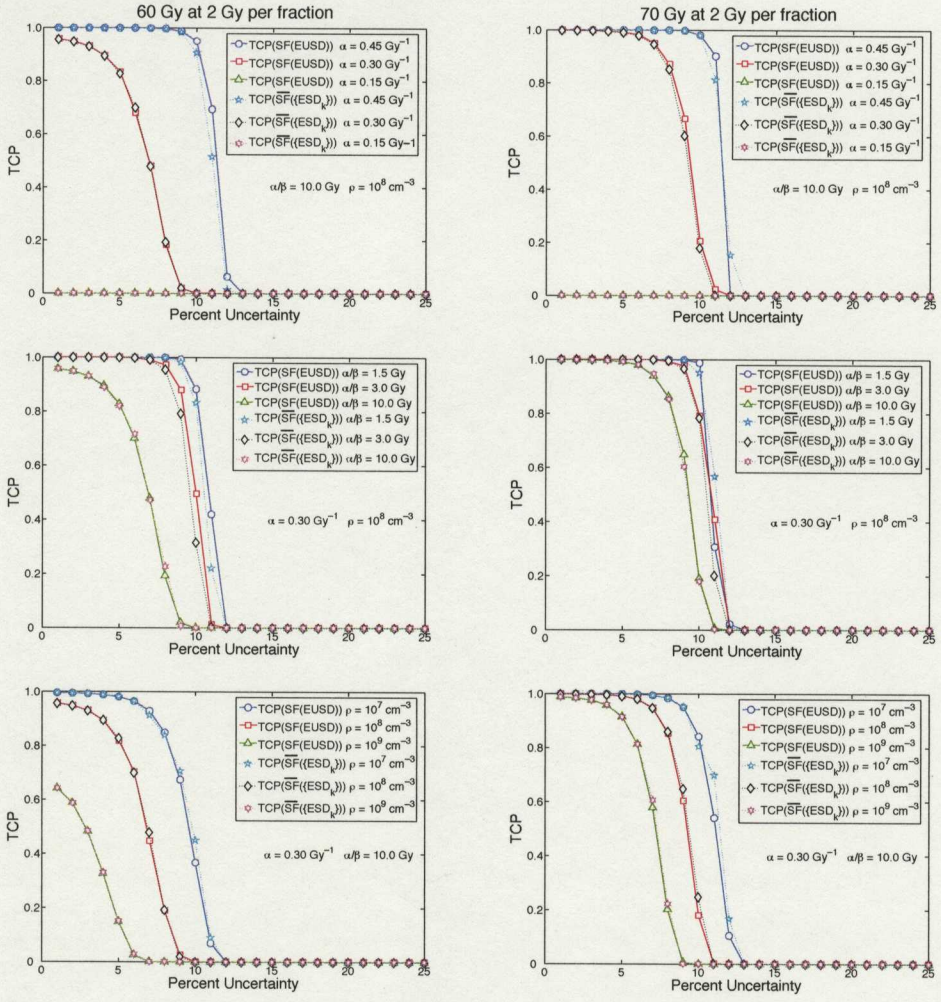

Figure 5.9: Tumour control probability for a uniform dose distribution modelled at 60 and 70 Gy at 2 Gy per fraction that incorporates inter-voxel mean dose fluctuations as well as an intra-voxel dose uncertainty.

analytically for the entire dose distribution or on a voxel-by-voxel basis.

Figure 5.9 shows the reduction in TCP as a function of dose uncertainty for a spatially uniform dose distribution calculated with various combinations of cell radiosensitivities and densities for a fixed voxel size of 1 cm^3. Previously, we showed that in combination, Eq. (4.25) and (4.26) could be used to evaluate EUSD for a

multi-voxel dose distribution that was assumed to have either a spatially uniform or non-uniform dose distribution. The data labeled TCP(SF(EUSD)) were calculated analytically using the derived expression for SF(EUSD). Calculating the mean expected survival fraction in this manner took into account the inter-voxel mean dose fluctuation as well as the intra-voxel dose uncertainty in one calculation. The data labeled TCP($\overline{SF}(\{ESD_k\})$) was evaluated using sampled mean voxel doses and the analytic expression to calculate SF(ESD) on a voxel-by-voxel basis.

Note, although the original application of TCP (as a function of mean survival fraction) was to analyze dose distributions that incorporate a physical dose non-uniformity, an extension of the evaluation of both spatial and probabilistic dose heterogeneities can be made using TCP(EUSD). This is consistent with our proposed extension of the definition of EUD as a method of incorporating dose uncertainties. Given the mathematical definition for the mean expect survival fraction, evaluation of TCP($\overline{SF}(\{ESD_k\})$) and TCP(EUSD) for the case of a spatially uniform dose distribution should naturally be the same and were included as a means of validation.

From Fig. 5.9 one can see that in each case the two methods of calculating TCP are equivalent. Clearly, accounting for the probabilistic dose heterogeneity that results from the inter-voxel mean dose fluctuation is correctly incorporated in the calculation of TCP through the concept of an equivalent uniform stochastic dose. In comparing Figs. 5.8 and 5.9 the inter-voxel mean dose fluctuation clearly reduces TCP in a similar manner to the increased reduction in ESD presented in Section 5.3.

Evaluating a multi-voxel dose distribution subject to a probabilistic dose heterogeneity will produce a TCP that is less than TCP calculated for one voxel. However, the relative influence of the radiosensitivity parameters and cell density will remain the same. In each case the relative reduction in TCP continues, yet each TCP curve shifts to a lower dose uncertainty. Clearly, the probabilistic dose heterogeneity is being

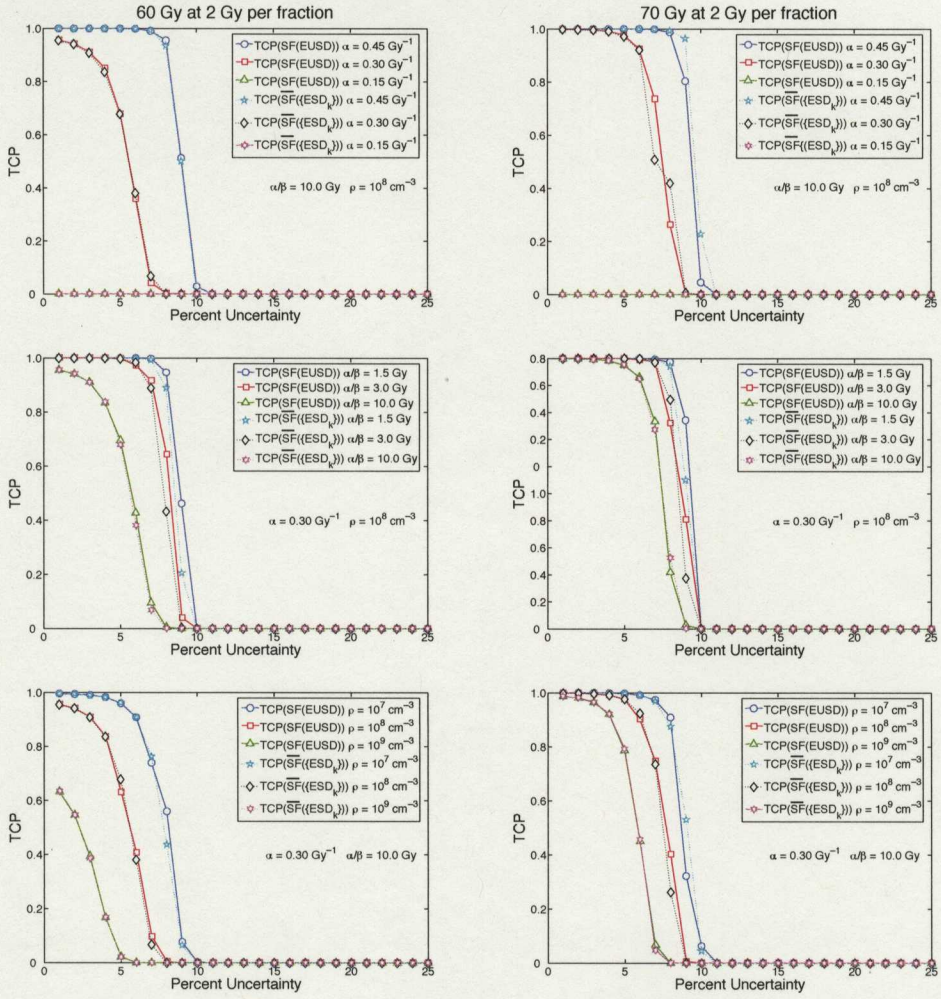

Figure 5.10: Tumour control probability for a spatially non-uniform dose distribution modelled at 60 and 70 Gy at 2 Gy per fraction that incorporates inter-voxel mean dose fluctuations as well as an intra-voxel dose uncertainty.

propagated through the calculation of TCP in the form of a reduced radiobiological response.

Figure 5.10 is the data for the modelled 60 and 70 Gy cases that incorporates a spatial dose heterogeneity. One can see that the spatially non-uniform dose distribution again degrades the radiobiological response of TCP. Each of the TCP curves are

shifted further to the left when compared to the spatially uniform dose distribution. For the generic combination of $\alpha = 0.30$ Gy^{-1}, $\alpha/\beta = 10.0$ Gy and $\rho = 10^9$ cm^{-3}, the drop from complete tumour control to no control happens at an uncertainty level of approximately 5% for the 60 Gy case and 8% for the 70 Gy case. As this is the most realistic model of a clinical dose distribution the reduction in TCP at uncertainty levels in this range should be consistent with other reported cases where TCP is reduced due to dose uncertainties.

5.5 Clinical Treatment plan evaluation using EUSD

To test the validity of evaluating clinical radiotherapy treatment plans using EUSD, three real IMRT head-and-neck treatment plans were modelled using the BEAMnrc-DOSXYZnrc Monte Carlo code. The prescription for each patient was 60 Gy to the PTV delivered in 25 fractions. This gave a fractional dose of 2.4 Gy. For simplicity we will refer to the three treatment plans as: Case #1, #2, #3. Each Case was modelled with 100, 10 and 2 million electron histories incident on the Bremsstrahlung target. Voxel dose and uncertainty values were extracted from the DOSXYZnrc dose matrix for the contoured PTV. The voxel number in each PTV was as follows: $\text{PTV}_{\#1} = 23,029$, $\text{PTV}_{\#2} = 7,277$ and $\text{PTV}_{\#3} = 7,846$. The voxel size was fixed at 0.25 cm^3 for all simulations. Shown in Figs. 5.11, 5.12 and 5.13 are the differential dose volume histograms (dDVHs)[1] and differential dose uncertainty histograms (dDUHs)[2] associated with the PTVs.

The dDUH scale was varied for each Case and history number to encompass the

[1] A differential dose volume histogram represents the dose elements within the PTV binned as a function of voxel dose.

[2] The differential dose uncertainty histogram represents the dose uncertainty elements within the PTV binned as a function of voxel dose uncertainty.

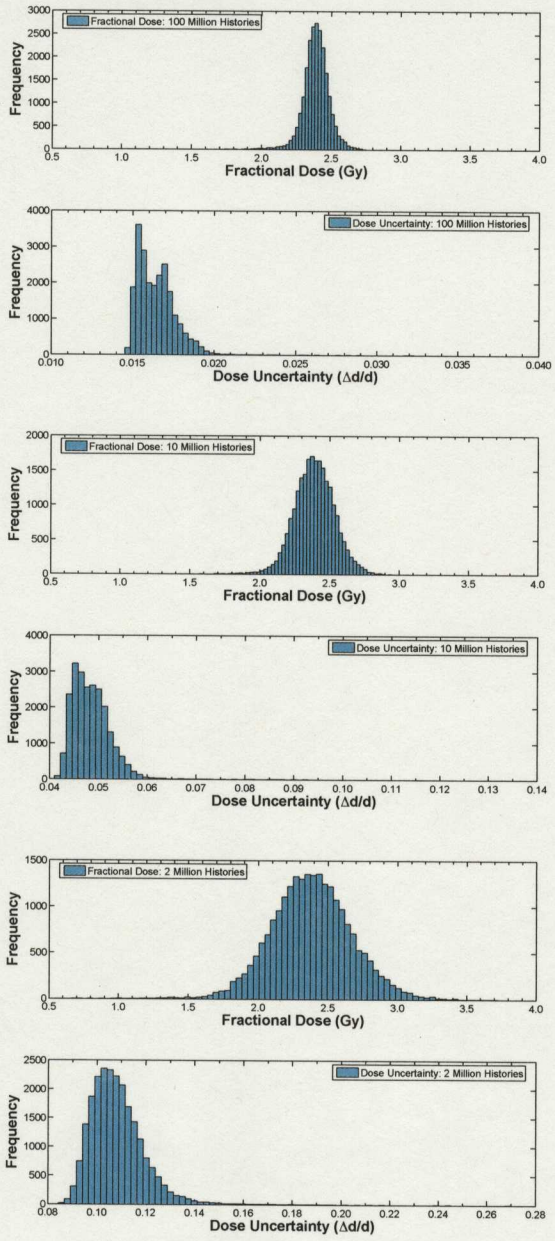

Figure 5.11: Differential dose volume histogram and differential dose uncertainty histogram for a clinical IMRT dose distribution calculated using the EGSnrc photon-electron Monte Carlo transport algorithms for 100 (top), 10 (middle) and 2 (bottom) million electron histories - Case #1.

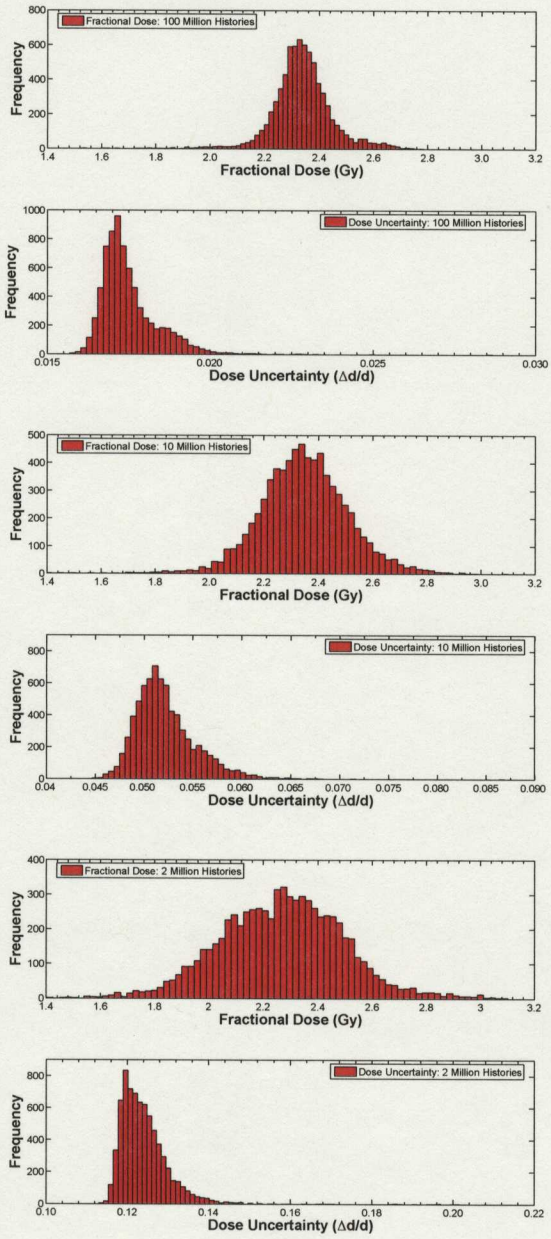

Figure 5.12: Differential dose volume histogram and differential dose uncertainty histogram for a clinical IMRT dose distribution calculated using the EGSnrc photon-electron Monte Carlo transport algorithms for 100 (top), 10 (middle) and 2 (bottom) million electron histories - Case #2.

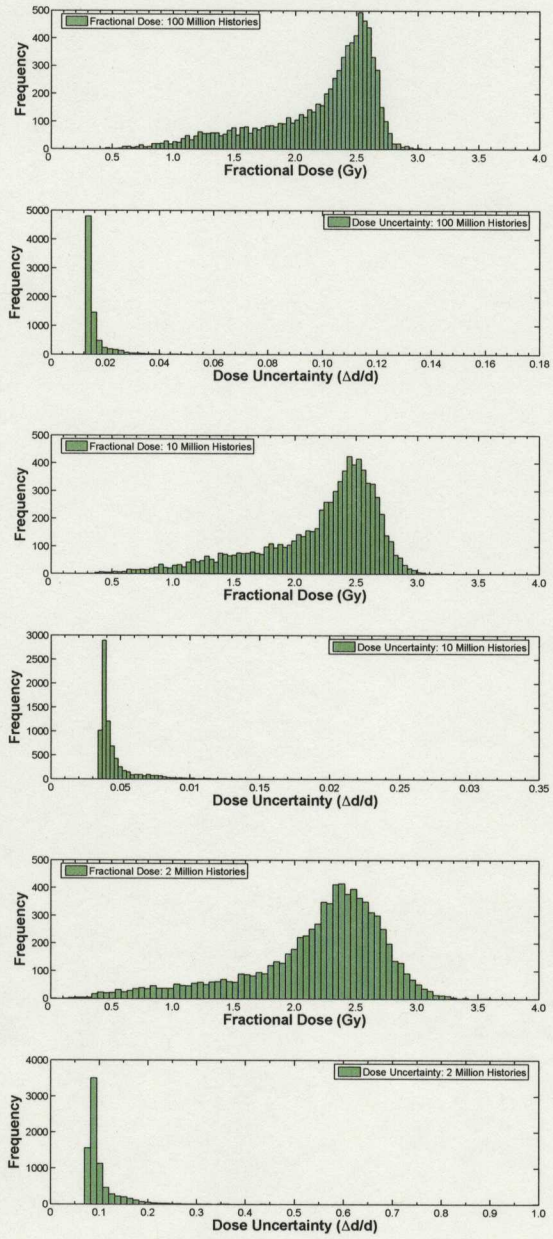

Figure 5.13: Differential dose volume histogram and differential dose uncertainty histogram for a real clinical IMRT treatment plan calculated using the EGSnrc photon-electron Monte Carlo transport algorithms for 100 (top), 10 (middle) and 2 (bottom) million electron histories - Case #3.

full range of dose uncertainty. One can see there is a clear shift in the dDUH peak as the history number is reduced. There is also a substantial increase in the maximum dose uncertainty. Both the shift in the dose uncertainty peak and the broadening of the dose uncertainty range are the result of the reduced number of electron histories used in the Monte Carlo simulations.

The inter-voxel fractional mean dose did not change with increased statistical dose uncertainty. This is clearly shown by the consistent dDVH peak location. Figures 5.11, 5.12 and 5.13 show that as the statistical dose uncertainty increases the dDVH widens; the width increase is a direct result of the decreased number of electron histories. This is consistent with the assumption made in the derivation of EUSD. We assumed that as the dose uncertainty increased there would be an increased fluctuation in the inter-voxel mean dose - which in turn produces a wider dDVH. This fluctuation was taken into account by incorporating $f_m(D)$ in the convolution equation (see Eq. (4.20)).

Shown in Table 5.4 are EUSD and TCP values calculated using the Monte Carlo simulation data. Cell density was set to $\rho = 10^7$ cm^{-3} to give, in combination with $\alpha = 0.30$ Gy^{-1} and $\alpha/\beta = 10.0$ Gy, a TCP of approximately 1 for the low uncertainty simulations. We note that evaluating TCP using a PTV volume is not strictly correct and GTV should be used to assess the true tumour control. The TCP analysis has been included here only to test the validity of the derived formalism. Therefore, the results should be interpreted as a relative TCP evaluation used to reveal only the impact of the increasing dose uncertainty.

It is evident that for each PTV dose distribution the statistical dose uncertainty increase results in an EUSD decrease. Clearly there is a correlation between the dDVH shape and the values listed in Table 5.4. For Cases # 1 and # 2 the relatively symmetric dDVHs are reflected in the EUSD and TCP values calculated from the

PTV data. Though TCP is high for a dose uncertainty up to 5%, increasing the dose uncertainty to approximately 10% reduces the tumour control to zero. This is consistent with the TCP results obtained using the derived analytic expression shown in the previous section.

It is clear from the evaluation of Case # 3 that a spatial dose heterogeneity can potentially have a large influence on the radiobiological outcome. If the PTV dose distribution does not provide nearly uniform coverage, the radiobiological evaluation of a planned treatment may show the plan to be problematic. One can clearly see that both spatial dose heterogeneity and dose uncertainty can significantly degrade radiobiological plan evaluation.

The radiobiological outcome for a planned treatment with a low TCP, and low levels of uncertainty, will itself be low. In fact, if the TCP is initially zero, incorporating a dose uncertainty cannot degrade the plan any further. This is exactly the situation for Case # 3; TCP is zero regardless of the number of histories used in the simulation.

The high spatial dose heterogeneity found in Case # 3 may be the result of low density regions within the PTV. Within a head-and-neck region a PTV contoured during the planning process may span a number of unavoidable air cavities; as a result, the PTV dose distribution will include low dose elements associated with the low density voxels. The result of having low dose elements within the PTV may be a substantial decrease in the radiobiological evaluation. This detail reveals the importance of using GTV in the evaluation of TCP but also highlights that combined methods of evaluation should be used in routine evaluation.

Note that for each modelled treatment the EUSD reduction is solely due to the decreasing number of electron histories and does not incorporate any physical dose uncertainties in the evaluation. If a physical dose uncertainty was to be included in

		PTV # 1		PTV # 2		PTV # 3	
History Number	Dose Uncertainty	EUSD	TCP	EUSD	TCP	EUSD	TCP
100×10^6	$\backsim 2\%$	51.14	0.897	54.03	0.968	28.90	0.000
10×10^6	$\backsim 5\%$	49.42	0.823	51.67	0.927	24.81	0.000
2×10^6	$\backsim 10\%$	38.58	0.000	39.76	0.000	19.94	0.000

Table 5.4: EUSD and TCP calculated for the three Monte Carlo calculated IMRT treatment plans. In each case the values were calculated with $\alpha = 0.30$ Gy^{-1}, $\alpha/\beta = 10.0$ Gy and $\rho = 10^7$ cm^{-3}.

the evaluation the radiobiological reduction would be greater.

In general, the dose distribution within the PTV will not be uniform. In using our analytic approach we assumed a theoretical non-unifrom dose distribution where the voxel dose was sampled from a Gaussian distribution. In evaluating the clinical IMRT treatment plans the Case specific spatial dose heterogeneity must be incorporated into the analytic evaluation. To account for the unavoidable spatial inhomogeneity the dose distribution calculated with 100 million electron histories will be considered equivalent to a PTV dose distribution with no statistical uncertainty. Assuming the dose distribution with $\lesssim 2\%$ statistical dose uncertainty is radiobiologically equivalent to a distribution with no dose uncertainty is consistent with the results shown in Fig. 5.1; where the difference between the case of no dose uncertainty and a case of 1.0% uncertainty was shown to be negligible[3].

Shown in Fig. 5.14 are EUSD and TCP values calculated analytically for the three IMRT plans. Equations (4.18) and (4.25) were used in a similar manner as before, yet the mean dose was substituted with the low dose uncertainty EUD. Using the assumption that the $\lesssim 2\%$ simulations are equivalent to a PTV dose distribution

[3]Calculating EUSD using the 100 million electron history simulation can be considered equivalent to calculating EUD.

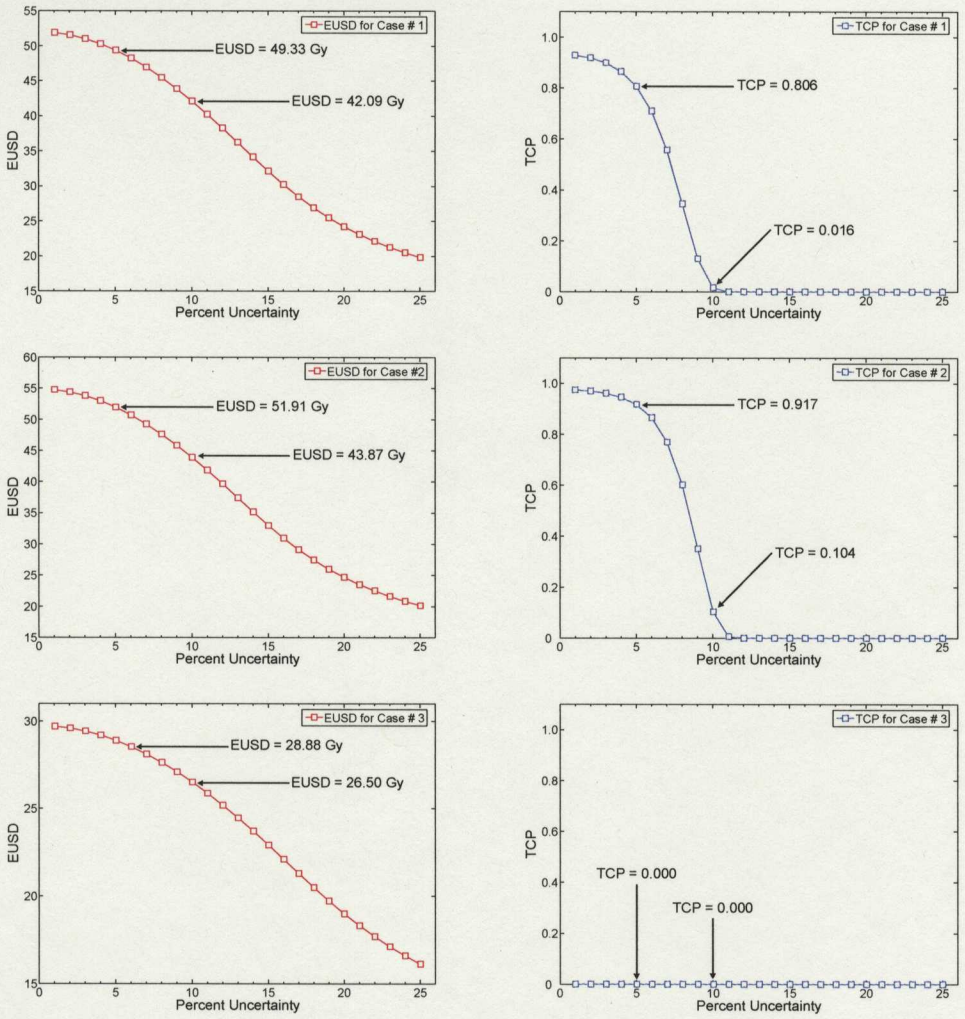

Figure 5.14: Three IMRT treatment plans evaluated using the derived formalism. The highlighted values at 5 and 10 % coincide with those in Table 5.4.

with no statistical uncertainty EUSD was used in this manner as a means of providing a single dose that characterizes the spatial PTV dose distribution. The other parameters used were as follows: $\alpha = 0.30$ Gy^{-1}, $\alpha/\beta = 10.0$ Gy, $\rho = 10^7$ cm^{-3}, $v = 0.25$ cm^3 and the number of fractions set at 25. The dose uncertainty was increased and the potential radiobiological degradation plotted in the same manner as before.

Highlighted on each graph are the values with dose uncertainties that corresponds to those given in Table 5.4. One can see that the analytic expression underestimates the EUSD and TCP reductions due to the modelled dose uncertainty increase. As the dose uncertainty increases beyond 5% the actual EUSD reduction is greater than that calculated analytically. The difference is a result of the large voxel dose uncertainty variation revealed in the dDUHs. This highlights one apparent limitation associated with the derived formalism; that only one dose uncertainty value can be input into the analytic expression. As seen in the dDUHs, the distribution of dose uncertainty is not constant throughout the PTV, as a result, any evaluation made using the analytical expression must be interpreted in context.

5.6 Interpretation of equivalent stochastic dose as a result of statistical dose uncertainty

In the previous sections we quantified the impact of dose uncertainty using the concept of an equivalent stochastic dose and tumour control probability. We have seen that the manifestation of dose variations that are either statistical or physical produce degraded radiobiological response in both tumour and tissue. If however, we assume that the modelled dose uncertainty is strictly statistical, then the results presented for each case can be interpreted as artificial with respect to the delivered dose distribution.

One example of a similar artifact is the underestimation of TCP as a function of statistical uncertainty reported by Buffa and Nahum [99]. The authors used EGS4 based Monte Carlo calculated dose distributions to quantify the reduction in TCP as a function of increased statistical uncertainty. They state the reduction was caused by a decrease in voxel dimension or a decrease in the number of simulated particle

histories. This is a natural consequence given dose uncertainty is calculated (for each voxel) as a function of 'energy depositing events' related back to the initial number of electron histories (Section 2.3.1). The statistical dose uncertainty will rise as either the initial number of electron histories is reduced or the size of each voxel is made smaller.

In a similar fashion, we can interpret the EUSD and TCP reductions found in this work as a result of an increased statistical uncertainty. The estimated change in TCP calculated using the EUSD formalism are consistent with the increased TCP, as a function of increased voxel size or number of histories, found by Buffa and Nahum. The authors found that varying the voxel size from 0.25 cm^3 to 0.5 cm^3 decreased the average dose uncertainty from approximately 10% to 3%. The relative change in TCP calculated for these same two cases was quoted at 80%. This is consistent with our findings; for the same range of dose uncertainty TCP degradation was of the same order.

To further the incorporation of statistical dose uncertainties into the evaluation of clinical Monte Carlo calculated dose distributions, Keall *et al* [100] state a 2% statistical dose uncertainty does not significantly affect isodose lines, DVHs or biological indices. The authors found a sharp drop in TCP as the standard deviation on the maximum dose in the PTV increased beyond 6%. The authors go on to state that systematic errors affect plan evaluation accuracy significantly more than random errors. From this, the authors suggest that Monte Carlo dose calculations will improve outcomes in radiation therapy as plans will be better modelled before treatment. Either way, the estimated dose uncertainty of approximately 6% is consistent with our results obtained through the implementation of TCP(EUSD).

One of the outcomes of the present work is that uncertainty levels acceptable for Monte Carlo calculated treatment plans can be found using the derived expression

(Eq. (4.25)). Using this equation, Monte Carlo uncertainty can be evaluated for any voxel or group of voxels in the dose matrix; including those within an organ at risk (OAR) and/or PTV. For the modelled dose distributions, a statistical uncertainty of 2% was found to result in an average EUSD of 98% with respect to the modelled mean dose and as the statistical uncertainty increased beyond 5% the ratio of EUSD to prescribed dose dropped rapidly. For radiosensitive tumours and late responding tissues a factor of 2 reduction in EUSD was evident when uncertainties increased to 10%.

A statistical uncertainty of 2% was found to result in a TCP not affected by the probabilistic dose heterogeneity. Consistent with the rapid drop in EUSD beyond a dose uncertainty of 5%, TCP was also found to drop significantly. These results are consistent with those presented by Keall *et al* and emphasize the importance for correct treatment plan evaluation when a statistical dose uncertainty is inherent in MC calculated dose distributions.

5.7 Interpretation of equivalent stochastic dose as a result of physical dose uncertainty

In contrast to the artificial impact of statistical dose uncertainties, physical dose uncertainties must be considered real and treatment plan evaluation procedures made to account for the probabilistic dose deposition. Generally, clinical evaluation procedures are based on static dose calculations where the CT data set is assumed to represent a spatially fixed patient. However, this assumption does not account for any of the well documented physical uncertainties due to organ motion or patient set-up. To address the limitations in static treatment planning, the derived formalism can be used to calculate an EUSD that incorporates regional dose uncertainties.

As an example of the difference between a static plan and a simulated treatment, Craig *et al* found a maximum dose error of 3%, 17% and 13% for prostate, lung and sinus treatments respectively. The authors do state that their results do not incorporate organ motion and that the quoted uncertainties could potentially be greater. Using estimates from this, and other similar studies, the impact of physical dose uncertainty due to set-up errors can be estimated without explicit simulation. The limitation of Eq. (4.25) is, of course, the assumed Gaussian form of the spatial dose distribution. Compliance to this assumption can be evaluated by producing differential dose volume histograms (dDVHs) for a planned treatment. Many dose distributions that do not cover severe tissue inhomogeneities do in fact provide near Gaussian dDVHs. Where this is not the case, the dDVH may be used as the representative distribution for $f_m(D) \otimes g(D)$ and SF(EUSD) evaluated by performing the subsequent convolution numerically.

Schaly *et al* [49] quantified possible levels of dose uncertainty due to internal organ motion for a prostate treatment. These values were calculated for single and multiple dose fractionations. For the rectum, bladder and seminal vesicles the dose uncertainty was found to be 29%, 2% and 24% over one fraction and 23%, 32% and 18% over 15 fractions respectively. Although these dose uncertainties are not associated with the tumour volume, they do show that the level of uncertainty on critical structures and organs at risk may be high and that accounting for the radiological response is important. Using the formalism presented in this work, in combination with EUD, TCP and other evaluative indices, clinical treatment plan evaluation may be made to incorporate dose uncertainties.

Physical dose uncertainties are often high in beam penumbral regions. Therefore, one application of EUSD could potentially be assessing the impact of dose uncertainty on the tissue/tumour response in penumbral regions, including critical

structures, OARs and normal tissues. Incorporating dose heterogeneities and physical dose uncertainties up to 25% ensured we covered a range of dose uncertainties that are possible for both PTV and non-PTV regions and is consistent with the range quoted by Schaly *et al* [49].

5.8 Implications of equivalent stochastic dose in treatment plan evaluation

Throughout this study we have assumed voxel dose to be a stochastic variable and established a convention to distinguish between physical and statistical dose uncertainty. Physical dose uncertainty was defined to be the result of treatment planning and/or dose delivery errors. Statistical dose uncertainty was associated exclusively with the inherent uncertainty in Monte Carlo calculated dose distributions. Given the distinction between physical and statistical dose uncertainty, the modelled reduction in EUSD can be interpreted in two ways. A reduction in EUSD that results from physical dose uncertainties can be considered real whereas the reduction due to statistical dose uncertainties seen as artificial. This is because statistical voxel dose uncertainty is not present in delivered dose distributions.

With reference made to the work of Buffa and Nahum and Keall *et al* we eluded to the possible degradation in TCP due to statistical dose uncertainties. Each of the studies focused on the reduction in TCP as a function of Monte Carlo dose uncertainty and found that the radiobiological response was degraded. Using our definitions of physical and statistical dose uncertainties, TCP as a function of ESD, could potentially be used to assess the radiobiological reduction as a function of both physical and statistical dose uncertainties concurrently.

One of the difficulties in comparing radiobiological indices (EUD, TCP and oth-

ers), calculated using different planning systems and Monte Carlo vs non-Monte Carlo algorithms, is that these radiobiological indices can be biased due to the different levels of uncertainty attributed to the calculated dose. Calculation of ESD could assist in overcoming this problem and may improve the comparison of radiobiological indices calculated with different levels of uncertainty.

This study focused on the impact dose uncertainties have on SF, EUD and TCP. Our formalism is naturally similar to EUD treatment plan evaluation and could be thought of as a natural extension to the original concept. Expansion of the work to include other evaluative methods is possible, yet the introduction of the ESD concept would require further study and will be the subject of future investigation.

An additional feature of the convolution technique presented here is the explicit inclusion of the number of fractions in the derived formalism, where the only assumption made is the probabilistic voxel dose. However, the assumption was made that all fraction doses were equal (Eq. (4.7)). Inter-fraction dose variations (van Herk [102]) were not therefore considered and the combined effect of the inter-fraction dose variations and total dose variations will be the subject of our future investigation.

Chapter 6

Conclusion

The goal of this study was to quantify the potential affects of dose uncertainty on the radiobiological treatment plan evaluation indices. As a means of evaluation we developed a formalism for assessing the impact of dose uncertainty on survival fraction at the intra and inter-voxel level. Dose uncertainties are divided into two categories: physical and statistical. Physical dose uncertainty is associated with the systematic and/or random errors incurred during treatment planning and/or delivery. The dose uncertainty associated with Monte Carlo calculated dose distributions are deemed statistical and noted as artificial with respect to the actual delivered dose. We refer to all dose uncertainties that arise from either calculation or delivery as stochastic. In addition to the designation between physical and statistical dose uncertainty, we make a distinction between spatial and probabilistic dose heterogeneity; the later being an artificial dose heterogeneity resulting from physical or statistical dose uncertainties.

To account for voxel dose uncertainty, we calculate the mean expected survival fraction for random dose deposition. Mathematically, the expression for the mean survival fraction is identical to that used by Niemierko in defining EUD. To distinguish between spatial and probabilistic dose variations, we define *equivalent stochastic dose* (ESD), as a voxel dose that gives the mean expected survival fraction for the

randomly deposited dose. For a probability density function $f(D)$, that represents the probabilistic voxel dose, SF(ESD) can be calculated by convolving $SF(D)$ with $f(D)$. In the case where the probability density function follows a Gaussian distribution, an analytic expression is derived for SF(ESD). The derived expression is verified using the Monte Carlo method and ESD values calculated with varied radiosensitivities for cases of 60 Gy and 70 Gy at 2 Gy per fraction. The analytic expression is also extended to account for a multi-voxel dose distribution that incorporates both probabilistic and spatial dose heterogeneities.

To account for probabilistic dose variations in TCP plan evaluation, we incorporate SF(ESD) into the calculation. At the intra-voxel level TCP was calculated as a function of the mean expected survival fraction which was evaluated analytically using the derived expression. To assess the impact of intra-voxel dose uncertainty and probabilistic inter-voxel mean dose fluctuations, we use the TCP model proposed by Niemierko and Goitein. The derived formalism was extended to account for both probabilistic and spatial dose heterogeneities on the calculation of TCP. The calculations were verified using the Monte Carlo method for cases of 60 and 70 Gy at 2 Gy per fraction for various combinations of radiosensitivities and cell densities.

The results show that the mean expected survival fraction increases with an increased dose uncertainty. This reduction was found to depend on the radiobiological parameters attributed to tissue and tumour. For dose uncertainties below approximately 5% the relative reduction in ESD was found to be less than 10%, when compared to the prescribed mean dose. However, as the dose uncertainty increased, the relative reduction increased non-linearly. In fact, at a dose uncertainty of 25% the ratio of ESD to mean prescribed dose was reduced by approximately 65%. Incorporating both probabilistic and spatial dose heterogeneities the relative reduction in EUSD to prescribed mean dose was reduced further. For a spatially non-uniform dose

distribution that included a dose uncertainty of 25%, the ratio of EUSD to prescribed mean dose reduced by approximately 80 %.

Using the ESD formalism, dose uncertainty was incorporated into the calculation of TCP. Incorporating SF(ESD) in the calculation of TCP revealed unique evaluative characteristics due to the modelled dose uncertainty. For various combinations of cell radiosensitivity and density the incorporation of an intra-voxel dose uncertainty resulted in a reduced TCP. For the various parameter combinations the reduction from TCP= 1 to TCP= 0 occurred at very distinct levels of dose uncertainty and in some cases the transition was very sharp.

Using either evaluative index the potential impact of both statistical and physical dose uncertainties can be quantified. Given that ESD can be interpreted as an extension of EUD, our formalism can easily be incorporated into current treatment plan evaluation methods. With the segregation of statistical and physical dose uncertainties, there is inherent in the application of ESD a layer of detail that could potentially become important as Monte Carlo methods become clinically viable. To date, most Monte Carlo dose calculations are used as a validation method for planned treatments. However, as Monte Carlo dose calculations are incorporated into the iterative methods used in treatment planning, an evaluative index that simultaneously combines both statistical and physical dose uncertainties in one formalism may become important. It is possible that the ESD concept presented in this work may satisfy this need.

Appendix A

Using the derived analytic expression in the evaluation of EUD

In developing the concept of an equivalent stochastic dose we calculated the mean expected survival fraction using Eq.(??). Note that the derived expression for the mean expected survival fraction, for the random voxel dose, is identical to Eq. (3.6) developed by Niemierko in defining EUD. Although the expressions are mathematically the same there is an important conceptual difference in interpretation.

Though mathematically identical, the difference between Eqs. (??) and (3.6) is that ESD is derived for a given random distribution of voxel dose and therefore is a probabilistic quantity. On the other hand, EUD was originally derived to account for non-uniform physical dose distributions and as a result is manifested as a physical quantity.

In this work we have categorized physical and probabilistic dose heterogeneity such that a physical dose heterogeneity was defined to be the result of physical inter-voxel dose non-uniformity, and a probabilistic dose heterogeneity defined to be the result of both physical and statistical dose uncertainties. Using these definitions one can see that EUD is an index used to quantify the radiobiological impact of a

physical dose heterogeneity; where as ESD is used to quantify the radiobiological impact of a probabilistic dose heterogeneity. Our convention will be to account for probabilistic dose heterogeneity through the use of ESD and EUSD but note that EUD could potentially comprise both spatial and probabilistic dose non-uniformity with an amended definition.

As noted, Eq. (??) is mathematically identical to that developed by Niemierko in defining EUD. Therefore, we can calculate an *equivalent uniform dose* for a given spatial dose distribution $g(D)$, such that

$$SF(EUD) = SF(D) \otimes g(D) \tag{A.1}$$

which is consistent with our inclusion of a physical dose heterogeneity in defining EUSD.

Appendix B

Published papers derived from this work

Included in this Appendix are the most recent published papers derived from this work.

G Cranmer-Sargison and S Zavgorodni (2005) EUD-based radiotherapy treatment plan evaluation: incorporating physical and Monte Carlo statistical dose uncertainties *Phys. Med. Biol.* **50** 4097-4109

TB, PBM, PMB/195849, 23/06/2005

INSTITUTE OF PHYSICS PUBLISHING PHYSICS IN MEDICINE AND BIOLOGY

Phys. Med. Biol. **50** (2005) 1–13 doi:10.1088/0031-9155/50/0/000

EUD-based radiotherapy treatment plan evaluation: incorporating physical and Monte Carlo statistical dose uncertainties

G Cranmer-Sargison[1] and S Zavgorodni[1,2]

[1] Department of Physics and Astronomy, University of Victoria, Victoria, BC, Canada
[2] Department of Medical Physics, British Columbia Cancer Agency, Vancouver Island Centre, Victoria, BC, Canada

E-mail: gcranmer@uvic.ca

Received 4 March 2005, in final form 2 June 2005
Published DD MMM 2005
Online at stacks.iop.org/PMB/50/1

Abstract

The purpose of this work is to quantify the impact of dose uncertainty on radiobiologically based treatment plan evaluation. Dose uncertainties are divided into two categories: physical and statistical. Physical dose uncertainty is associated with the systematic and/or random errors incurred during treatment planning and/or delivery. The dose uncertainty associated with Monte Carlo calculated dose distributions is deemed statistical and noted as artificial with respect to the actual delivered dose. We will refer to all dose uncertainties that arise from either calculation or delivery as stochastic. Both physical and statistical dose uncertainties are considered at the intra- and inter-voxel levels. To account for voxel dose uncertainty, we calculate the mean survival fraction (SF) for the random dose deposition. Mathematically, the expression for the mean survival fraction is identical to that used by Niemierko (1997 *Med. Phys.* **24** 103–10) in defining equivalent uniform dose (EUD). To distinguish between spatial and probabilistic dose variations, we define *equivalent stochastic dose* (ESD) as a voxel dose that gives the mean expected survival fraction for the randomly deposited dose. For a probability density function $f(D)$, that represents the probabilistic voxel dose, SF(ESD) can be calculated by convolving SF(D) with $f(D)$. In the case where the probability density function follows a Gaussian distribution, an analytic expression is derived for SF(ESD). The derived expression is verified using the Monte Carlo method and ESD values calculated with varied radiosensitivities for cases of 60 and 70 Gy at 2 Gy per fraction. The analytic expression is also extended to account for a multi-voxel dose distribution that incorporates a spatial dose heterogeneity. The results show that survival fraction increases with an increased dose uncertainty. This reduction depends on radiobiological parameters attributed to tissue and tumour. For tissue, ESD drops to 55% of

0031-9155/05/000001+13$30.00

the mean physical dose when the dose has a 10% intra- and inter-voxel dose uncertainty and inhomogeneity.

(Some figures in this article are in colour only in the electronic version)

1. Introduction

There are a number of inherent uncertainties in all radiotherapy treatment planning and delivery. Two broad categorizations can be made to separate the uncertainties that result from the planning process with those due to treatment delivery. Treatment planning uncertainties can encompass patient CT data set limitations (Gagné and Robinson 2004), the assumed static nature of clinical treatment plans (Booth and Zavgorodni 2001, Craig *et al* 2003 and Schaly *et al* 2004) as well as the statistical uncertainty associated with Monte Carlo (MC) dose calculation algorithms (Verhaegen and Seuntjens 2003). Accounting for dose uncertainties that are either physical or statistical has become an important issue in modern radiotherapy.

Treatment delivery uncertainties are essentially geometric in nature and are mainly due to patient set-up errors. Many have investigated the application and limitation of convolution techniques in modelling the impact of patient position uncertainties on delivered dose distributions (Leong 1987, Lujan *et al* 1999, Zavgorodni 2000, McCarter and Beckham 2000). To extend the convolution technique to Monte Carlo calculated dose distributions, Beckham *et al* (2002) investigated the difference between fluence convolution and dose matrix convolution. As an extension of this work, Stapleton *et al* (2005) implemented the fluence-convolution method to include Monte Carlo calculated dynamic IMRT treatment plans.

The inherent statistical uncertainty associated with MC calculated dose arises from the random sampling used and is therefore not present in dose distributions calculated using analytic techniques. In fact, the uncertainty manifests itself as an artificial increase in dose heterogeneity. A number of investigators (Sempau and Bielajew 2000, Jiang *et al* 2000) have explored the effects of MC uncertainty on calculated dose distributions and dose–volume histograms (DVHs), whereas others have specifically investigated the effects of MC uncertainty on radiological predictive indices (Buffa and Nahum 2000, Keall *et al* 2000, Kawrakow 2004). It has been shown that an increase in MC statistical uncertainty broadens the DVH and results in an underestimation of the tumour control probability (TCP). It is generally agreed that an average dose uncertainty of 2% will not noticeably change TCP and as the radiosensitivity uncertainty increases, the relative impact of MC uncertainty will be reduced.

Niemierko (1997) developed the concept of *equivalent uniform dose* (EUD) as a method of summarizing and reporting inhomogeneous dose distributions. EUD is equated with a uniform dose that results in the same survival fraction as does the heterogeneous dose distribution. Ebert (2000) found that EUD varied insignificantly in comparison to TCP for time-independent factors such as cell density, cell radiosensitivity, radiosensitivity heterogeneity and α/β ratio. The author indicates that both TCP and EUD be used concurrently in the evaluation of irradiation strategies, but suggests that EUD may provide a more stable and less deceptive indicator of relative effects.

In this study we investigate the impact of radiotherapy dose uncertainty on survival fraction. Dose uncertainties are divided into two categories: physical and statistical. Physical dose uncertainty is defined to be any physically discernible uncertainty resulting from systematic and/or random errors in treatment planning and/or delivery. Statistical dose uncertainty is associated exclusively with dose distributions calculated using Monte Carlo

electron–photon transport algorithms. We will refer to all dose uncertainties that arise from either calculation or delivery as stochastic. In addition to the designation between physical and statistical dose uncertainties, we make a distinction between spatial and probabilistic dose heterogeneities; the latter being an artificial dose heterogeneity resulting from physical or statistical dose uncertainty. We developed the concept of *equivalent stochastic dose* (ESD) and derive an analytic expression for SF(ESD) as a means of assessing the impact of radiotherapy dose uncertainty. This concept allows for the combination of statistical and physical dose uncertainties in a formalism that quantifies the impact of each concurrently and demonstrates that EUD can potentially account for both spatial and probabilistic dose non-uniformities with an amended definition.

2. Methods

2.1. Mean survival fraction for random voxel dose

Consider a stochastic process, where the total dose delivered to a voxel is a random event. Given the random nature of the voxel dose, we can estimate the mean expected survival fraction as

$$\overline{\mathrm{SF}}(\{D_i\}) = \frac{1}{N}\sum_{i=1}^{N}\mathrm{SF}(D_i), \tag{1}$$

where N is the number of sampled D_i from a probability density function $f_v(D)$ that represents the probabilistic dose to a voxel. The survival fraction can be calculated, in the simplest case, as

$$\mathrm{SF}(D_i) = \exp\left\{-\alpha D_i - \frac{\beta}{n}D_i^2\right\}, \tag{2}$$

where α and β are the radiosensitivity parameters and n is the number of fractions in a planned treatment (Fowler 1989).[3]

Equation (1) is mathematically identical to that developed by Niemierko (1997) in defining *equivalent uniform dose*. In a similar fashion, we define *equivalent stochastic dose* as the dose to a voxel that results in a mean expected survival fraction given a set of random events depositing doses D_i according to a probability density function $f_v(D)$. Given this definition, SF(ESD) can be written as

$$\mathrm{SF(ESD)} = \overline{\mathrm{SF}}(\{D_i\}). \tag{3}$$

Using equations (2) and (3), an expression for ESD is obtained, such that

$$\mathrm{ESD} = \frac{1}{2}\sqrt{\frac{\alpha^2 n^2}{\beta^2} - \frac{4n}{\beta}\ln\{\overline{\mathrm{SF}}(\{D_i\})\}} - \frac{n\alpha}{2\beta}. \tag{4}$$

Note that in this definition of ESD, the probability density function $f_v(D)$ and the mean voxel dose are assumed to be known.

When N is large, the calculation of $\overline{\mathrm{SF}}(\{D_i\})$ and therefore SF(ESD), results in a convolution,

$$\mathrm{SF(ESD)} = \mathrm{SF}(D) \otimes f_v(D). \tag{5}$$

[3] Cell proliferation is not considered in this paper for the sake of simplicity. Given that cell proliferation is independent of dose, it will not alter the results presented in this work.

Similarly, an *equivalent uniform dose* can be calculated for a given spatial dose distribution $g(D)$, such that

$$\mathrm{SF(EUD)} = \mathrm{SF}(D) \otimes g(D). \tag{6}$$

Though mathematically identical, the difference between equations (5) and (6) is that ESD is derived for a given stochastic distribution of voxel dose and therefore is a probabilistic quantity, whereas EUD has been derived for a physical dose distribution and as a result is manifested as a physical quantity. For the purpose of this paper, we will account for probabilistic dose heterogeneity through the use of ESD. We note that EUD can potentially comprise both spatial and probabilistic dose non-uniformities with an amended definition.

So far we have only considered ESD for a single voxel and have shown this to be mathematically equivalent to convolving $\mathrm{SF}(D)$ with $f_{\mathrm{v}}(D)$. Now, let us look at a multi-voxel distribution where the dose in each voxel is random. Given the assumed random nature associated with the deposited dose, each voxel dose will converge to a different random value D_k that is distributed with a probability density function $f_{\mathrm{m}}(D)$. Using equation (5) with D_k, survival fractions $\mathrm{SF}(\mathrm{ESD}_k)$ can be calculated for each voxel (producing a distribution of ESD_k). The mean expected survival fraction for a multi-voxel domain is then expressed as

$$\overline{\mathrm{SF}}(\{\mathrm{ESD}_k\}) = \frac{1}{M}\sum_{k=1}^{M} \mathrm{SF}(\mathrm{ESD}_k), \tag{7}$$

where M is the number of voxels in the distribution. When the number of voxels is large, calculating the mean expected survival fraction again results in convolution.

We now amend the definition of ESD given in equation (5) to subsume both the random voxel dose and the inter-voxel ESD uncertainty by including the probability density function $f_{\mathrm{m}}(D)$ of D_k. So far equation (5) has reflected the probabilistic nature of the intra-voxel dose, assuming that the mean voxel dose was known. Now, survival fraction has to be further convolved with $f_{\mathrm{m}}(D)$ to reflect the variability in the mean values of the voxel dose. As a result, the equivalent stochastic dose for spatially uniform multi-voxel distribution subject to voxel dose uncertainty becomes

$$\mathrm{SF(ESD)} = \mathrm{SF}(D) \otimes f_{\mathrm{v}}(D) \otimes f_{\mathrm{m}}(D). \tag{8}$$

This shows that the statistical dose fluctuations produce a probabilistic inter-voxel dose heterogeneity in ESD_k, that can be accounted for in a similar fashion to a physical dose heterogeneity (equation (6)).

Given a dose distribution that is spatially not uniform, another distribution representing the physical dose heterogeneity can be included in equation (8). We define an *equivalent uniform stochastic dose* (EUSD) that encompasses random voxel dose, inter-voxel noise as well as a spatial dose non-uniformity. The survival fraction associated with EUSD, for a known spatial dose distribution is then

$$\mathrm{SF(EUSD)} = \mathrm{SF}(D) \otimes f_{\mathrm{v}}(D) \otimes f_{\mathrm{m}}(D) \otimes g(D), \tag{9}$$

where $g(D)$ represents the physical distribution of dose about a mean and is easily derived from the differential dose–volume histogram (dDVH) generated by a commercial treatment planning system. Note that equation (8) is just a special case of equation (9) and that multi-voxel dose distributions should, in general, be evaluated using EUSD.

2.2. An analytic expression for mean survival fraction for stochastically deposited dose

Let us develop a specific case of equation (5) where the probability density function is assumed Gaussian with a mean dose D, such that

$$f(D - D'; \sigma^2) = \frac{1}{\sqrt{2\pi}\sigma} \exp\left\{-\frac{(D - D')^2}{2\sigma^2}\right\}, \tag{10}$$

where σ is the standard deviation. If we now substitute equations (2) and (10) into equation (5), the survival fraction associated with the *equivalent stochastic dose* becomes

$$\mathrm{SF(ESD)} = \frac{1}{\sqrt{2\pi}\sigma} \int \exp\left\{-\alpha D' - \frac{\beta}{n} D'^2 - \frac{(D - D')^2}{2\sigma^2}\right\} \mathrm{d}D' \tag{11}$$

$$= \frac{1}{\sqrt{2\pi}\sigma} \int \exp\left\{-\left[D'^2\left(\frac{\beta}{n} + \frac{1}{2\sigma^2}\right) + D'\left(\alpha - \frac{D}{\sigma^2}\right) + \frac{D^2}{2\sigma^2}\right]\right\} \mathrm{d}D'. \tag{12}$$

Upon integration over all positive dose values ($0 \leqslant D' \leqslant \infty$), an analytic solution is found, giving

$$\mathrm{SF(ESD)} = \frac{1}{2^{3/2}\sigma}\left(\frac{\beta}{n} + \frac{1}{2\sigma^2}\right)^{-1/2}\left(1 - \mathrm{erf}\left(\frac{\alpha - \frac{D}{\sigma^2}}{2\sqrt{\frac{\beta}{n} + \frac{1}{2\sigma^2}}}\right)\right)$$

$$\times \exp\left\{\frac{\left(\left(\alpha - \frac{D}{\sigma^2}\right)^2 - 4\left(\frac{\beta}{n} + \frac{1}{2\sigma^2}\right)\frac{D^2}{2\sigma^2}\right)}{4\left(\frac{\beta}{n} + \frac{1}{2\sigma^2}\right)}\right\}. \tag{13}$$

SF(ESD) can now be found knowing only the mean dose and standard deviation for each voxel, and ESD is calculated using equation (4).

It is well known that the convolution of any number of Gaussian distributions is itself Gaussian. Therefore, equation (13) can be applied to encompass a case where many random processes and a Gaussian spatial non-uniformity contribute to the calculation of survival fraction (equation (9)). A set of convolved Gaussian distributions can be represented by modifying equation (10), such that

$$f\left(D - D'; \sum \sigma_k^2\right) = \frac{1}{\sqrt{2\pi \sum \sigma_k^2}} \exp\left\{-\frac{(D - D')^2}{2\sum \sigma_k^2}\right\}, \tag{14}$$

where the standard deviation is now a sum of squares. Equation (13) can then be used to account for multiple random processes as well as spatial dose non-uniformities such that σ^2 represents the combined variance of the individual processes $\left(\sigma^2 = \sum \sigma_k^2\right)$. An example of this would be the case where $f_{\mathrm{v}}(D)$, $f_{\mathrm{m}}(D)$ and $g(D)$ of equation (9) each take the form of a Gaussian.

2.3. Verification of ESD equation using the Monte Carlo method

The derivation and implementation of equation (13) was verified using Monte Carlo modelling. This verification was performed for three cases: modelling a randomly deposited voxel dose, modelling a uniform dose delivered randomly to a multi-voxel phantom and modelling a randomly delivered spatially non-uniform dose to a multi-voxel phantom.

To model a voxel dose delivered through a stochastic process, values of D_{v} were randomly generated 1.0×10^5 times from a Gaussian probability density function $f_{\mathrm{v}}(D)$. The simulation was run with a standard deviation that increased in 0.5% increments from 0.5% to 25%. The

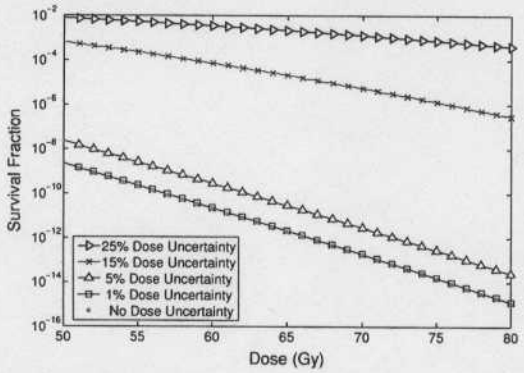

Figure 1. SF as a function of dose for various levels of statistical uncertainty calculated using equation (13). The modelled treatment was fixed at 2 Gy per fraction, with $\alpha = 0.30\ \mathrm{Gy}^{-1}$ and $\alpha/\beta = 10$ Gy. The SF with no dose uncertainty was calculated using the LQ equation (equation (2)).

mean expected survival fraction was calculated at each level of uncertainty and compared to that predicted by equation (13). This range was chosen to cover potential physical and statistical dose uncertainties not only in the PTV, but also in any organs at risk (OARs), where both physical (due to beam penumbra) and statistical (due to lower number of particles transported through these regions) uncertainties are usually higher.

As a further test, an inter-voxel ESD uncertainty was introduced into a multi-voxel phantom. Each mean voxel dose (D_{m}) was first sampled from a Gaussian distribution $f_{\mathrm{m}}(D)$ centred about a uniform multi-voxel mean dose D. To represent a volume of interest, the number of voxels was fixed at $j = 2.5 \times 10^3$. To model voxel dose uncertainty, values of D_{v} were randomly generated 1.0×10^5 times from a Gaussian probability density function $f_{\mathrm{v}}(D)$ centred about D_{m}. The standard deviation of $f_{\mathrm{v}}(D)$ was assumed to be equal to that of $f_{\mathrm{m}}(D)$. The mean expected survival fraction was calculated for each level of uncertainty and compared to that predicted using equation (13) where the total variance incorporated both the variance of $f_{\mathrm{v}}(D)$ and $f_{\mathrm{m}}(D)$.

In a similar manner to Ebert (2000), a spatially Gaussian heterogeneous dose distribution was also modelled. The standard deviation of the physical dose distribution was taken to be the same as that of the statistical distributions $f_{\mathrm{v}}(D)$ and $f_{\mathrm{m}}(D)$. The mean values of this normally distributed multi-voxel dose (D_{g}) were sampled 2.5×10^3 times from a Gaussian distribution centred on the prescribed mean dose D. The inter-voxel ESD uncertainty and intra-voxel dose uncertainty were each modelled as above. The results were compared with those derived using equation (13) noting that the variance was now the sum of three variances.

3. Results

Using equation (13) the survival fraction was calculated for a clinically relevant dose range with increasing levels of uncertainty (figure 1). The calculated survival fractions respond as expected given the mathematically equivalent (equations (5) and (6)) and well-documented effect of dose heterogeneity on SF. One can see that the difference between the case of no dose uncertainty and the case of 1.0% uncertainty is negligible, but as the dose uncertainty increases to 25% the SF increases by ~7 orders of magnitude. With a dose uncertainty increase, the

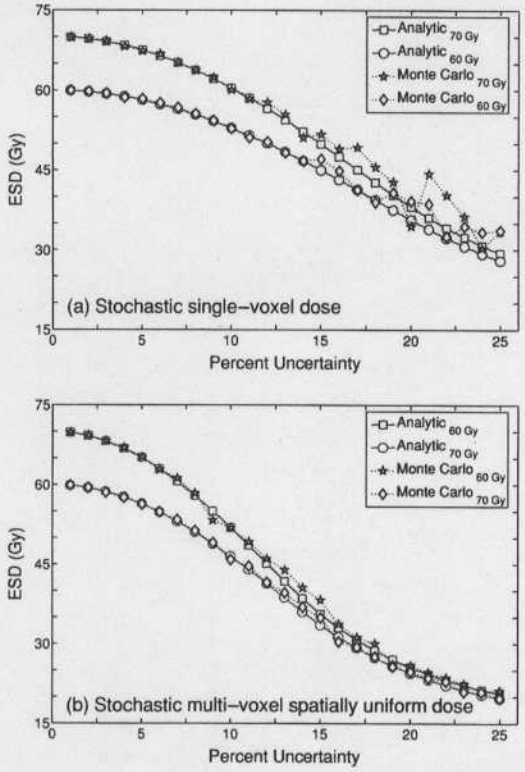

Figure 2. (a) ESD for a single voxel, where dose is stochastically deposited and therefore has an associated uncertainty. (b) Multi-voxel uniform dose distribution modelled with an inter-voxel noise and an intra-voxel uncertainty. The additional impact of the inter-voxel noise can be seen when compared to the graph above. In both cases, the ESD reduction due to the dose uncertainties is evident and is correctly modelled using the derived expression.

slope of the SF curve flattens and represents a reduction in cell kill with respect to higher voxel dose. Analogous to the effect of spatial dose heterogeneity (Tomé and Fowler 2002), an increase in dose uncertainty gives a greater probability of low dose values, producing 'probabilistic cold spots' that result in a reduced biological effect. The declining slope of SF highlights the fact that 'probabilistic cold spots' have a large impact on overall cell kill while 'probabilistic hot spots' have minimal impact. This is similar to the results presented by Halloway *et al* (2002) for a modelled spatial dose heterogeneity.

Figure 2 represents a comparison between ESD calculated using equation (13) with that obtained from modelling, using the Monte Carlo method, dose deposited to (a) a single voxel and (b) a multi-voxel phantom. One can see that the derived expression correctly accounts for the modelled stochastic voxel dose in both cases. At increased levels of dose uncertainty, the impact of the stochastic process is evident in the reduced ESD. In fact, as the voxel dose uncertainty increases, the difference between the two cases of 60 and 70 Gy decreases; the reduction being the result of the non-linear response of SF to dose variations. The increased probability in a low voxel dose precipitates the effect more readily at 70 Gy than at 60 Gy and emphasizes the need for accurate voxel dose uncertainty estimation.

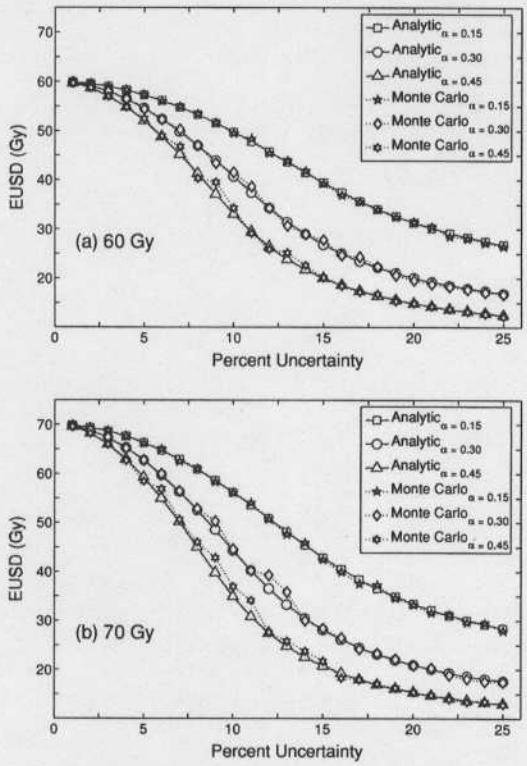

Figure 3. EUSD for a Gaussian dose distribution modelled with an inter-voxel noise and an intra-voxel uncertainty. The derived expression and sampled data are in excellent agreement and show the impact of the dose heterogeneity, inter-voxel noise and voxel dose uncertainty for various α values ($\alpha/\beta = 10.0$). Shown are cases with mean dose of (a) 60 Gy and (b) 70 Gy at 2 Gy per fraction.

Figure 2(b) shows that as the standard deviations in the intra- and inter-voxel dose distributions increase, a substantial reduction in ESD occurs. If we assume the modelled uncertainty is strictly statistical, then the results for this case can be interpreted as the reduction in EUD for a spatially uniform, multi-voxel dose distribution subject to Monte Carlo uncertainty.

Shown in figures 3 and 4 are calculated (equation (13)) and Monte Carlo generated data for a spatial dose non-uniformity that incorporates inter- and intra-voxel uncertainties. Obviously, equation (13) correctly models the spatial non-uniformity and is capable of simulating both stochastic and spatial dose heterogeneities. Incorporating a spatial non-uniformity to the modelled multi-voxel distribution results in a further reduction in EUSD when compared to the spatially uniform case. In addition, figures 3 and 4 each show the effect stochastic dose uncertainties have on tumour and tissues with different α and α/β values. One can see that the derived expression is valid for the various radiosensitivities used in this work.

Table 1 displays the ratios of EUSD to a planned homogeneous mean dose of 60 and 70 Gy at 2 Gy per fraction. It is apparent that dose uncertainty has a greater effect on radiosensitive tumours and less effect on radioresistant tumours. For a dose heterogeneity and uncertainty

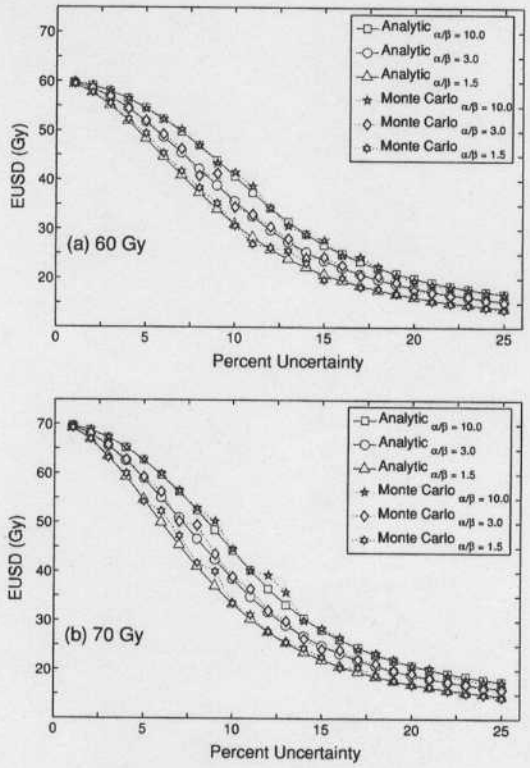

Figure 4. EUSD for a Gaussian dose distribution modelled with an inter-voxel noise and an intra-voxel uncertainty. The derived expression and sampled data are in excellent agreement and show the impact of the dose heterogeneity, inter-voxel noise and voxel dose uncertainty for various α/β values ($\alpha = 0.30$). Shown are cases with mean dose of (a) 60 Gy and (b) 70 Gy at 2 Gy per fraction.

Table 1. Relative EUSD taken with respect to the prescribed homogeneous mean dose of 60 and 70 Gy for various α values ($\alpha/\beta = 10.0$). The physical dose distribution is considered Gaussian with a standard deviation equivalent to the level of dose uncertainty.

	Relative EUSD 60 Gy treatment plan			Relative EUSD 70 Gy treatment plan		
Standard	α (Gy^{-1})			α (Gy^{-1})		
deviation (%)	0.15	0.30	0.45	0.15	0.30	0.45
2	0.992	0.985	0.977	0.991	0.983	0.974
5	0.955	0.906	0.867	0.947	0.896	0.847
10	0.829	0.692	0.552	0.803	0.633	0.499
15	0.657	0.462	0.334	0.612	0.402	0.296
25	0.447	0.280	0.208	0.406	0.252	0.185

of 2%, the relative difference between the mean dose and EUSD is on average 2%, but the difference inflates to a point where a dose heterogeneity and uncertainty of 25% results in

Table 2. Relative EUSD taken with respect to the prescribed homogeneous mean dose of 60 and 70 Gy for various α/β values ($\alpha = 0.30$). The physical dose distribution is considered Gaussian with a standard deviation equivalent to the level of dose uncertainty.

	Relative EUSD 60 Gy treatment plan			Relative EUSD 70 Gy treatment plan		
Standard deviation (%)	α/β (Gy) 1.5	3.0	10.0	α/β (Gy) 1.5	3.0	10.0
2	0.963	0.976	0.985	0.965	0.972	0.983
5	0.807	0.863	0.906	0.782	0.843	0.895
10	0.517	0.594	0.692	0.477	0.550	0.633
15	0.415	0.394	0.462	0.315	0.356	0.402
25	0.233	0.257	0.280	0.211	0.231	0.252

a reduction in EUSD by 75%. Comparing the cases of 60 and 70 Gy, one can see that the relative reduction in EUSD is more significant for higher dose.

Table 2 displays the ratio of EUSD to the modelled homogeneous mean dose of 60 and 70 Gy for $\alpha/\beta = 1.5, 3.0$ and 10.0 Gy^{-1}. One can see that as the α/β ratio increases, the relative EUSD also increases. This indicates that the dose variations are affecting late responding tissues to a greater degree than the early responding ones. For each level of probabilistic dose heterogeneity and voxel dose uncertainty, the variation of the α/β ratio affects EUSD less than variations in α. This is due to the high number of fractions (30 and 35) used in each case and is consistent with the known relative importance between α and β values in fractionated treatments.

4. Discussion

Throughout this study we have assumed voxel dose to be a stochastic variable and established a convention to distinguish between physical and statistical dose uncertainties. Physical dose uncertainty has been defined to be the result of treatment planning and/or dose delivery errors. Whereas, statistical dose uncertainty has been associated exclusively with the inherent uncertainty in Monte Carlo calculated dose distributions. Given the distinction between physical and statistical dose uncertainties, the modelled reduction in EUSD can be interpreted in two ways. A reduction in EUSD that results from physical dose uncertainties is considered real whereas the reduction due to statistical dose uncertainties seen as artificial. This is because statistical voxel dose uncertainty is not present in delivered dose distributions.

One example, of such an artefact, is the underestimation of TCP as a function of statistical uncertainty reported by Buffa and Nahum (2000). The authors state that this was caused by the decrease in voxel dimension or a decrease in the number of particle histories. Similarly, the EUSD reduction in our case can be seen as a result of increased statistical uncertainty and would therefore be an artefact of a Monte Carlo simulation.

Keall *et al* (2000) established that a 2% statistical dose uncertainty does not significantly affect isodose lines, DVHs or biological indices, and found a sharp drop in TCP as the standard deviation on D_{max} increased beyond 6%. One of the outcomes of the present paper is that uncertainty levels acceptable for Monte Carlo calculated treatment plans can be found by using the derived expression (equation (13)). Using this equation, MC uncertainty can be evaluated for any voxel or group of voxels in the dose matrix, including those within an organ at risk (OAR) and/or PTV. For the modelled dose distributions, a statistical uncertainty

of 2% was found to result in an average EUSD of 98% with respect to the modelled mean dose, and as the statistical uncertainty increased beyond 5%, the ratio of EUSD to prescribed dose dropped rapidly. For radiosensitive tissues and late responding tumours, a factor of 2 reduction was evident when uncertainties increased to 10% (tables 1 and 2). These results are consistent with those presented by Keall *et al* and emphasize the importance for correct treatment plan evaluation when a statistical dose uncertainty is inherent in MC calculated dose distributions.

In contrast to the artificial impact of statistical uncertainties on EUSD, physical dose uncertainty must be considered real and treatment plan evaluation procedures made to account for the probabilistic dose deposition. Generally, clinical evaluation procedures are based on static dose calculations where the CT data set is assumed to represent a spatially fixed patient. However, this assumption does not account for any of the well-documented physical dose uncertainties. To address the limitations in static treatment planning, the derived formalism can be used to calculate an EUSD that incorporates regional dose uncertainties.

As an example of the difference between a static plan and a simulated treatment, Craig *et al* (2003) found a maximum dose error of 3%, 17% and 13% for a prostate, lung and sinus treatments, respectively. Craig *et al* state that their results do not incorporate organ motion and that the quoted uncertainties could potentially be greater. Using estimates from this and other similar studies, the impact of physical dose uncertainty due to organ motion and set-up errors can be estimated without explicit simulation. The limitation of equation (13) is, of course, the assumed Gaussian form of the spatial dose distribution. Compliance to this assumption can be evaluated by producing differential dose–volume histograms (dDVHs) for a planned treatment. Many dose distributions that do not cover severe tissue inhomogeneities do in fact provide near Gaussian dDVHs. Where this is not the case, EUSD can be evaluated numerically using equation (9).

Physical dose uncertainties are often high in beam penumbral regions. Therefore, one application of EUSD could potentially be assessing the impact of dose uncertainty on the tissue/tumour response in penumbral regions, including critical structures, OARs and normal tissues. Incorporating physical dose heterogeneities and physical dose uncertainties up to 25% ensured that we covered a range of dose uncertainties that are possible for both PTV and non-PTV regions.

One of the difficulties in comparing radiobiological indices (EUD, TCP, NTCP and others), calculated using different planning systems and Monte Carlo versus non-Monte Carlo algorithms, is that these radiobiological indices can be biased due to the different levels of uncertainty attributed to the calculated dose. Calculation of ESD could assist in overcoming this problem and may improve the comparison of radiobiological indices calculated with different levels of uncertainty.

This study focused on the effects dose uncertainties have on SF and EUD. Our formalism is naturally similar to, and could be treated as an extension of the EUD concept. It also readily accommodates GEUD (Niemierko 1999). Expansion of the work to include TCP and NTCP is possible, yet the introduction of the ESD concept into TCP (Webb and Nahum 1993, Niemierko and Goitein 1993) and NTCP models requires further study and will be the subject of future investigation.

An additional feature of the convolution technique presented here is the explicit inclusion of the number of fractions in the derived formalism, where the only assumption made is the probabilistic voxel dose. However, the assumption was made that all fraction doses were equal (equation (2)). Inter-fraction dose variations (van Herk 2003 and Zavgorodni 2004) were not therefore considered and the combined effect of the inter-fraction dose variations and total dose variations will be the subject of our future investigation.

5. Conclusion

In this work, statistical and physical dose uncertainties have been combined in a formalism that describes both concurrently. MC dose uncertainty is deemed statistical whereas any dose uncertainty that results from treatment planning and/or dose delivery errors is grouped as physical. The effect of probabilistic dose deposition that results from either category of dose uncertainty can be quantified by defining an *equivalent stochastic dose* as the dose that results in a mean survival fraction for a given random event. The formalism simultaneously accounts for a spatial dose heterogeneity and can therefore be used in the evaluation of radiotherapy treatment plans.

Acknowledgments

The authors would like to acknowledge Andrew Jirasek, Karl Bush and Wayne Beckham for their valuable discussions and comments during the preparation of this manuscript.

References

Beckham W A, Keall P J and Siebers J V 2002 A fluence-convolution method to calculate radiation therapy dose distributions that incorporate random set-up error *Phys. Med. Biol.* **47** 3465–73

Booth J T and Zavgorodni S F 2001 Modelling the dosimetric consequences of organ motion at CT imaging on radiotherapy treatment planning *Phys. Med. Biol.* **46** 1369–77

Buffa F M and Nahum A E 2000 Monte Carlo dose calculations and radiobiological modelling: analysis of the effect of the statistical noise of the dose distributions on the probability of tumour control *Phys. Med. Biol.* **45** 3009–23

Craig T, Battista J and Van Dyk J 2003 Limitations of a convolution method for modeling geometric uncertainties in radiation therapy: I. The effect of shift invariance *Med. Phys.* **30** 2001–11

Ebert M A 2000 Viability of the EUD and TCP concepts as reliable dose indicators *Phys. Med. Biol.* **45** 441–57

Fowler J F 1989 The linear-quadratic formula and progress in fractionated radiotherapy *Br. J. Radiol.* **62** 679–94

Gagné I M and Robinson D M 2004 The impact of tumor motion upon CT image integrity and target delineation *Med. Phys.* **31** 3378–92

Holloway L, Hoban P and Metcalfe P 2002 Radiobiological indices that consider volume: a review *Australas. Phys. Eng. Sci. Med.* **25** 47–57

Jiang S B, Pawlicki T and Ma C M 2000 Removing the effect of statistical uncertainty on dose–volume histograms from Monte Carlo dose calculations *Phys. Med. Biol.* **45** 2151–61

Kawrakow I 2004 The effect of Monte Carlo statistical uncertainty on the evaluation of dose distributions in radiation therapy planning *Phys. Med. Biol.* **49** 1549–56

Keall P J, Jeraj R and Mohan R 2000 The effect of dose calculation uncertainty on the evaluation of radiotherapy plans *Med. Phys.* **27** 478–84

Leong J 1987 Implementation of random positioning error in computerised radiation treatment planning systems as a result of fractionation *Phys. Med. Biol.* **32** 327–34

Lujan A, Ten Haken R Larsen E and Balter J 1999 Quantization of setup uncertainties in 3D dose calculations *Med. Phys.* **26** 2397–402

McCarter S D and Beckham W A 2000 Evaluation of the validity of a convolution method for incorporating tumour movement and set-up variations into radiotherapy treatment planning system *Phys. Med. Biol.* **45** 923–31

Niemierko A 1997 Reporting and analyzing dose distributions: a concept of equivalent uniform dose *Med. Phys.* **24** 103–10

Niemierko A 1999 A generalized concept of equivalent uniform dose (EUD) *Med. Phys.* **26** 1100 (abstract)

Niemierko A and Goitein M 1993 Implementation of a model for estimating tumor control probability for an inhomogeneously irradiated tumor *Radiother. Oncol.* **29** 140–47

Schaly B, Kempe J A, Bauman G S, Battista J J and Van Dyk J 2004 Tracking the dose distribution in radiation therapy by accounting for variable anatomy *Phys. Med. Biol.* **49** 791–805

Sempau J and Bielajew A F 2000 Towards the elimination of Monte Carlo statistical fluctuation from dose volume histograms for radiotherapy treatment planning *Phys. Med. Biol.* **45** 131–57

Stapleton S, Zavgorodni S, Popescu I A and Beckham W A 2005 Implementation of random set-up errors in Monte Carlo calculated dynamic IMRT treatment plans *Phys. Med. Biol.* **50** 429–39

Tomé W A and Fowler J F 2002 On cold spots in tumor subvolumes *Med. Phys.* **29** 1590–98

van Herk M 2003 Biologic and physical fractionation effects of random geometric errors *Int. J. Radiat. Oncol. Biol. Phys.* **57** 1460–71

Verhaegen F and Seuntjens J 2003 Monte Carlo modelling of external radiotherapy photon beams *Phys. Med. Biol.* **48** R107–64

Webb S and Nahum A E 1993 A model for calculating tumour control probability in radiotherapy including the effects of inhomogeneous distributions if dose and clonogenic cell density *Phys. Med. Biol.* **38** 653–66

Zavgorodni S F 2000 Treatment planning algorithm corrections accounting for random setup uncertainties in fractionated stereotactic radiotherapy *Med. Phys.* **27** 685–90

Zavgorodni S F 2004 The impact of inter-fraction variations on biological equivalent dose (BED): the concept of equivalent constant dose *Phys. Med. Biol.* **49** 5333–45

Bibliography

[1] McKinnell R G, Parchment R E, Perantoni A O and Pierce G B 2000 *The Biological Basis of Cancer* Cambridge University Press, New York, NY

[2] Coutard H 1934 Principles of x-ray therapy of malignant disease *Lancent* **2** 1-8

[3] Grubbe E H 1933 Priority in the therapeutic use of x-rays *Radiology* **21** 1212-17

[4] Brady L W, Kramer S, Levitt S H, Parker R G and Powers W E 2001 Radiation Oncology: Contributions of the United States in the last years of the 20^{th} century Radiology **219** 1-5

[5] Jones L, Hoban P and Metcalfe P 2001 The use of the linear quadratic model in radiotherapy: a review *Australas. Phys. Eng. Sci. Med.* **24** 132-46

[6] del Regato J A 1995 One hundred years of radiation oncology, *Current Radiation Oncology*, Oxford University Press Inc., New York, NY

[7] Dobbs J, Barrett A and Ash D 1999 *Practical Radiotherapy Planning*, Oxford University Press Inc., New York, NY

[8] Glatstein E, Lichter A S, Fraass B A, Kelly B A and van De Geijn J 1985 The imaging revolution and radiation oncology: use of CT, ultrasound, and NMR for localization, treatment planning and treatment delivery *Int. J. Radiat. Oncol. Biol. Phys.* **11** 299-314

[9] ICRU Report 50 1993 Prescribing, recording and reporting photon beam therapy International Commission on Radiation Units and Measurements, Bethesda MD

[10] ICRU Report 62 1999 Prescribing, recording and reporting photon beam therapy (Supplement to ICRU Report 50) International Commission on Radiation Units and Measurements, Bethesda MD

[11] Aaltonen-Brahme P, Brahme A, Lax I, Levernes S, Naslund I, Reitan J, Turesson I 1997 Specification of dose delivery in radiation therapy *Acta. Oncologica* **36**, suppl. 10

[12] Dobbs H J, Parker N J, Hobday P and Husband J E 1983 The use of CT in radiotherapy treatment planning *Radiother. Oncol.* **37** 133-141

[13] Hendee W R and Ibbott G S 1996 *Radiation Therapy Physics* Mosby-Year Book Inc., St. Louis, MI

[14] Langer M 2003 *What is different about IMRT?*, Intensity-Modulated Radiation Therapy: The state of the art, AAPM 2003 Summer School published proceedings

[15] Khan F M 2003 *The Physics of Radiation Therapy*, Lippincott Williams and Wilkins, Philadelphia, PA

[16] Webb S 2001 *Intensity Modulated Radiation Therapy*, Institute of Physics Publishing, Bristol and Philadelphia

[17] Takahashi S 1969 Conformation radiotherapy, rotation techniques as applied to radiography and radiotherapy *Acta. Radiat. Oncol. Biol. Phys.* **242**

[18] Boyer A L 2002 The physics of intensity-modulated radiation therapy *Physics Today* September

[19] Brahme A 1996 Recent developments in radiation therapy planning and treatment optimization *Australas.Phys. Eng. Sci. Med.* **19** 53-66

[20] MacKenzie M A, Lachaine M, Murray B, Fallone B G, Robinson D and Field G C 2002 Dosimetric verification of inverse planned step and shoot multileaf collimator fields from a commercial treatment planning system *J Appl Clin Med Phys.* **3** 97-109

[21] Bortfeld T, Bürkelbach J, Boesecke R and Schlegel W 1990 Methods of image reconstruction from projections applied to conformation therapy *Phys. Med. Biol.* **35** 1423-34.

[22] Boyer A L 1997 Verification and delivery of intensity-modulated treatments with dynamic multileaf collimator *Proc. 12th Int. Conf. on the Use of Computers in Radiation Therapy* Salt Lake City, May 1997, 13-16

[23] Boyer A L and Strait 1997 Delivery of intensity-modulated treatments with dynamic multileaf collimator *Proc. Meeting: intensity-modulated Radiation Therapy: A clinical perspective* London, 26 June 1997, 11-16

[24] Webb S 1989 Optimisation of conformal radiotherapy dose distributions by simulated annealing *Phys. Med. Biol.* **34** 1349-70

[25] De Meerleer G O, Vakaet L A, De Gersem W R, De Wagter C, De Naeyer B, and De Neve W 2000 Radiotherapy of prostate cancer with or without intensity modulated beams: A planning comparison *Int. J. Radiat. Oncol. Biol. Phys.* **47** 639648.

[26] Goitein M and Niemierko A 1996 Intensity modulate therapy and inhomogeneous dose to the tumor: A note of Caution *Int. J. Radiat. Oncol. Biol. Phys.* **36** 519-22

[27] Rogers D W O 1995 Monte Carlo Techniques in Radiotherapy *CAP. Phys.* **22**, 503-524

[28] Cranmer-Sargison G, Beckham W A and Popescu I A 2004 Modelling an extreme water-lung interface using a single pencil beam algorithm and the Monte Carlo method *Phys. Med. Biol.* **49** 1557-67

[29] Verhaegen F and Seuntjens J 2003 Monte Carlo modelling of external radiotherapy photon beams *Phys. Med. Biol.* **48** R107-R164

[30] Sobol I M 1974 *The Monte Carlo Method*, University of Chicago Press, Chicago IL

[31] Nelson W R, Hirayam H and Rogers D W O 1985 The EGS4 Code System *Stanford Linear Accelerator Center Report No. SLAC-265*

[32] Rogers D W O, Faddegon B A, Ding G X, Ma C M, Wei J, and Mackie T R 1995 BEAM: A Monte Carlo code to simulate radiotherapy treatment units *Med. Phys.* **22** 503-524

[33] Karzmarh C J, Nunan C S and Tanabe E 1992 *Medical Linear Accelerators*, McGraw-Hill Companies Health Professions Divi, Columbus, OH

[34] Rogers D W O, Ma C M, Walters B R B, Ding G X, Sheikh-Bagheri D and Zhang G 2001 BEAMnrc Users Manual *National Research Council of Canada, Ottawa* **PIRS-0509(A)revG**

[35] Walters B R B and Rogers D W O 2001DOSXYZnrc Users Manual *National Research Council of Canada, Ottawa* **PIRS-794**

[36] Ma C M and Rogers D W O 2004 BEAMDP as a General-Purpose Utility *National Research Council of Canada, Ottawa* **PIRS-509e(rev A)**

[37] Kawrakow I, Fippel M and Friedrich K 1996 3D electron dose calculation using a Voxel based Monte carlo algorithm (VMC) *Med. Phys.* **23** 445-457

[38] Walters B R B, Kawrakow I and Rogers D W O 2002 History by History statistical estimators in the BEAM code system *Med. Phys.* **29** 2745-52

[39] Ma C M, Pawlicki T, Jiang S B, Li S, Deng J, Mok E, Kapur A Xing L, Ma L and Boyer A L 2000 Monte Carlo verification of IMRT dose distributions from a commercial treatment planning optimization system *Phys. Med. Biol.* **45** 2483-95

[40] Chen Y, Boyer A L and Ma C M 2000 Calculation of x-ray transmission through a multileaf collimator *Med. Phys.* **27** 1717-26

[41] Kim J O, Siebers J V, Arnfield M R and Mohan R 2001 A Monte Carlo study of radiation transport through multileaf collimators *Med. Phys.* **28** 2497-506

[42] Keall Pj, Siebers J V, Arnfield M R, Kim J O and Mohan R 2001 Monte Carlo dose calculations for dynamic IMRT treatments *Phys. Med. Biol.* **46** 929-41

[43] Siebers J V, Keall P J, Kim O and Mohan R 2002 A method for photon beam Monte Carlo multileaf collimator particle transport *Phys. Med. Biol.* **47** 3225-49

[44] Popescu I A, Shaw C P, Zavgorodni S F and Beckham W A 2005 Absolute dose calculations for Monte Carlo simulations of radiotherapy beams *Phys. Med. Biol.* **50** 3375-92

[45] Urie M M, Goitein M, Doppke K, Kutcher J G, LoSasso T, Mohan R, Munzenrider J E, Sontag M and Wong J W 1991 The role of uncertainty analysis in treatment planning *Int. J. Radiat. Oncol. Biol. Phys.* **21** 91-107

[46] Langen K M and Jones D T L 2001 Organ motion and its management *Int. J. Radiat. Oncol. Biol. Phys.* **50** 265-78

[47] Gagné I M and Robinson D M 2004 The impact of tumor motion upon CT image integrity and target delineation *Med. Phys.* **31** 3378-92

[48] Booth J T, Zavgorodni S F 2001 Modelling the dosimetric consequences of organ motion at CT imaging on radiotherapy treatment planning *Phys. Med. Biol.* **46** 1369-77

[49] Schaly B, Kempe J A, Bauman G S, Battista J J and Van Dyk J 2004 Tracking the dose distribution in radiation therapy by accounting for variable anatomy *Phys. Med. Biol.* **49** 791-805

[50] Balter J M, Ten Haken R K, Lawrence T S, Lam K L and Robertson J M 1996 Uncertainties in CT-based radiation therapy treatment planning associated with patient breathing *Int. J. Radiat. Oncol. Biol. Phys.* **36** 167-74

[51] Chetty I J, Rosu M, McShan D L, Fraass B A, Balter J M and Ten Haken R K 2004 Accounting for center-of-mass target motion using convolution methods in Monte Carlo-based dose calculations of the lung *Med. Phys.* **31** 925-32

[52] Goitein M 1985 Calculation of the uncertainty in the dose delivered during radiation therapy *Med. Phys.* **12** 608-12

[53] Craig T, Battista J and Van Dyk J 2003 Limitations of a convolution method for modeling geometric uncertainties in radiation therapy. I. The effect of shift invariance *Med. Phys.* **30** 2001-11

[54] Powers E L 1962 Considerations of Survival Curves and Target Theory *Phys. Med. Biol.* **7** 3-28

[55] Lee D E *Actions of Radiation on Living Cells*, Cambridge University Press, UK

[56] Pizzarello D J and Witcofski R L 1975 *Basic Radiation Biology*, Lea & Febiger, Philadelphia, PA

[57] Steel G G 2002 *Basic Clinical Radiobiology* , Oxford University Press, New York, NY

[58] Chadwick K H and Leenhouts H P 1973 A molecular theory of cell survival *Phys. Med. Biol.* **18** 78-87

[59] Leenhouts H P and Chadwick 1990 The influence of dose rate on the dose-effect relationship *J. Radiol. Prot.* **10** 95-102

[60] Tobias C A, Blakely E A, Ngo F Q H and Yang T C Y 1980 The repair-misrepair model of cell survival *Radiation Biology in Cancer Research* Raven Press, New York, NY

[61] Lea D E 1946 *Actions of Radiations on Living cells* Cambridge University Press, UK

[62] Hagen U 1989 Biochemical aspects of radiation biology *Experientia* **45** 7-12

[63] Michalik V and Frankenberg D 1996 Two types of double strand breaks in electron and photon tracks and their relation to exchange-type chromosome aberrations *Radiat. and Enviro. Biol. Phys.* **35** 163-169

[64] Sachs R K, Hahnfeld P and Brenner D J 1997 The link between low-LET dose-response relations and the underly

[65] Hall E J 2000 *Radiobiology for the radiologist*, Lippincott Williams & Wilkins, Philadelphia, PA

[66] Van Dyk J —it The Modern Technology of radiation Oncology Medical Physics Publishing, Madison, WI

[67] Fowler J F 1984 40 years of radiobiology: its impact on radiotherapy *Phys. Med. Biol.* **29** 97-113

[68] Fowler J F 1989 The linear-quadratic formula and progress in fractionated radiotherapy *Br. J. Radiol.* **62** 679-94

[69] H E Johns and J R Cunningham 1983 *The Physics of Radiology*, Charles C Thomas, Springfield, Illinois

[70] Metcalfe P, Kron T and Hoban P 1997 *The Physics of Radiotherapy X-Rays from Linear Accelerators*, Medical Physics Publishing, Madison, Wisconsin

[71] Niemierko A 1997 Reporting and analyzing dose distributions: A concept of equivalent uniform dose *Med. Phys.* **24** 103-10

[72] Holloway L, Hoban P, Metcalfe P 2002 Radiobiological indices that consider volume: a review *Australas. Phys. Eng. Sci. Med.* **25** 47-57

[73] Webb S and Nahum A E 1993 A model for calculating tumour control probability in radiotherapy including the effects of inhomogeneous distributions of dose and clonogenic cell density *Phys. Med. Biol.* **38** 653-666

[74] Webb S, Evans P M, Swindell W and Deasy J O 1994 A proof that uniform dose gives the greatest TCP for fixed integral dose in the planning target volume *Phys. Med. Biol.* **39** 2091-98

[75] Niemierko A and Goitein M 1993 Implementation of a model for estimating tumor control probability for an inhomogeneously irradiated tumor *Radiother. Oncol.* **29** 140-7

[76] Brenner D J 1993 Dose, volume and tumor control predictions in radiotherapy *Int. J. Radiat. Oncol. Biol. Phys.* **26** 171-79

[77] Zagars G K, Schultheiss T E and Peters L J 1987 Inter-tumor heterogeneity and radiation dose-control curves *Radiother. Oncol.* **8** 353-62

[78] Ebert M A and Hoban P W 1996 Some characteristics of tumour control probability for heterogeneous tumours *Phys. Med. Biol.* **41** 2125-33

[79] Sempau J and Bielajew A F 2000 Towards the elimination of Monte Carlo statistical fluctuation from dose volume histograms fro radiotherapy treatment planning *Phys. Med. Biol.* **45** 131-157

[80] Jiang S B, Pawlicki T and Ma CM 2000 Removing the effect of statistical uncertainty on dose-volume histograms from Monte Carlo dose calculations *Phys. Med. Biol.* **45** 2151-61

[81] Kawrakow I 2004 The effect of Monte Carlo statistical uncertainty on the evaluation of dose distributions in radiation therapy planning *Phys. Med. Biol.* **49** 1549-56

[82] 2004 The impact of inter-fraction dose variation on biological equivalent dose (BED): the concept of equivalent constant dose *Phys. Med. Biol.* **49** 5333-45

[83] Leong J 1987 Implementation of random positioning error in computerised radiation treatment planning systems as a result of fractionation *Phys. Med. Biol.* **32** 327-34

[84] Lujan A, Ten Haken R Larsen E and Balter J 1999 Quantization of setup uncertainties in 3-D dose calculations *Med. Phys.* **26** 2397-402

[85] Zavgorodni S F 2000 Treatment planning algorithm corrections accounting for random setup uncertainties in fractionated stereotactic radiotherapy *Med. Phys.* **27** 685-90

[86] McCarter S D and Beckham W A 2000 Evaluation of the validity of a convolution method for incorporating tumour movement and set-up variations into radiotherapy treatment planning system *Phys. Med. Biol.* **45** 923-31

[87] Rudat V, Flentje M, Oetzel D, Menke M, Schlegel W and Wannenmacher M 1994 Influence of the position error on 3D conformal dose distributions during fractionated radiotherapy *Radiother. Oncol.* **33** 56-63

[88] Song W, Battista J and Van Dyk J 2004 Limitations of a convolution method for modeling geometric uncertainties in radiation therapy: the radiobiological dose-per-fraction effect *Med. Phys.* **31** 3034-45

[89] Bel A, van Herk and Lebesque J V 1996 Target margin for random geometrical treatment uncertainties in conformal therapy *Med. Phys.* **23** 1537-45

[90] Beckham W A, Keall P J and Siebers J V 2002 A fluence-convolution method to calculate radiation therapy dose distributions that incorporate random set-up error *Phys. Med. Biol.* **47** 3465-73

[91] Stapleton S, Zavgorodni S, Popescu I A and Beckham W A 2005 Implementation of random set-up errors in Monte Carlo calculated dynamic IMRT treatment plans *Phys. Med. Biol.* **50** 429-39

[92] Eugene Butkov 1968 *Mathematical Physics* Addison-Wesley Publishing Company, Reading, Mass.

[93] K. F. Riley 1974 *Mathematical Methods for the Physical Sciences*, Cambridge University Press, New York NY

[94] Roberts S A and Hendry J H 1998 A realistic closed-form radiobiological model of clinical tumour-control data incorporating intertumor heterogeneity *Int. J. Radiat. Oncol. Biol. Phys.* **41** 689-699

[95] Cho J B C, van Herk M, Mijnheer B J and Bartelink H 2002 The effect of set-up uncertainties, contour changes, and tissue inhomogeneities on target dose-volume histograms *Med. Phys.* **29** 2305-18

[96] Ebert M A 2000 Viability of the EUD and TCP concepts as reliable dose indicators *Phys. Med. Biol.* **45** 441-57

[97] Tomé W A and Fowler J F 2002 On cold spots in tumor subvolumes *Med. Phys.* **29** 1590-98

[98] Tomé W A and Fowler J F 2000 The selective boosting of tumor subvolumes *Int. J. Radiat. Oncol. Biol. Phys.* **48** 593-99

[99] Buffa F M, Nahum A E 2000 Monte Carlo dose calculations and radiobiological modelling: analysis of the effect of the statistical noise of the dose distributions on the probability of tumour control *Phys. Med. Biol.* **45** 3009-23

[100] Keall P J, Jeraj R and Mohan R 2000 The effect of dose calculation uncertainty on the evaluation of radiotherapy plans *Med. Phys.* **27** 478-484

[101] Wigg D R 2001 *Applied radiobiology and bioeffect planning*, Medical Physics Publishing, Madison, WI

[102] van Herk M 2003 Biologic and physical fractionation effects of random geometric errors *Int. J. Radiat. Oncol. Biol. Phys.* **57** 1460-71